MODELING AND SIMULATION OF MAGNETIC TRANSMISSION LINES

Name: Muhammad Shamaas

Registration ID: 2018-MS-EE-4

Supervisor: Dr. Muhammad Asghar Saqib

DEPARTMENT OF ELECTRICAL ENGINEERING
UNIVERSITY OF ENGINEERING AND TECHNOLOGY LAHORE

Contents

List of Figures

List of Symbols

Symbol	Definition	Equation
q	Strength of magnetic poles	(1.1)
r	Distance between magnetic poles	(1.1)
F	Force between magnetic poles	(1.1)
$\boldsymbol{B}$	Magnetic flux density vector	(1.2)
$\boldsymbol{E}$	Electric field intensity vector	(1.2)
$\boldsymbol{F_{EM}}$	Lorentz force vector	(1.2)
e	Electric charge	(1.2)
$\boldsymbol{v}$	Velocity vector	(1.2)
$\boldsymbol{F_{loop}}$	Force on current loop	(1.3)
I	Electric conduction current	(1.3)
$\boldsymbol{dl}$	Infinitesimal length vector	(1.3)
$\boldsymbol{T}$	Torque vector	(1.4)
$\boldsymbol{m}$	Magnetic dipole moment vector	(1.4)
μ_B	Bohr magneton	(1.5)
g_L	Orbital angular momentum g-factor	(1.5)
g_S	Spin angular momentum g-factor	(1.5)
$\boldsymbol{L}$	Orbital angular momentum	(1.5)
$\boldsymbol{S}$	Spin angular momentum	(1.5)
$\hbar$	Reduced Planck constant	(1.5)
m_e	Electron mass	(1.5)
E	Energy	(1.6)
$\boldsymbol{J}_{ij}$	Heisenberg exchange constant between two states	(1.7)
$\boldsymbol{M}$	Magnetization	(1.8)
χ_m	Magnetic susceptibility	(1.8)
$\boldsymbol{H}$	Magnetization field vector	(1.8)
μ_0	Free space permeability	(1.9)
$\boldsymbol{J}_{bound}$	Bound electric conduction current	(1.10)
d	Width of magnetic strip	(1.12)
$\alpha_x\alpha_y\alpha_z$	Direction cosines	(1.13)
K_a	Anisotropy constant	(1.13)
E_M	Magnetostatic energy	(1.12)
E_{MCA}	Magneto-crystalline anisotropy energy	(1.13)
E_{MS}	Magnetostriction energy	(1.14)
λ_{ms}	Magnetostriction constant	(1.14)
σ_s	Mechanical stress	(1.14)
E_{DW}	Domain wall Energy	(1.15)
a	Atomic spacing	(1.15)
T_c	Curie temperature	(1.15)
μ	Magnetic permeability	(1.16)
T	Temperature	(1.17)
M_0	Spontaneous magnetization	(1.19)
α	Temperature exponent for susceptibility	(1.20)
β	Temperature exponent for magnetization	(1.21)
W_H	Hysteresis loss energy	(1.22)

P_H	Hysteresis density	(1.24)
B_{max}	Magnetic saturation flux density	(1.24)
f	Frequency	(1.24)
P_e	Eddy current loss density	(1.25)
ρ	Electrical resistivity	(1.25)
ε	Electrical permittivity	(1.26)
ε_0	Electrical permittivity of free space	(1.26)
ε'	Real part of electrical permittivity	(1.26)
ε''	Imaginary part of electrical permittivity	(1.26)
ω	Radian frequency	(1.26)
μ'	Real part of magnetic permeability	(1.27)
μ''	Imaginary part of magnetic permeability	(1.27)
$tan\delta_d$	Dielectric loss tangent	(1.28)
$tan\delta_b$	Diamagnetic loss tangent	(1.29)
$tan\delta_H$	Hysteresis loss tangent	(1.30)
$tan\delta_E$	Eddy current loss tangent	(1.30)
$tan\delta_r$	Residual loss tangent	(1.30)
$tan\delta$	Total loss tangent	(1.30)
$\boldsymbol{D}$	Electric flux density vector	(2.1)
σ	Electric conductivity	(2.1)
ρ_v	Volume charge density	(2.4)
ρ_s	Surface charge density	(2.5)
J_s	Surface current density	(2.6)
γ	Propagation constant	(2.9)
α	Attenuation constant	(2.11)
β	Phase constant	(2.11)
δ	Skin depth	(2.12)
u	Phase velocity	(2.13)
λ	Wavelength	(2.14)
η	Intrinsic impedance	(2.15)
β_o	Free space phase constant	(2.16)
μ_r	Relative permeability	(2.16)
ε_r	Relative permittivity	(2.16)
u_o	Free space phase velocity	(2.17)
λ_o	Free space wavelength	(2.18)
η_0	Free space intrinsic impedance	(2.19)
$\boldsymbol{S}$	Poynting vector	(2.22)
$\hat{\boldsymbol{n}}$	Surface normal vector	(2.22)
$\boldsymbol{J}$	Electric conduction current density vector	(2.25)
W_e	Electric energy	(2.27)
W_m	Magnetic energy	(2.28)
$\boldsymbol{I}$	Wave intensity	(2.29)
$\boldsymbol{g}$	Momentum density of wave	(2.30)
c	Speed of light	(2.30)
$\boldsymbol{P}$	Radiation pressure	(2.31)
F	Force	(2.31)
A	Area	(2.31)
p	Momentum	(2.31)
$\boldsymbol{\mathcal{R}}_m$	Magnetic reluctance	(3.1)
$\boldsymbol{\phi}_m$	Magnetic flux	(3.1)

$\boldsymbol{\mathcal{F}}_m$	Magnetomotive force	(3.1)
$\emptyset$	Phase angle of magnetic reluctance	(3.1)
P_e	Electric power	(3.2)
I_e	Electric conduction current	(3.2)
R_e	Electric resistance	(3.2)
P_m	Magnetic power	(3.3)
V_T	Generator terminal voltage	(3.4)
E_A	Generated electromotive Force	(3.4)
I_A	Armature current	(3.4)
R_A	Armature resistance	(3.4)
R_S	Series field winding resistance	(3.4)
I_L	Terminal current	(3.5)
I_F	Shunt field winding current	(3.5)
R_F	Shunt field winding resistance	(3.5)
$\mathcal{F}_{net}$	Net magnetomotive force	(3.7)
$\mathcal{F}_F$	Shunt field magnetomotive force	(3.7)
$\mathcal{F}_{SE}$	Series field magnetomotive force	(3.7)
$\mathcal{F}_{AR}$	Armature reaction magnetomotive force	(3.7)
N_F	Shunt field winding turns	(3.8)
I_F^*	Net Field Current	(3.8)
N_{SE}	Series field winding turns	(3.8)
k	Voltage constant	(3.9)
ϕ_m	Magnetic flux	(3.9)
ω_m	Rotor mechanical speed	(3.9)
V_e	Electrical voltage	(3.10)
N	Gyration constant	(3.10)
$I_{m,disp}$	Magnetic displacement current	(3.12)
V_m	Magnetic voltage	(3.13)
$\mathcal{F}_m$	Magnetomotive force	(3.13)
Φ_{Pm}	Magnetic flux stored in permeance	(3.14)
P_m	Magnetic permeance	(3.14)
v_{Pm}	Magnetic voltage of permeance	(3.14)
i_{Pm}	Magnetic displacement current of permeance	(3.15)
L_m	Magnetic inductance	(3.16)
A	Area of magnetic core	(3.16)
l	Length of magnetic core	(3.16)
λ_p	Flux linkage of primary winding	(3.17)
Vp	Voltage of primary winding	(3.17)
D	Duty cycle	(3.17)
T_s	Switching period	(3.17)
V_s	Source voltage	(3.17)
ΔB	Maximum change in magnetic flux	(3.18)
$V_{Diode,on}$	Turn on voltage of diode	(3.19)
l_m	Mean path length of magnetic core	(3.20)
R_c	Resistance of core	(3.22)
L_{filter}	Filter Inductance	(3.23)
C_{filter}	Filter Capacitance	(3.24)
L_T	Transverse inductance of magnetic transmission line	(3.33)
C_L	Longitudinal capacitance of magnetic transmission line	(3.34)

Φ_e	Electric flux	(3.34)
P_{av}	Average power	(3.43)
P_{loss}	Dissipated power	(3.45)
G_L	Longitudinal Conductance of magnetic transmission line	(3.46)
L_L	Longitudinal inductance of electric transmission line	(3.58)
C_T	Transverse capacitance of electric transmission line	(3.60)
P	Wave power	(4.17)
$\boldsymbol{P}$	Polarization vector	(4.18)
ε_∞	Permittivity at infinite frequency	(4.20)
μ_∞	Permeability at infinite frequency	(4.21)
σ_D	Electric conductivity	(4.22)
σ_B	Magnetic conductivity	(4.23)
σ_n	Oscillator strength at nth resonance frequency	(4.22)
γ_n	Oscillator damping ration at nth resonance frequency	(4.22)
ω_n	nth resonance frequency	(4.22)
$\chi^{(2)}$	Pockels nonlinearity coefficient	(4.24)
$\chi^{(3)}$	Kerr nonlinearity coefficient	(4.24)
$\boldsymbol{b}_n$	Bias vector for gyromagnetic precession	(4.26)
Z_w	Intrinsic wave impedance	(5.2)
$\mathcal{R}_{mskin}$	Magnetic reluctance	(5.4)

Abstract

Magnetic Transmission Line is the dual counterpart of Electric Transmission Line [22] - [26]. Its theory encompasses a diverse range of applications including Transformers, Dynamic Machines, Microwave Generators, Tuners, Couplers, Isolators, Power Dividers etc. Intrinsically, Magnetic Transmission Line is made from a non-conducting magnetic material, with a high permeability [22] - [26]. It transmits Magnetic Flux as the effective Magnetic charge. Time varying magnetic flux results in a Magnetic Displacement Current inside the Transmission Line. This produces a gradient Magnetic Field; with Fields Lines that spread radially outwards. The magnetic displacement current and magnetic voltage due to this Magnetic Field is measured in Volts and Amperes respectively. Although, the operation of a Magnetic Transmission Line does not involve electric charges, Magnetic Displacement Current produces an Electric Field with closed Field Lines encircling the Magnetic Transmission Line [22] - [26]. Together, the Electric and Magnetic Fields transmit Energy along the direction of propagation. These relations were modeled using Maxwell's Equations and magnetic circuits to study the time and frequency domain behavior of Magnetic Transmission Lines [22] - [26]. Furthermore, Finite Difference Time Domain [68] - [69], [64] Electromagnetic Field Simulations [39] were carried out in MEEP [52] Simulator for anisotropic, inhomogeneous, non-linear Magnetic Transmission Lines [40], [65], [43], [22] - [26], [8].

The Magnetic Transmission Line model is valuable for the design of Magnetic Elements like Ferromagnetic Inductors, Transformers and Filters [22] - [26], [17], [20]. The conventional design of Magnetic Elements is an iterative procedure. The hit and trial procedure involves many approximations like uniform field inside core, minimal flux leakage and constant magnetic permeability. There is no shortage of empirical formulas for designing Magnetic Cores and estimating Magnetic Losses [35-36], [20]. The derived formulas are specific for a narrow frequency band or the particular core shape and size. The Magnetic Transmission Line [22] - [26] model can be extended to design accurate models for transient analysis of magnetic elements [20].

Acknowledgements

First of all, thanks to Allah who made it possible for me to complete this thesis.

I am thankful to my supervisors Dr. Muhammad Asghar Saqib, Dr. Syed Abul Rehman Kashif, Dr. Syed Shah Irfan Hussain and Dr. Farhan Mahmood whose stimulating suggestions supported me throughout the research for this thesis.

Especially, I would like to give my special thanks to my teachers whose care and struggle enabled me to stay focused in my quest for knowledge.

My former colleagues supported me in my research work. I want to thank them for all their help, support, interest and valuable hints. Especially I am obliged to my friends and family for their support.

1. Introduction to Solid State Magnetism

The first chapter is dedicated to a brief review of the nature of Magnetic materials and the transmission of magnetic information using magnetic dipoles. Section 1.1. presents a summary of Magnetic Dipoles and Bulk Magnetization. Section 1.2. discusses the AC properties and losses of magnetic materials [35-36], [20]. Section 1.3. presents a literature review of Magnetic Transmission Lines [22] - [26] with major emphasis on the recent research on Giant Magnetoresistance [66], Magnetic Capacitance [74], [73], Magnetic Memory [41], Spintronic and Nanomagnetic Logic Devices [63], [42], [38], [34], [5], [15], [19], [30].

Magnetic Transmission Lines [22] - [26] are designed to transmit electromagnetic energy using strong magnetic fields. They are made of magnetic materials having very high magnetic permeability and a strong affinity for magnetic flux. When an external magnetic field is applied, magnetic dipoles react to align with it. This large scale cooperation enhances the Magnetic Flux Density inside the magnetic material. When the applied field is varied, the changing Magnetic Flux Density transmits the magnetic information across the magnetic material [13]. This phenomenon is called Magnetic Transmission [22] - [26].

It is important to note that charge transport is not involved in magnetic communication. Isolated Magnetic charges do not exist and magnetic conduction current can never flow in a Magnetic Transmission Line [22] - [26]. Magnetic Transmission is only possible through the alignment of magnetic dipoles in response to a stimulating Magnetomotive Force. This is termed as Magnetic Displacement Current.

Magnetic Transmission does not involve the flow of Electric charges either. Magnetic materials are very poor electric conductors; hence electric currents cannot transmit information across a Magnetic Transmission Line [22] - [26]. Changing Magnetic Fields produce Electric Fields which are transmitted through electric displacement currents. This causes polarization of atoms in the dielectric [50] magnetic medium which transmits Electric information across the Magnetic Material. Together, the Electric and Magnetic Fields transmit Electromagnetic Energy along the direction of propagation [55].

The following sections will elaborate on the subject of Magnetic Materials. A brief account on the losses [35-36], [20] in Magnetic Transmission Lines [22] - [26] will be given as well.

1.1. Nature of Magnetic Materials

The basic building blocks of magnetic materials are fictitious magnetic monopoles which can be considered as magnetic charge carriers. In nature, magnetic monopoles always exist in pairs called magnetic dipoles. A monopole can have either positive or negative charge which is responsible for the magnetic field around it. The force between monopoles is proportional to the strength of the poles (q) and inversely proportional to the square of distance (r) between them:

$$F \propto \frac{q_1 q_2}{r^2} \tag{1.1}$$

Dipoles result from the microscopic bound currents due to the electrons circulating around the nucleus. The effect of each tiny magnet is similar to the effect of a current flowing in a loop. The identification of the North and South poles is dictated by the Flemming's right hand rule.

Whenever a moving charge q is placed in an electromagnetic field, it experiences a force called Lorentz Force [55]. The direction of the force represents the direction of least pressure in the electromagnetic field. Lorentz Force depends on the velocity of the charge and the strength of the electric and magnetic fields:

$$\boldsymbol{F_{EM}} = e(\boldsymbol{E} + \boldsymbol{v} \times \boldsymbol{B}) \tag{1.2}$$

If an orbiting electron is placed in a magnetic field, the net Ampere force on the current loop is:

$$\boldsymbol{F_{loop}} = \oint I\boldsymbol{dl} \times \boldsymbol{B} \tag{1.3}$$

The Force will produce a Torque which will rotate the tiny magnet in the direction of applied field resulting in the transmission of magnetic information. The Torque can be represented in terms of the magnetic dipole moment normal to the current loop:

$$\boldsymbol{T} = \boldsymbol{m} \times \boldsymbol{B} \tag{1.4}$$

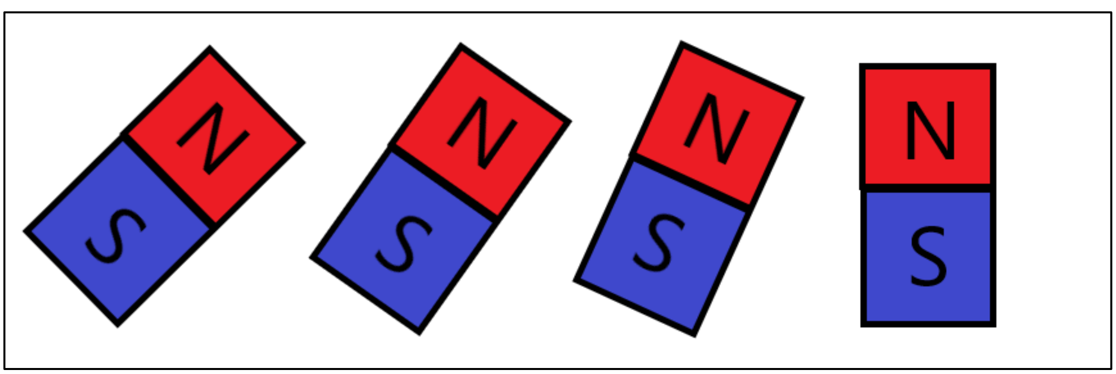

Figure 1: Magnetic Transmission through transfer of Torque

The magnetic dipole moment $\hat{\boldsymbol{\mu}}$ of an orbiting/spinning electron is related to the g-factors for the spin and orbital angular momentum, the spin angular momentum operator $\hat{\boldsymbol{S}}$ and the orbital angular momentum operator $\hat{\boldsymbol{L}}$ [6], [15]:

$$\boldsymbol{m} = \mu_B(g_L\boldsymbol{L} + g_S\boldsymbol{S}) \tag{1.5}$$

where $g_L = 1, g_S = 2.0023, \mu_B = \frac{q\hbar}{2m_e}$.

The magnetic field of the orbiting electron interacts with its spin to produce intrinsic spin-orbit interaction [15]. Hence the moment attains discrete values depending on the spin and orbital quantum numbers [42]. The net magnetic moment of an atom or ion is the vector sum of the orbital and spin moments of all electrons in its outer shell. The energy levels of an electron split in a magnetic field due to Zeeman splitting and Heisenberg exchange interaction [15], [6]:

$$E = -\boldsymbol{m}.\boldsymbol{B} \tag{1.6}$$

$$E = -\sum_{ij}\boldsymbol{J}_{ij}\boldsymbol{S}_i.\boldsymbol{S}_j + \mu_B g_S \sum_{\boldsymbol{j}}\boldsymbol{S}_i.\boldsymbol{B} \tag{1.7}$$

where $\boldsymbol{J}_{ij}$is the exchange constant between state i and j.

Two dipoles attract each other if unlike poles are close to each other. On the other hand, two dipoles repel each other if like poles are closer. Inside an unmagnetized material, the magnetic dipoles are optimally oriented hence the net torque is zero. Only a few orientations can result in a net zero torque on all the dipoles in a magnetic material. Dipoles tend to align parallel to neighboring dipoles due to positive exchange interactions so that the lowest energy state can be achieved.

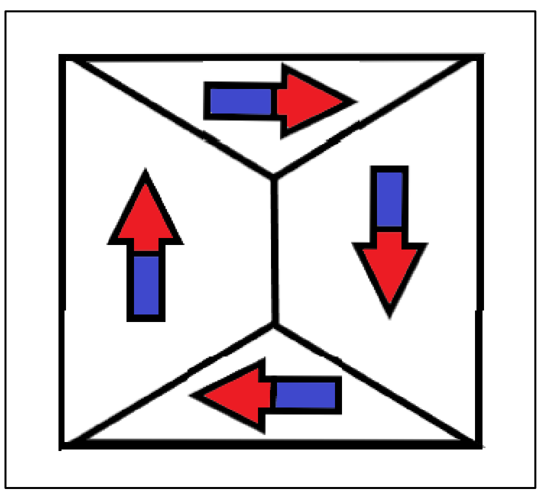

Figure 2: A minimum energy state configurations achieved by cooperation of neighboring domains

Atoms contain orbitals with discrete levels of energy for accommodating electrons. Electrons try to occupy the lowest energy orbitals first to minimize the energy of the system. An electron with clockwise spin can pair with an electron having anticlockwise spin. Hence, the clockwise spin cancels the effect of anticlockwise spin and no magnetic moment results [15].

An external magnetic field can cause a mechanical torque on a magnetic dipole. The moment tries to turn the dipole in the direction that decreases the overall energy of the system. Only unpaired spins contribute to the net magnetic moment. The resulting spin and orbital moments add up to produce a net Magnetization Vector Field M inside the magnetic material [15]. This field is proportional to the magnetic susceptibility of the material χ_m:

$$\boldsymbol{M} = \chi_m \boldsymbol{H} \tag{1.8}$$

The Magnetic Field inside a magnetic material can be represented by a flow of magnet field lines [13]. The number of lines passing through a region of space is called Magnetic Flux (equivalent to magnetic charge). Magnetic Flux Density (B) represents the number of flux lines per unit area:

$$\boldsymbol{B} = \mu_0(\boldsymbol{H} + \boldsymbol{M}) \tag{1.9}$$

Iron, Nickel and Cobalt contain 4, 3 and 2 unpaired electrons per atom respectively [53]. Hence, the effect of Magnetization is very strong in these special elements and their alloys. Large scale cooperation between magnetic dipoles causes an enhanced Magnetic moment. Due to the high magnetic susceptibility, they are used in the production of Ferromagnetic and Ferrimagnetic materials [53].

The microscopic bound current responsible for producing magnetic dipoles cancels out inside a uniformly magnetized material. A net bound current flows at the surface of the material. If **M** is non-uniform, the bound current will be non-zero inside the material as well.

$$\boldsymbol{J}_{bound} = \nabla \times \boldsymbol{M} \tag{1.10}$$

$$\nabla . \boldsymbol{H} = -\nabla . \boldsymbol{M} \tag{1.11}$$

The parallel alignment of magnetic dipoles causes the creation of magnetic domains [27] to reduce the magnetic potential energy stored in the Magnetic Flux Lines. The Magnetic energy consists of the following:

1. Magnetostatic Energy: The energy needed to place the magnetic poles in a specific geometric configuration e.g. magnetized state [27] is proportional to the width of the magnetic strip (d) and the value of applied Magnetic Field Intensity (H). Transformers are made using insulated sheets of steel having high electrical resistance [17], [27]. Rolling of the sheets aligns the Magnetic domains and reduces the Magnetostatic Energy [27]. The expression for this energy is given below

$$E_M \propto H^2 d \tag{1.12}$$

2. Magneto-crystalline Anisotropy Energy: For crystalline structures with repeating atomic units, the domain magnetization tends to align along one direction more easily than other directions. Magneto-crystalline Anisotropy Energy is greater in hard direction as compared to the easy direction [27]. It depends on the anisotropy constants (K_a) and direction cosines (α_i) which project magnetization on the different axes e.g.

$$E_{MCA} = K_a(\alpha_x\alpha_y + \alpha_y\alpha_z + \alpha_z\alpha_x) \tag{1.13}$$

3. Magnetostrictive Energy: Magnetization and Demagnetization can cause changes in the dimensions of the magnetic materials [27]. These stresses are caused by shifting of atomic planes e.g. during alignment of domains. Magnetostrictive Energy represents the elastic potential energy stored in the constricted atomic configuration. It is proportional to the magnetostriction constant λ_{ms} and applied stress σ_s.

$$E_{MS} \propto \frac{3}{2}\lambda_{ms}\sigma_s \tag{1.14}$$

4. Domain Wall Energy: A Domain wall is a region where the Magnetization in one domain gradually changes to the direction of a neighboring domain [27]. Domain Wall Energy represents the energy in the transition region. It is related to Anisotropy Constant (K_a), Curie Point (T_c) and atomic spacing (a).

$$E_{DW} \propto \sqrt{\frac{K_a T_c}{a}} \tag{1.15}$$

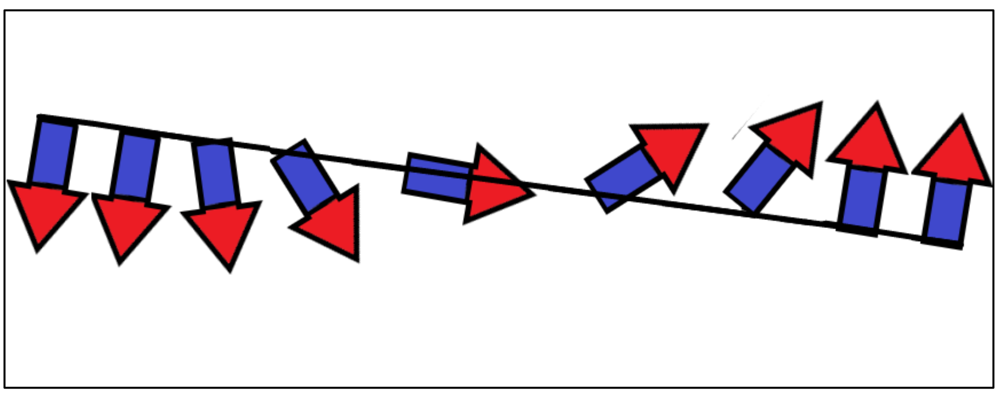

Figure 3: Tansition of spin direction at a domain boundary

Naturally, the size and direction of magnetic domains [27] is chosen to minimize the overall magnetic energy of the system. If an unmagnetized material is placed in an external magnetic field, the domains may have to align in a hard direction for Magnetization of the material. Work will be done to align the domains in the special configuration so that the preferable domains grow in size while the unfavorable domains shrink. This will involve displacement of atomic planes and domain boundaries. Hence the overall stored magnetic energy of the system will increase during magnetization [27].

When a demagnetized material is placed in an increasing Magnetic Field, the domain walls will start reversible movements and rotations. The Magnetization will start to increase slowly as shown in the Figure 4 below. This corresponds to the elastic phase with minimum magnetic susceptibility. Later on, the domain wall motions increase greatly. Large scale irreversible atomic plane displacements correspond to the partial magnetism phase in magnetization curve. During this phase, the material exhibits the highest magnetic susceptibility. Soon the majority of domains get aligned with the magnetic field. In the last phase, a large amount of energy is needed to rotate the remaining domain magnetization hence the material exhibits a saturating magnetic susceptibility. At high fields, the induction saturates at Bmax.

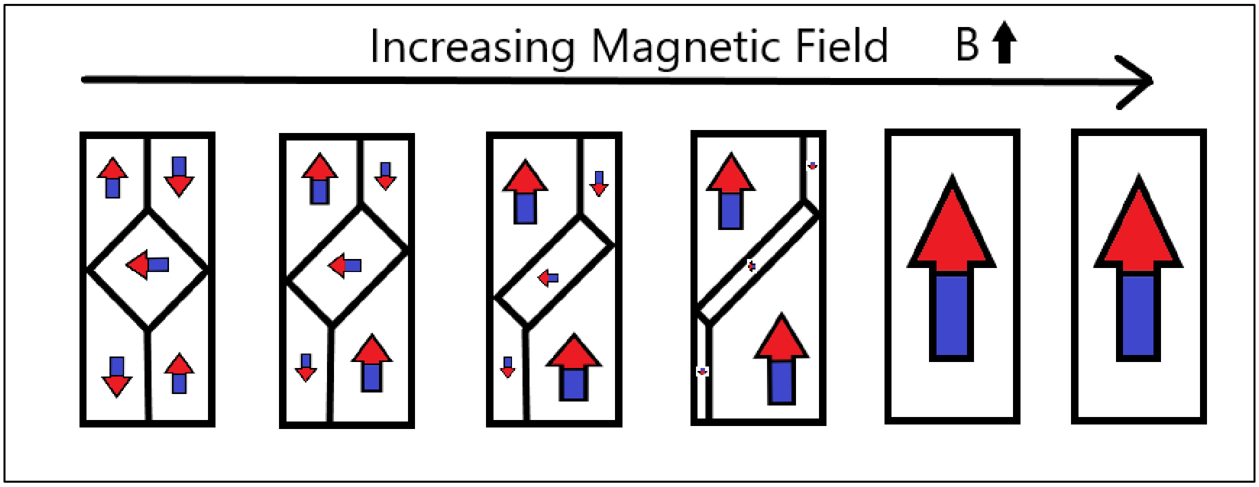

Figure 4: Effect of Applied Field on Magnetic domains

If the applied field of the saturated material is decreased, the magnetic domains start to reverse their direction [27]. Initially, the material exhibits a small magnetic susceptibility. This resistance results because the majority of domains are aligned in the easy direction. The favorable domains had shrunk during the magnetization. Work must be done to expand the favorable domain walls in the reverse direction. As a result, demagnetization does not follow the curve of the original magnetization. When the applied field is decreased further, the magnetic susceptibility of the material starts to increase as more domains start to align in the reverse direction [58].

The induction lags the applied field hence some remnant induction remains when applied field is reduced to zero. In order to demagnetize the material, some extra amount must be applied. This amount is called the coercive force. As the field keeps decreasing, the domains start aligning in the hard direction. Once all the domains have aligned, the material saturates in the reverse direction.

If the material is now magnetized again, the response will contain all the phases described earlier. The induced field will start to increase slowly, followed by a phase of large magnetic susceptibility and end by saturating.

Hysteresis [44-46] can also be experienced in a single domain particle as dictated by the Stoner-Wohlfarth model [58], [48]. In actual anisotropic materials, susceptibility is represented by a tensor [48]. When a ferromagnetic material is magnetized, the susceptibility follows the blue curve χ_m^+. In order to reduce its magnetization to zero, the applied field is decreased. The anisotropic behavior can explain the hysteresis in ferromagnetic materials.

The slope of the B-H curve is called permeability [58]. It is closely related to the magnetic susceptibilityχ_m.

$$\mu = \frac{B}{H} = \mu_0(1 + \chi_m) \tag{1.16}$$

When the material is saturated, the magnetic susceptibility becomes zero. Hence the permeability reduces to μ_0. Besides Magnetic Field Intensity, permeability is strongly dependent on chemical composition, crystal structure, stress, temperature and time after magnetization [58].

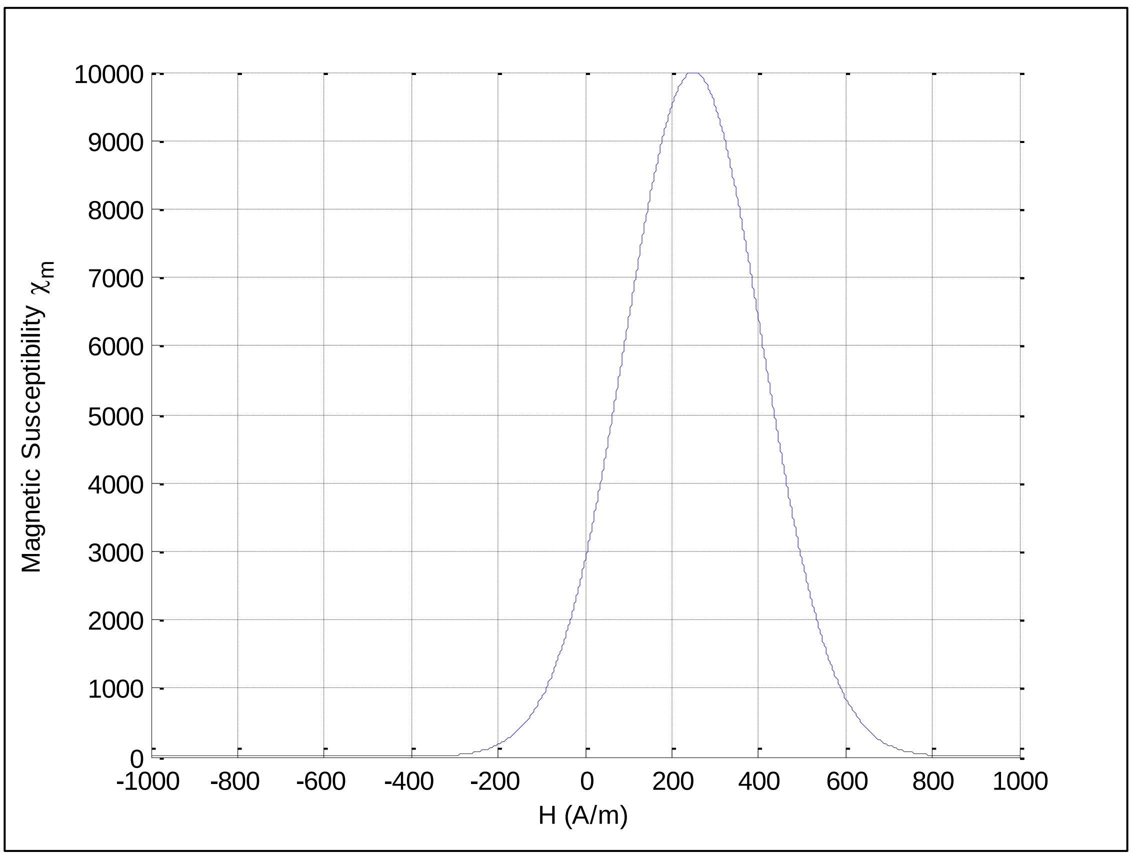

Figure 5: Variation of Magnetic Susceptibility with applied Magnetic Field

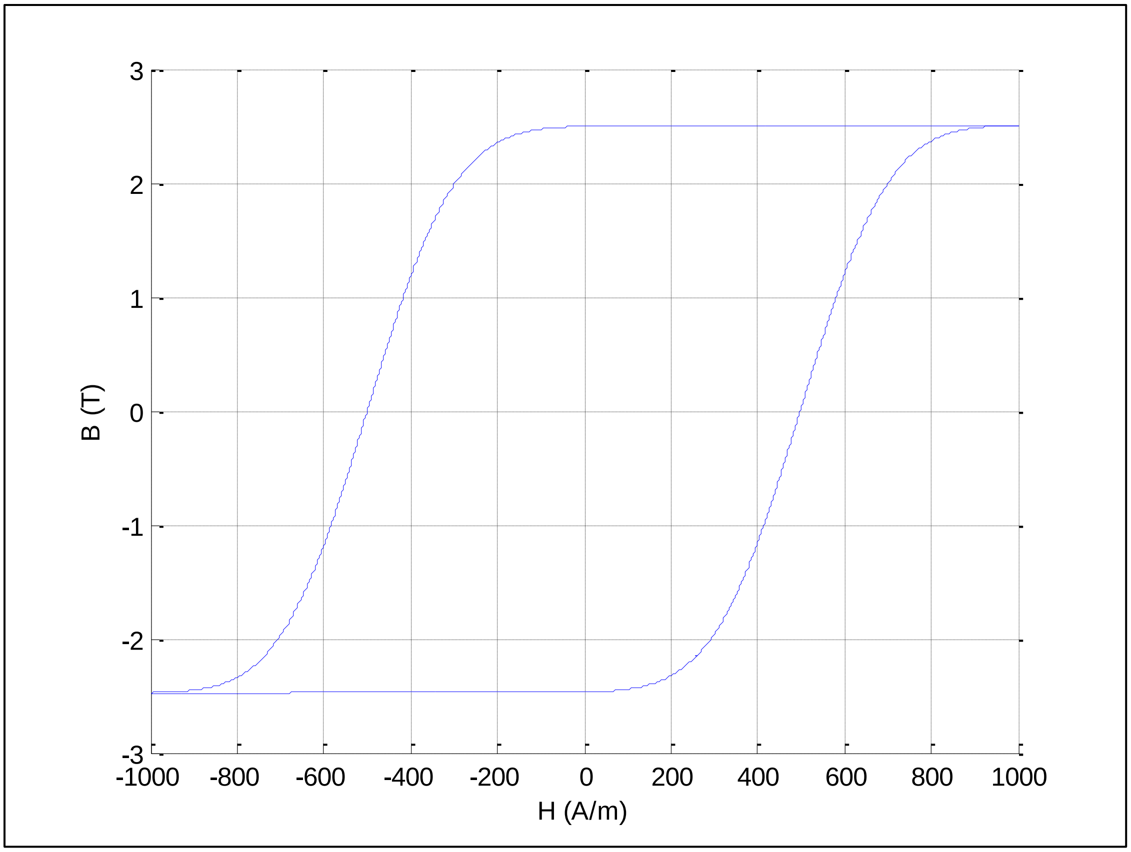

Figure 6: Hysteresis Loop for a nonlinear ferromagnetic material

According to the Curie Weiss Law [6], the susceptibility decreases rapidly when the temperature is increased beyond the Curie temperature T_c, when the ferromagnet becomes a paramagnet.

$$\chi_m \propto \frac{1}{T - T_c} \tag{1.17}$$

According to the Landau mean-field theory for ferromagnetism [62], [6], the Magnetization is related to temperature by the relation:

$$M \propto \sqrt{(T_c - T)} \tag{1.18}$$

The Spin Wave Theory of Felix Bloch [15], [6] states that Magnons carry quantized energy and momentum at T > 0 K. Each Magnon has spin $\hbar$. Their exchange interactions are responsible for the delocalized spin transitions inside the ferromagnet which reduce the magnetization from the maximum value $\lim_{T \to 0\,K} M = M_0$.

The Bloch relation for the Magnetization is given below.

$$M = M_0\left(1 - \sqrt[\frac{3}{2}]{\frac{T}{T_c}}\right) \tag{1.19}$$

The experimental results deviate from the theoretical formulas near the Curie Temperature. From experiments, it has been concluded that ferromagnetic materials have the following exponential relations for susceptibility and Magnetization near Curie temperature [15], [6]:

$$\chi_m \propto \frac{1}{(T - T_c)^{\alpha}} \tag{1.20}$$

$$M \propto (T - T_c)^{\beta} \tag{1.21}$$

1.2. AC Losses in Magnetic Materials

After the brief introduction of Magnetic Transmission in the last section, this section will explain the different mechanisms of AC losses [35-36], [20] in ferromagnetic materials.

The cyclic magnetization of a Magnetic Material causes many energy losses [35-36], [58]. The atomic plane displacements and domain wall rotations cause mechanical losses in the material. Induced voltages cause circulating currents and electrical losses. At microwave frequencies, magnetic resonance and complex permeability [72], [70], [58], [35-36], [12], [16] can cause a significant increase in the losses [35-36]. The various loss mechanisms [20] are:

1. Hysteresis Losses: During the traversal of magnetization loop, energy is lost as heat during irreversible domain changes [58], [35-36], [48], [44-46]. The permeability changes with position, the applied field strength, time after demagnetization (disaccommodation), frequency and temperature [35-36], [58], [20], [44-46]. Fields inside Anisotropic media can be represented by a 3×3 permeability/ magnetic susceptibility tensor [58]:

$$\begin{bmatrix} \boldsymbol{B_x} \\ \boldsymbol{B_y} \\ \boldsymbol{B_z} \end{bmatrix} = \begin{bmatrix} \mu_{xx} & \mu_{xy} & \mu_{xz} \\ \mu_{yx} & \mu_{yy} & \mu_{yz} \\ \mu_{zx} & \mu_{zy} & \mu_{zz} \end{bmatrix} \begin{bmatrix} \boldsymbol{H_x} \\ \boldsymbol{H_y} \\ \boldsymbol{H_z} \end{bmatrix} \tag{1.22}$$

   This hysteresis loss [44-46] is equal to the area inside the DC hysteresis loop [48], [58]:

$$W_H = \int \boldsymbol{B}\, \boldsymbol{dH} \tag{1.23}$$

   Hysteresis loss increases with the applied field strength and frequency [58], [20], [44-46]. The empirical formula for Hysteresis Loss Density [48] is:

$$P_H \propto B_{max}^n f \tag{1.24}$$

2. Eddy Current Losses: Ferromagnetic materials are semiconductors with resistivity (ρ) ranging from 0.1Ωm to greater than 1MΩm. The associated permittivity causes dielectric losses [50], [35-36]. Whenever a changing electromagnetic field is impressed induced voltages are developed in the material [55]. These generate circulating eddy currents in the material and produce Ohmic losses [20], [35-36], [58].

   These losses can be reduced by using thin laminated magnetic films or magnetic grains for manufacturing. The Eddy current losses [35-36], [20] depend on the frequency (f), the applied field intensity (B_{max}) and the resistivity (ρ) or conductivity ($\sigma = \frac{1}{\rho}$) [58]. The empirical formula for Eddy Current Loss Density is:

$$P_e \propto \frac{(B_{max} f)^2}{\rho} \tag{1.25}$$

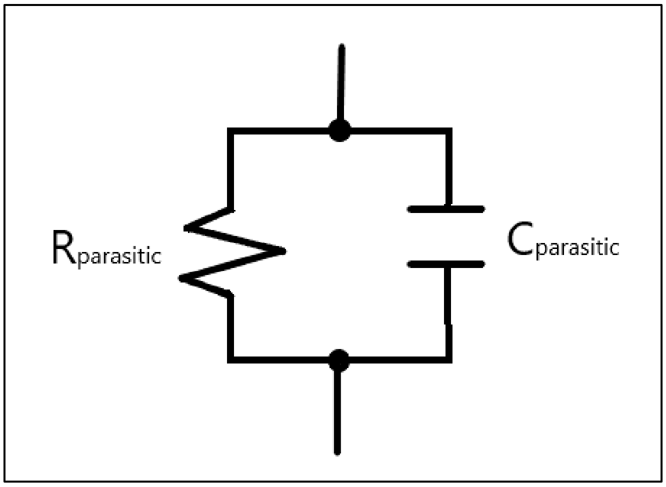

Figure 7: Dielectric circuit model for Ferromagnetic material

The Eddy Current Losses [20] can be enhanced at high frequencies due to dimensional resonance [12], [13], [35-36]. If a dimension of the magnetic material is equal to a quarter multiple of the electromagnetic wavelength, a standing wave can develop inside it. Under this condition, the in-phase flux cancels the anti-phase flux so the observed permittivity and permeability drops to zero [55]. The resulting Eddy Current loss shows a peak during resonance [58], [12]. We can represent complex permittivity and complex permeability [72], [70] as:

$$\varepsilon = \varepsilon_0(\varepsilon' - j(\varepsilon'' + \frac{\sigma}{\omega})) \tag{1.26}$$

$$\mu = \mu_0(\mu' - j\mu'') \tag{1.27}$$

The real part is responsible for the displacement current, whereas the imaginary part contributes to the conduction current. During Dimensional Resonance [12], the electric conductance of the magnetic material increases greatly. Hence the material acts like an electric conductor with a very low resistivity [58]. Although Magnetic conduction currents do not exist, Magnetic displacement currents can flow inside a magnetic material [13]. When the real permeability drops, the magnetic displacement currents are restricted and the magnetic susceptibility falls. This causes failure of the magnetic system. The associated loss tangents are:

$$tan\delta_d = \frac{\varepsilon''}{\varepsilon'} \tag{1.28}$$

$$tan\delta_b = \frac{\mu''}{\mu'} \tag{1.29}$$

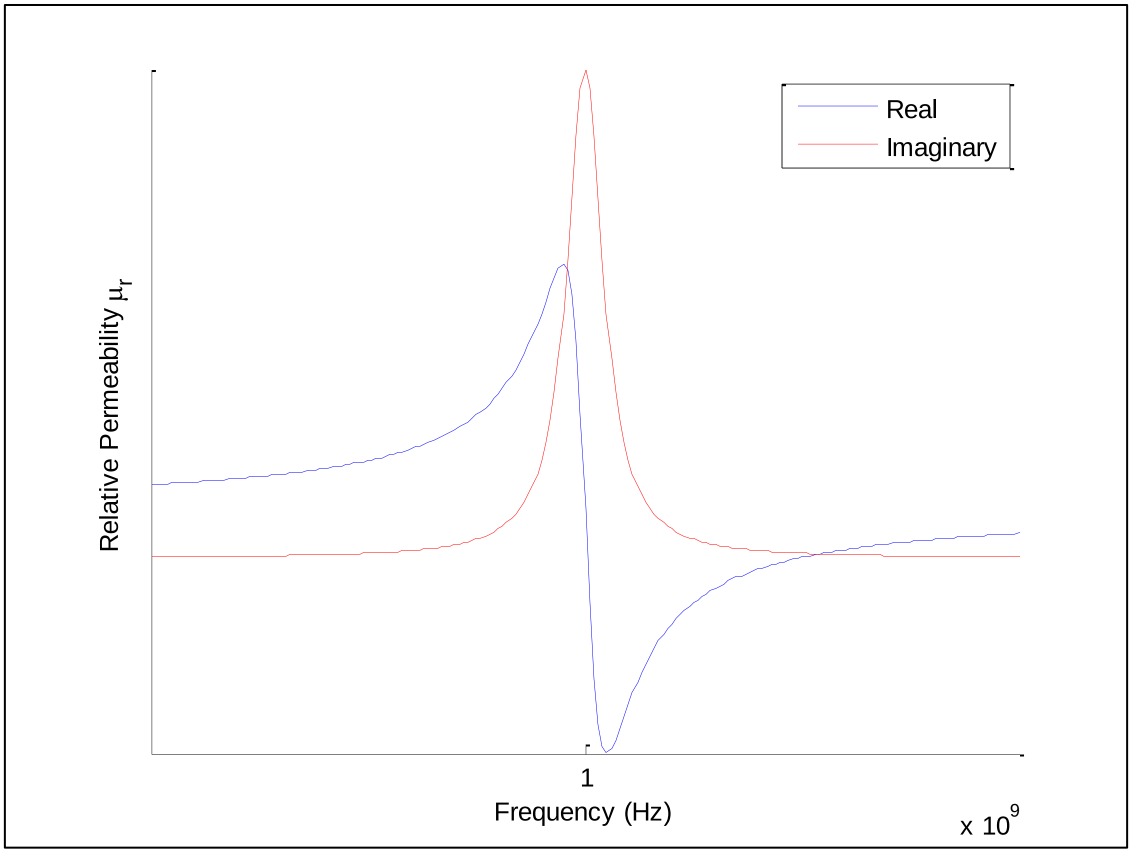

Figure 8: Frequency dependance of Permeability

3. Residual Losses: Besides hysteresis loss [48], [44-46] and eddy current loss, several processes can contribute to losses [35-36], [13], [20] when the eddy currents are negligible and the applied flux density is extremely small. These stray losses [51] are independent of the flux density but they increase with frequency [58]. The associated loss tangent is $tan\delta_r$.

The total loss tangent due to hysteresis loss [48], [44-46], eddy current loss and residual loss [51], [20] is expressed as:

$$tan\delta = tan\delta_H + tan\delta_E + tan\delta_r \tag{1.30}$$

In conclusion, the losses due to hysteresis [48], [44-46], Eddy currents [35-36], Piezomagnetism [35-36], Magnetoresistance [66], Magnetostriction [35-36] and other residual loss mechanisms [51], [20] can be expressed as heat losses across an effective resistance or conductance.

1.3. Literature Review

This section presents a literature review of Magnetic Transmission Lines [22] - [26] in context of the recent research on Giant Magnetoresistance [66], Magnetic Capacitance [74], [73], Magnetic Memory [41], Spintronic and Nanomagnetic Logic Devices [63], [42], [38], [34], [5], [15], [19], [30].

Faria [22] - [26] presented a Time and Frequency domain theory of multi-wire magnetic transmission lines based on the matrix theory of multi-conductor electric transmission lines. For magnetic transmission lines, transverse impedance and the longitudinal admittance determine the propagation constants for the wave modes [22] - [26]. Simulations showed that they exhibit super-luminal phase velocity and almost zero attenuation dispersion [72], [16]. He also established a relationship between voltages and currents at the multi-conductor transmission line ports by employing the transmission matrix techniques. Mathematical models were developed for studying the Frequency Domain Behavior of non-uniform Magnetic Transmission Lines [22] - [26]. Solutions to Electromagnetic equations were presented in the form of a superposition of natural modes of propagation [55]. The Magnetic Transmission Line exhibited the behavior of a high pass filter, blocking all DC signals. DC signals produce the most severe transients in Electric Transmission Lines [9]; which behave like a low pass filter. Moreover, he developed a model for ideal transformers using magnetic transmission line theory [22] - [26], [10].

Antonini [4] presented an in-depth analysis of meta-material transmission lines [10]. The ladder network structure of the transmission line was used to obtain dominant zeros and poles. This lead to a rational form of the two port network transfer function. The rational form of the transfer functions provided an efficient time-domain macro model; which accurately captured the physics of composite meta-material transmission lines [4], [10].

Caloz and Itoh [11] also presented non-linear [40] electromagnetic meta-material Transmission Lines [10] focusing on their complex permittivity and permeability [72]. They used the transmission matrix method to formulate equations for the dispersive [72], [16], distributed non-linear system [40], [8]. These results are very useful in understanding the complex dispersive [72] and radiative nature of Magnetic Transmission Lines [22] - [26].

Edwards and Steer [15] compared copper, ferrite meta-conductor and magnetized permalloy meta-conductor based coplanar waveguides. Magnetized ferrite layer provided some skin effect suppression compared to copper waveguide; however, permalloy provided the most uniform current profile. Some applications of Ferrite materials are high frequency phase shifters, circulators and isolators [53], [33], [27]. Phase shifters used in test and measurement systems can be controlled using the bias magnetic field. Electronically controlled phase shifters are used in phase array antennas for steering antenna beam in space. Microwave circulators [58] use ferrites to separate received and transmitted waves in radar systems [33], [16], [53]. Magnetized films also act as Radio Frequency selective limiters. Microwave Ferrite isolators are used for unidirectional transmission in plasma systems [49], [16], [27]. Their blocking capability protects precious microwave sources [54].

Neuber et al. [16], [17] presented gyromagnetic Non Linear Transmission Lines [62], [61], [71] constructed out of nickel-zinc (NiZn), magnesium-zinc (MgZn), manganese-zinc (MnZn) and yttrium iron garnet (YIG) ferrites [58], [53], [33], [27]. Biased Anisotropic Magnetic Transmission lines [22] - [26] functioned as microwave sources [54] because of Gyromagnetic Precession [71], [62], [61], [54]. Their performance strongly depended on Magnetic Saturation experienced at high biasing Field Strengths.

Paul [56] has presented Time domain and frequency domain Lumped Inductive-Capacitive Coupling Circuits [39], [18] for cross talk between different Electric Transmission Line Conductors. The generator-receptor model is well suited for studying Radiated/ Conducted Emissions and Susceptibility. Such models must be developed for Magnetic Transmission Lines [22] - [26] as well; to study their Electromagnetic Interference and Electromagnetic Compatibility [55].

Paul, Whites and Nasar [55] have presented a step-by-step method to solve the Maxwell's equations in sinusoidal steady state; due to a given current distribution in a homogeneous, linear, isotropic medium. First, magnetic potential field is calculated at all desired points in space, due to the current distribution. The curl of the magnetic potential field is used to obtain the magnetic field. The Divergence of the magnetic potential field is used to obtain the scalar Electric Potential. In turn, the magnetic potential field and the gradient of the electric potential are used to derive the Electric field. The procedure is much more complicated for waveguides in inhomogeneous, anisotropic, and non-linear media [40], [8]; hence, numerical methods [21] are suggested where a closed form solution is not possible.

Er-Ping [21] has discussed a wide range of standard time and frequency domain Computational Electromagnetics [14], [12], [21] Methodologies. Time Domain Methods [39] include Analytical Methods, Finite Difference Methods (FDTD) [64], [43], [9], Finite Integral Methods (FIT), Finite Volume Methods (FVTD), Fast Multipole Method (FMM), Partial Element Equivalent Circuit Method (PEEC), Transmission Line Method (TLM) [43] etc. Frequency Domain Methods include Method of Moments (MoM), Finite Element Method (FEM), Geometric Theory of Diffraction (GTD), Physical Theory of Diffraction (PTD) etc. He compared Finite Difference Methods, Method of Moments and Finite Element Method, in respect of Principle, geometry materials, Meshing, Matrix Equation and Boundary Treatment. He gave a list of commercially available simulators along with some common applications like high-speed electronics [58], photonics [12], [15], microwave circuits [16], integrated circuits and Antennas. The Finite Difference Method can obtain response over a broad band of frequencies for many non-linear [40], [8] and inhomogeneous media without using matrix equations [9], [43]. This method is well suited for simulation of dispersive [72], [16], non-uniform Magnetic Transmission Lines [22] - [26].

This chapter discussed the nature of Magnetic materials and the transmission of magnetic information using magnetic dipoles and Bulk Magnetization. The AC losses [20] of magnetic materials include hysteresis losses [48], [44-46], eddy current losses and residual losses [51] due to complex permeability and permittivity [35-36], [72], [70]. A literature review of Magnetic Transmission Lines [22] - [26] in context of recent research on Ferromagnetic Modeling and Simulation [18].

Chapter 2 will discuss the propagation of electromagnetic waves in anisotropic, inhomogeneous, dispersive [72], [44-46], [16] Ferromagnetic materials as dictated by the Maxwell's Laws [55].

Chapter 3 presents three different models for Magnetic Elements: Reluctance Model [11], Permeance-Capacitance Model [73], [44-46], [32], [2], [3] and the Magnetic Transmission Line Model [22] - [26].

Chapter 4 is dedicated to computational electrodynamics [21] i.e. the low frequency and high frequency methods for solving Maxwell's equations [55]. An overview of Finite Difference Time Domain method [68] - [69], [64], [43], [39], [9] is presented which solves partial differential equation using leapfrog method. The MEEP [52] simulator uses this method for evolving electromagnetic fields in anisotropic, inhomogeneous, dispersive [72], [16] Ferromagnetic materials.

2. Wave Propagation in Magnetic Materials

This chapter will discuss the propagation of electromagnetic waves in anisotropic, inhomogeneous, dispersive [72], [16] Ferromagnetic materials as dictated by the Maxwell's equations [55]. Section 2.1 discusses Plane wave propagation in ferromagnetic materials. Section 2.2 is devoted to the power flow analysis of electromagnetic waves travelling through magnetic materials.

2.1. Plane Wave Propagation

Ideal Magnetic Transmission Lines [22] - [26] can be modeled as linear, isotropic, homogeneous media which follow Maxwell's equations [55]:

1. Ampere's Law [55]

$$\nabla \times \boldsymbol{H} = \sigma \boldsymbol{E} + \frac{d\boldsymbol{D}}{dt} \tag{2.1}$$

2. Faraday's Law [55]

$$\nabla \times \boldsymbol{E} = -\mu_0 \frac{d\boldsymbol{B}}{dt} \tag{2.2}$$

3. Gauss' Laws

$$\nabla . \boldsymbol{D} = \rho_v \tag{2.3}$$
$$\nabla . \boldsymbol{B} = 0 \tag{2.4}$$

subject to the following boundary conditions [55]:

1. The perpendicular components of **B** and **D** follow these conditions:

$$B_{\perp 1} = B_{\perp 2} \; and \; D_{\perp 1} - D_{\perp 2} = \rho_s \tag{2.5}$$

2. The parallel components of **H** and **E** follow these conditions:

$$H_{\parallel 1} - H_{\parallel 2} = J_s \; and \; E_{\parallel 1} = E_{\parallel 2} \tag{2.6}$$

The solution is given by the Helmholtz Equations [55]:

$$\nabla \times \nabla \times \boldsymbol{E} = -\frac{\partial(\nabla \times \boldsymbol{B})}{\partial t} = \mu\sigma \frac{\partial \boldsymbol{E}}{\partial t} + \mu\varepsilon \frac{\partial^2 \boldsymbol{E}}{\partial t^2} \tag{2.7}$$

$$\nabla \times \nabla \times \boldsymbol{H} = \sigma(\nabla \times \boldsymbol{E}) + \frac{\partial(\nabla \times \boldsymbol{D})}{\partial t} = \mu\sigma \frac{\partial \boldsymbol{H}}{\partial t} + \mu\varepsilon \frac{\partial^2 \boldsymbol{H}}{\partial t^2} \tag{2.8}$$

For sinusoidal steady state:

$$\boldsymbol{\nabla}^2 \boldsymbol{E} = \gamma^2 \boldsymbol{E} \tag{2.9}$$

$$\nabla^2 \boldsymbol{H} = \gamma^2 \boldsymbol{H} \tag{2.10}$$

$$\gamma = \sqrt{j\omega\mu\sigma - \omega^2\mu\varepsilon} = \alpha + j\beta \tag{2.11}$$

The propagation constant (γ) dictates the wave propagation in the medium. The attenuation constant (α) represents the loss or attenuation of fields. The skin depth (δ) is defined as the penetration measured from the surface at which the amplitude reduces by a factor of 1/e:

$$\delta = \frac{1}{\alpha} = \sqrt{\frac{2}{\omega\mu\sigma}} \tag{2.12}$$

The phase constant β dictates the phase velocity (u) and wavelength (λ):

$$u = \frac{\omega}{\beta} \tag{2.13}$$

$$\lambda = \frac{2\pi}{\beta} \tag{2.14}$$

The ratio of matching Electric Field Intensity $\boldsymbol{E}^{+}/\boldsymbol{E}^{-}$ and Magnetic Field Intensity $\boldsymbol{H}^{+}/\boldsymbol{H}^{-}$ determines the intrinsic impedance of the material:

$$\eta = \frac{j\omega\mu}{\gamma} = \sqrt{\frac{j\omega\mu}{\sigma_e + j\omega\varepsilon}} \tag{2.15}$$

For lossless magnetic materials with very small σ_e,

$$\beta \approx \beta_o\sqrt{\mu_r\varepsilon_r} \tag{2.16}$$

$$u \approx \frac{u_o}{\sqrt{\mu_r\varepsilon_r}} \tag{2.17}$$

$$\lambda \approx \frac{\lambda_o}{\sqrt{\mu_r\varepsilon_r}} \tag{2.18}$$

$$\eta \approx \eta_0\sqrt{\frac{\mu_r}{\varepsilon_r}} \tag{2.19}$$

where β_o, u_o, $\lambda_o$and $\eta_0$represent the free space phase constant, phase velocity wavelength and intrinsic impedance respectively.

Considering plane wave propagation in the z direction, the solution is:

$$E_x(z) = E_m^{+}e^{-\alpha z - j\beta z + j\theta^{+}} + E_m^{-}e^{\alpha z + j\beta z + j\theta^{-}} \tag{2.20}$$

$$H_y(z) = \frac{E_m^{+}}{\eta}e^{-\alpha z - j\beta z + j\theta^{+} - j\theta_\eta} - \frac{E_m^{-}}{\eta}e^{\alpha z + j\beta z + j\theta^{-} - j\theta_\eta} \tag{2.21}$$

2.2. Power Flow Analysis

The power flow density of an electromagnetic wave is given by the Poynting vector **S**. It has the units of W/m^2. The Poynting flux is indicative of the amount of power flowing across a surface:

$$\oint \boldsymbol{S}.\hat{\boldsymbol{n}}\, dS = \int (\boldsymbol{E} \times \boldsymbol{H}) dS \tag{2.22}$$

$$= \boldsymbol{\nabla}.(\boldsymbol{E} \times \boldsymbol{H}) \tag{2.23}$$

The expression can be expanded using the following formula:

$$\boldsymbol{\nabla}.(\boldsymbol{E} \times \boldsymbol{H}) = -\mathbf{E}.(\boldsymbol{\nabla} \times \boldsymbol{H}) + \mathbf{H}.(\boldsymbol{\nabla} \times \boldsymbol{E}) \tag{2.24}$$

$$= -\mathbf{E}.\left(\boldsymbol{J} + \frac{\partial \boldsymbol{D}}{\partial t}\right) + \mathbf{H}.\left(-\frac{\partial \boldsymbol{B}}{\partial t}\right) \tag{2.25}$$

The flow of Poynting flux can be separated into the Ohmic Power dissipation, Electric Power flow and Magnetic Power flow:

$$-\oint \boldsymbol{S} dS = \frac{1}{2}\int \boldsymbol{E}.\boldsymbol{J}\, dV + \int \boldsymbol{E}.\frac{\partial \boldsymbol{D}}{\partial t}\, dV + \int \boldsymbol{H}.\frac{\partial \boldsymbol{B}}{\partial t}\, dV \tag{2.26}$$

From these expressions, it is clear that the Electric Energy and Magnetic Energy of a system is:

$$W_e = \int \boldsymbol{D}.\boldsymbol{E}\, dV \tag{2.27}$$

$$W_m = \int \boldsymbol{B}.\boldsymbol{H}\, dV \tag{2.28}$$

The average power transported per unit area is the Intensity of the Electromagnetic Wave:

$$\boldsymbol{I} = < \boldsymbol{S} > \tag{2.29}$$

Electromagnetic Waves also carry momentum and the momentum density stored in the fields is

$$\boldsymbol{g} = \frac{1}{c^2}\boldsymbol{S} \tag{2.30}$$

The Momentum transferred to a surface results in a radiation pressure

$$\boldsymbol{P} = \frac{F}{A} = \frac{1}{A}\frac{\Delta p}{\Delta t} = \frac{1}{A}\frac{< \boldsymbol{g} > A\, c\, \Delta t}{\Delta t} = < \boldsymbol{g} > A\, c \tag{2.31}$$

3. Magnetic Circuit Modeling

In this chapter, three different Magnetic circuit models will be presented: The Reluctance Model [11], The Permeance-Capacitance Model [73], [44-46], [32], [2], [3] and The Magnetic Transmission Line Model [22] - [26]. It is understood that magnetic monopoles do not exist and Magnetic conduction current cannot flow. Any reference to the flow of Magnetic displacement current is meant to indicate the flow of Magnetic Displacement Current i.e. the rate of change of Magnetic Flux.

The Reluctance Model [11] is the oldest and most popular model, even though it is not a power invariant model [28]. It only has one component called the Magnetic Reluctance which resists the flow of Magnetic Flux [11]. The model does not have energy storage elements.

The Permeance-Capacitance Model [73], [44-46], [32], [28], [2], [3] overcomes the weaknesses of the Reluctance Model [11] by considering the rate of change of Magnetic Flux as the Magnetic displacement current. It is a power invariant model [28] because it correctly encompasses the transformation of Magnetic and Electric Energy [32]. This model has the shortcoming that it does not incorporate Electric Energy Storage in a Magnetic material [35-36], [20].

The Magnetic Transmission Line [22] - [26] model improves the Permeance-Capacitance Model [73], [44-46], [32], [2], [3], [28] by including a component for Electric Energy Storage and a component for magnetization, polarization and conduction losses [35-36], [20].

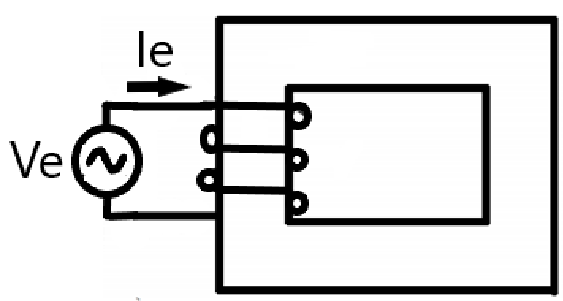

Figure 9: A Magnetic core excited by an electric current

3.1. Reluctance Model

This section discusses the age old Reluctance model [11] for magnetic elements. The model contains a single element for representing the relationship between magnetic voltage and magnetic flux.

H. A. Rowland's Law (1873) [55] is the counterpart of G. Ohm's Law (1827) for Magnetic circuits [11]. Complex Reluctance Model defines Magnetic reluctance as the ratio of sinusoidal Magnetomotive Force and sinusoidal Magnetic Flux [11].

$$\boldsymbol{\mathcal{R}}_m = \frac{\boldsymbol{\mathcal{F}}_m}{\boldsymbol{\phi}_m} = \frac{\oint \boldsymbol{H}.dl}{\int \boldsymbol{B}.dS} = |\boldsymbol{\mathcal{R}}_m|e^{j\emptyset} \tag{3.1}$$

Lossy Complex Magnetic Reluctance is non-linear and varies with the magnetic field. It resists both Magnetic flux and changes in Magnetic flux [11].

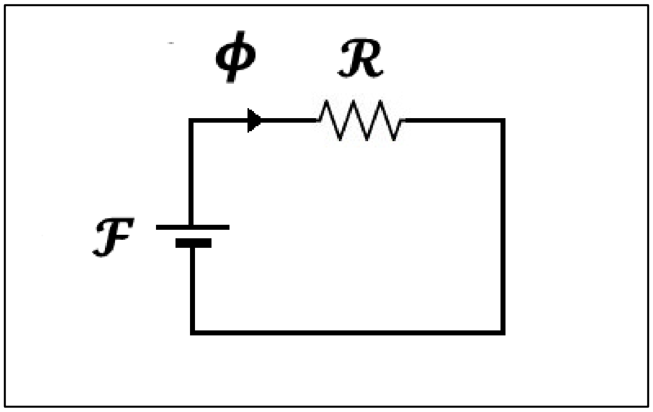

Figure 10: Reluctance model for Magnetic Core

In 1969, R. W. Buntenbach proved that the Reluctance model [11], [55] is not power invariant [28]. Reluctance Power Loss cannot be calculated using Joule Heating Law (1842) analogy due to dimensional inconsistency [28]:

$$[P_e] = [I_e^2][R_e] = Ampere.Volt \tag{3.2}$$

$$but$$

$$[P_m] \neq [\boldsymbol{\phi}_m^2][|\boldsymbol{\mathcal{R}}_m|] = Volt.Second.Ampere \tag{3.3}$$

Hence this is not an accurate model for Power and Energy Flow.

3.1.1. Application

This section presents the reluctance model for a Compounded DC Generator [11] with both a series and a shunt field winding. The series field inductance L_S has N_{SE} turns. The series field winding resistance is represented by R_S. The shunt field winding inductance L_F has N_F turns. The shunt field winding resistance is represented by R_F. The armature winding resistance is represented by R_A.

The Electric circuit equations are

$$V_T = E_A - I_A(R_A + R_S) \tag{3.4}$$

$$I_L + I_F = I_A \tag{3.5}$$

$$I_F = \frac{V_T}{R_F} \tag{3.6}$$

The magnetic circuit equations are

$$\mathcal{F}_{net} = \mathcal{F}_F \pm \mathcal{F}_{SE} - \mathcal{F}_{AR} \tag{3.7}$$

$$N_F I_F^* = N_F I_F \pm N_{SE} I_A - \mathcal{F}_{AR} \tag{3.8}$$

The generated electric voltage is related to the Magnetic Flux and rotor speed by the following equation

$$E_A = k\phi\omega_m \tag{3.9}$$

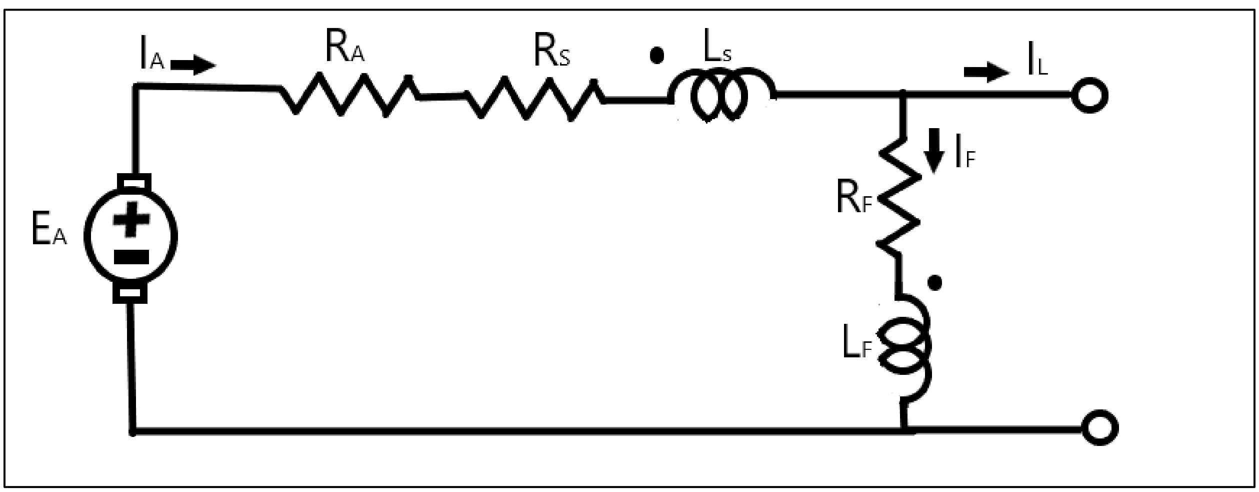

Figure 11: Model for Cumulatively Compounded DC Motor

Ferromagnetic materials are non-linear [48], [8], [39] as their permeability varies with the strength of applied field intensity. At high magnetic field intensity, the material saturates, limiting further increase of Magnetic Flux [48]. Hence, the susceptibility decreases rapidly.

A Compounded DC Generator was simulated in Simulink as shown in Figure 12. The generator parameters were the following: R_A=0.19 Ω, R_S=0.02 Ω, R_F=20-50Ω, N_F=1000 turns, N_S=20 turns and rated speed=1800 rpm.

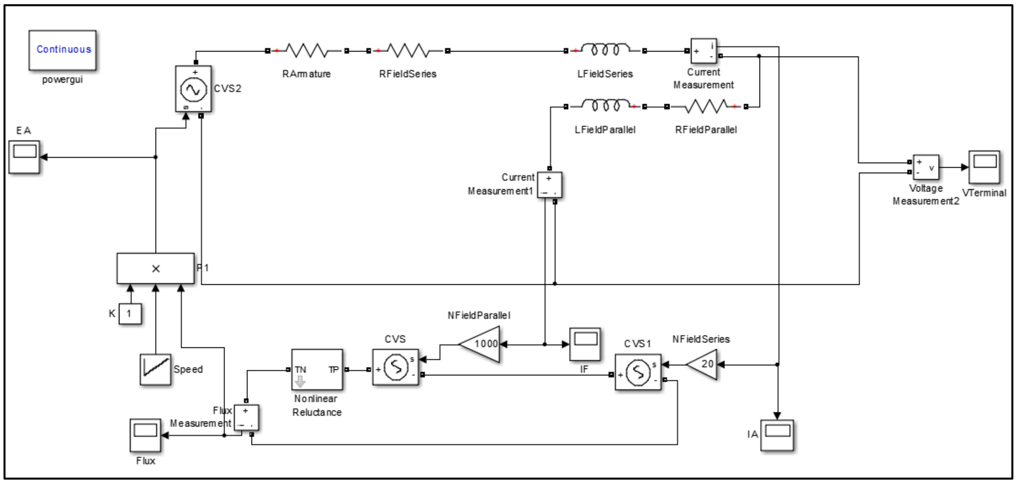

Figure 12: Simulink Model for Cumulatively Compounded DC Generator

The Reluctance Model preserves the integrity of the machine's geometry [11]. It decouples the electrical system from the magnetic system. The magnetic paths in the core are represented using an equivalent nonlinear reluctance element shown in Figure 13.

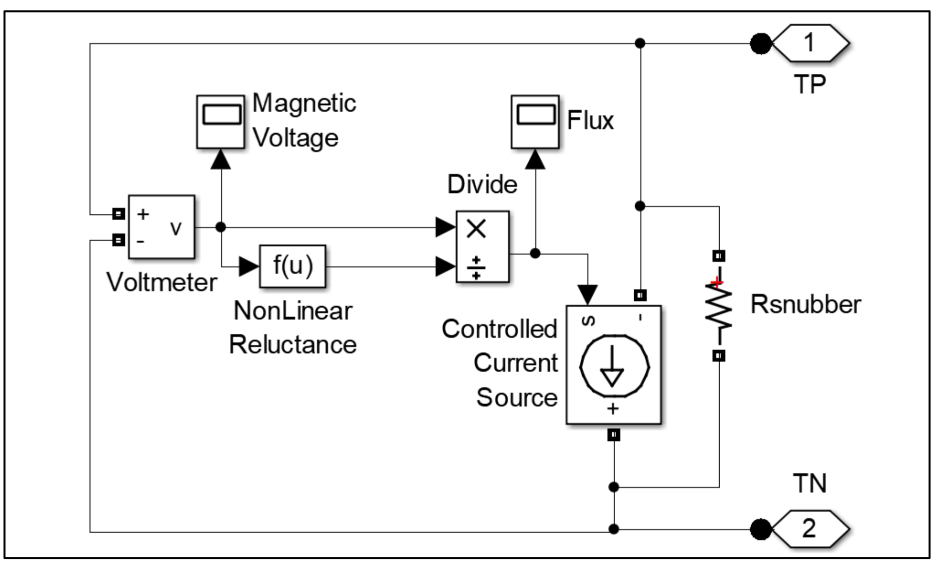

Figure 13: Simulink Model for Nonlinear Permeance

The rotor mechanical speed was increased from 500 to 2000 rpm in steps of 500rpm as shown in Figure 14. The Field currents, generated Magnetomotive force, Electromotive force and Terminal voltage are also shown. Clearly, the results do not increase linearly with speed.

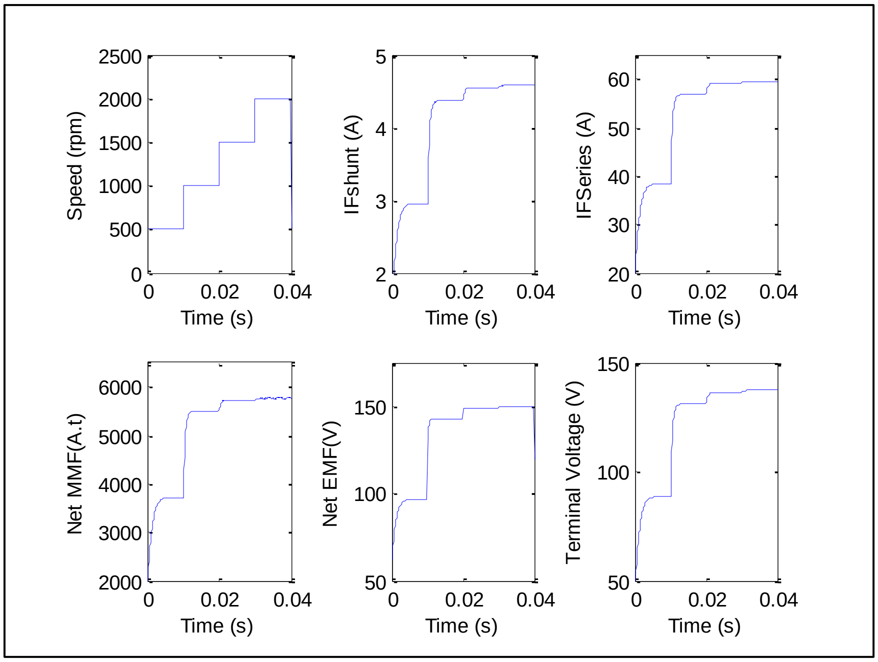

Figure 14: Evolution of Field Currents, Net MMF, Generated EMF and Terminal Voltage upon change of Rotor speed

The nonlinear Terminal voltage versus rotor speed curve is shown in Figure 15.

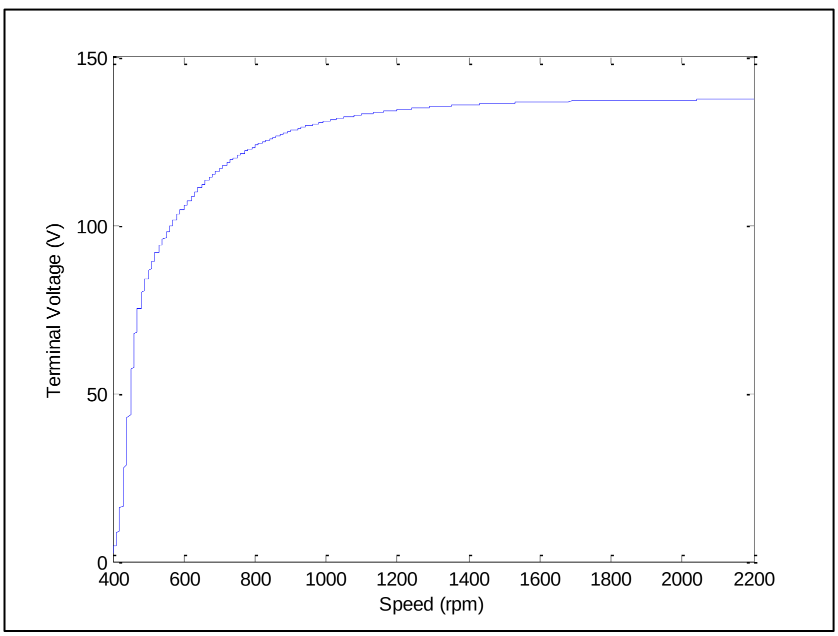

Figure 15: Variation of Terminal Voltage with rotor speed

Clearly, the Reluctance model is only suitable for steady state simulations of machines if the reluctance profile of the magnetic core and the voltage constant is already known.

3.2. Permeance-Capacitance Model

This section presents the power invariant Permeance-Capacitance model [73], [44-46], [32], [28], [2], [3] for a Transformer based on the gyrator theory. The model is valuable for modeling nonlinear magnetic materials with hysteresis losses.

In 1948, B. Tellegen's Gyrator theory was devised to describe power invariant transformation of magnetic and electric quantities in a transformer [32], [3], [28]. The dual effort and flow quantities are related by the gyration constant (N). According to M. Faraday's Law (1831) [55], Electric Voltage is responsible for producing Magnetic Displacement Current which is defined as the rate of change of magnetic flux.

$$V_e = -N\frac{d\phi_m}{dt} \qquad [Volt] \tag{3.10}$$

$$\oint \boldsymbol{E}.dl = -\frac{d}{dt}\int \boldsymbol{B}.dS$$

$$= -\mu_0\frac{d}{dt}\int \boldsymbol{H}.dS - \mu_0\frac{d}{dt}\int \boldsymbol{M}.dS \tag{3.11}$$

Magnetic Displacement Current is the rate of change of Magnetic Flux which results from the polarization of Magnetic Dipoles. For a magnetic core, the magnetic displacement current and Magnetomotive Force are given by:

$$I_{m,disp} = \frac{d\phi_m}{dt} = -\frac{1}{N}V_e \qquad [Volt] \tag{3.12}$$

According to A. Ampere's Law (1861) [55], Magnetic Voltage is responsible for producing Electric Conduction Current [55].

$$V_m = \mathcal{F}_m = NI_e \qquad [Ampere] \tag{3.13}$$

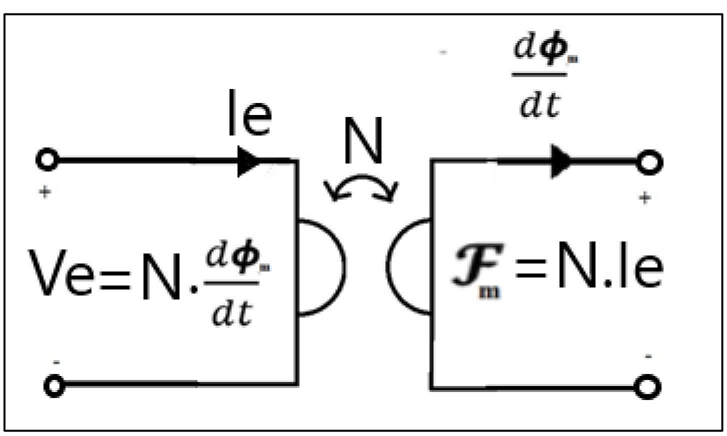

Figure 16: Gyrator Model for power invariant transformation of Electric and Magnetic quantities

R. W. Buntenbach proposed Power Invariant Permeance-Capacitance Model (1969) [73], [44-46], [32], [28], [2], [3] to replace Reluctance Model.

Magnetic Permeance [44-46], [32], [2], [3] is defined as a magnetic capacitor which stores magnetic flux measured in Volt-seconds.

$$\Phi_{Pm}(t) = P_m v_{Pm}(t) \qquad [Volt.s] \tag{3.14}$$

It resists changes in Magnetic voltage.

$$i_{Pmdisp}(t) = P_m \frac{dv_{Pm}(t)}{dt} \quad [Volt] \tag{3.15}$$

This Permeance is measured in units of Henry. It is closely related to Magnetic Reluctance and Magnetic Inductance of the core.

$$P_m = \frac{1}{\boldsymbol{\mathcal{R}}_m} = \frac{L_m}{N^2} = \mu\frac{A}{l} \ [Henry] \tag{3.16}$$

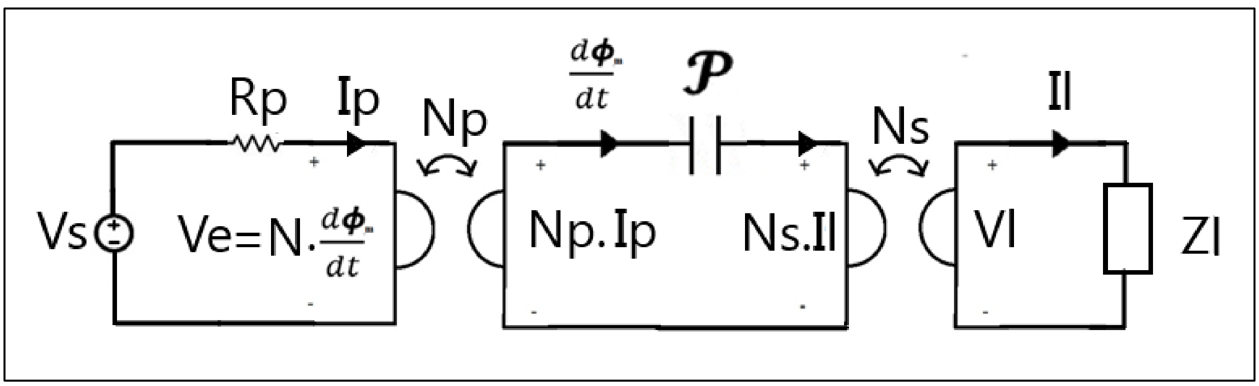

Figure 17: Permeance-Capacitance model for Transformer

3.2.1.Application

This section presents a Permeance-Capacitance Model [73], [44-46], [32], [2], [3] for a full bridge Isolated Buck Converter. The electrical circuit is shown in Figure 18.

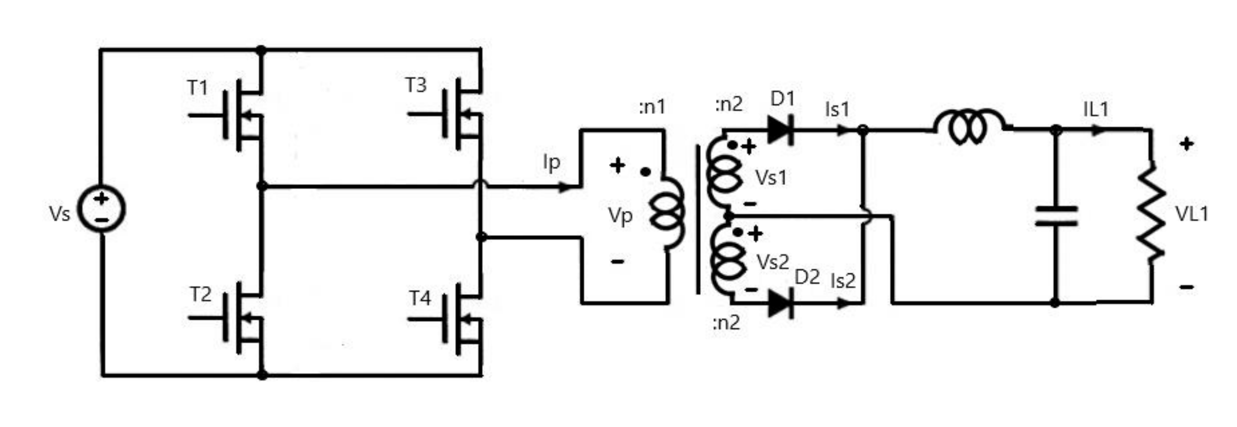

Figure 18: Electrical circuit for Full Bridge Isolated Buck Converter

The switching table for the switches and diodes is given below.

	Transistors				Diodes	
Time Interval	T1	T2	T3	T4	D1	D2
$0 < t \leq DT_s$	ON	OFF	OFF	ON	ON	OFF
$DT_s < t \leq T_s$	OFF	ON	OFF	ON	ON	ON
$T_s < t \leq (1+D)T_s$	OFF	ON	ON	OFF	OFF	ON
$(1+D)T_s < t \leq 2T_s$	ON	OFF	ON	OFF	ON	ON

The design parameters are given in the table below

Parameter	Symbol	Value
Source Voltage	V_s	160 V
Load 1 Voltage	V_{L1}	5 V $\pm$ 5%
Load 1 Current	I_{L1}	100 A $\pm$ 5%
Core cross-sectional area	A_c	2.26cm^2
Core Magnetic Path Length	l_m	9.58 cm
Peak Flux Density	ΔB	0.08 T
Core relative Permeability	μ	3500
Core Resistivity	ρ	0.02 Ωm
Switching Frequency	F_s	150 kHz
Duty Cycle	D	0.75

The Design Procedure had the following steps:

1. Applied Primary winding flux

$$\lambda_p = \int_0^{Ts} Vp(t)\,dt = DT_sV_s = (0.75)\left(\frac{1}{150\;kHz}\right)(160\;V) = 8\times10^{-4}\;V.s \tag{3.17}$$

2. Turns of Primary winding

$$n_1 = \frac{\lambda_p}{2\Delta BA_c} = \frac{(8\times10^{-4}\;V.s)}{2(0.08\;T)(2.26\times10^{-4}m^2)} \approx 22 \tag{3.18}$$

3. Turns of Secondary windings

$$n_2 = \frac{V_{L1}+V_{Diode,on}}{Vs}n_1 = \frac{(5+2)\times22}{160} \approx 1 \tag{3.19}$$

4. Core Permeance

$$P_{m,max} = \frac{\mu A_c}{l_m} = \frac{(3500\times4\pi\times10^{-7})(2.26\times10^{-4}m^2)}{(9.58\times10^{-2}m)} = 10.3\;\mu H \tag{3.20}$$

$$P_{m,min} = \frac{\mu_o A_c}{l_m} = \frac{(4\pi\times10^{-7})(2.26\times10^{-4}m^2)}{(9.58\times10^{-2}m)} = 2.94\;nH \tag{3.21}$$

5. Core Resistance

$$R_c = \frac{\rho l_m}{A_c} = \frac{(0.02\;\Omega\mathrm{m})(9.58\times10^{-2}m)}{(2.26\times10^{-4}m^2)} = 8.48\Omega \tag{3.22}$$

6. Load Filter Design

$$L_{filter} = \frac{(1-D)T_s}{\Delta I_{L1}}V_{L1} = \frac{(0.25)\left(\frac{1}{150\;kHz}\right)}{\left(\frac{5}{100}\times100\;A\right)}(5\;V) = 1.7\mu H \tag{3.23}$$

$$C_{filter} = \frac{(1-D)T_s}{\Delta V_{L1}}I_{L1} = \frac{(0.25)\left(\frac{1}{150\;kHz}\right)}{\left(\frac{5}{100}\times5\;V\right)}(100\;A) = 67nF \tag{3.24}$$

The equivalent circuit for the converter is shown in Figure 19. It shows the primary voltage as a PWM Voltage source V_p. The primary winding resistance is represented by R_p. The primary current is converted to Magnetomotive force across the gyrator with gyration constant n_1. The nonlinear core Permeance is represented by element P. The secondary side consists of two gyrators with gyration constant n_2. Each gyrator senses the Magnetic voltage and generates proportional secondary current. The secondary side circuit consists of a rectifier circuit and a filter circuit to provide constant voltage and current to the load.

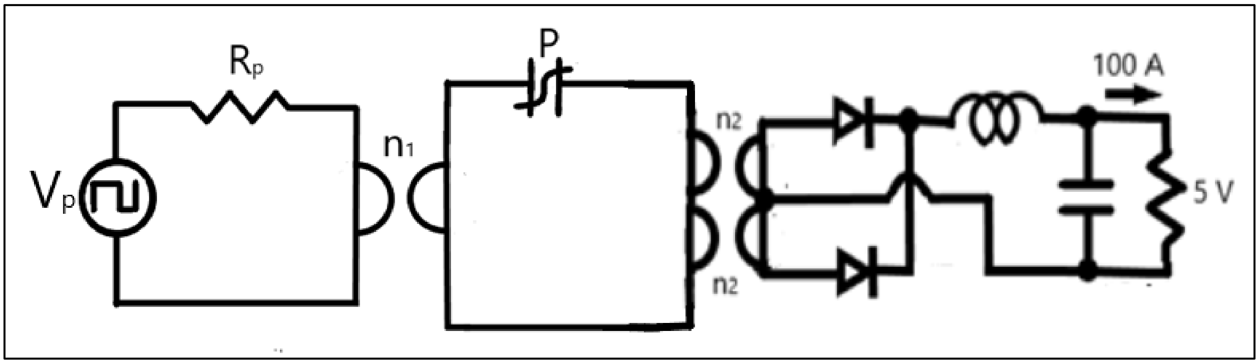

Figure 19: Equivalent converter circuit with gyrators and nonlinear core Permeance

The Simulink Model for the nonlinear Permeance is shown in Figure 20. It incorporates a resistance R_m that reduces the Magnetic Voltage of the Capacitance C_m. The current across the Capacitance is the derivative of its magnetic flux linkage.

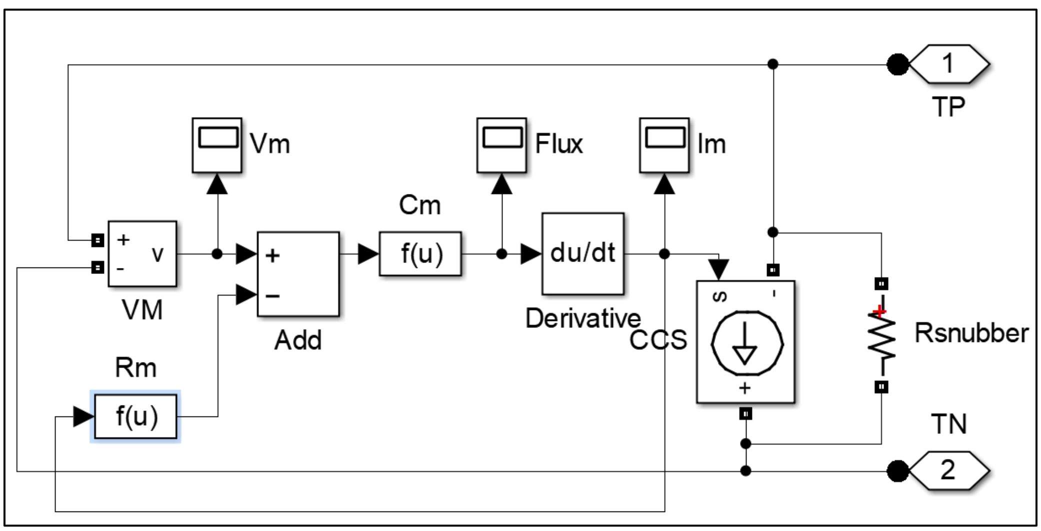

Figure 20: Simulink Model for nonlinear Permeance

The Flux response of nonlinear Permeance for voltage variation is recorded in Figure 21. The slope of the Flux-voltage curve gives the instantaneous Permeance. The area between the two curves represents the magnetic hysteresis loss across the resistance R_m.

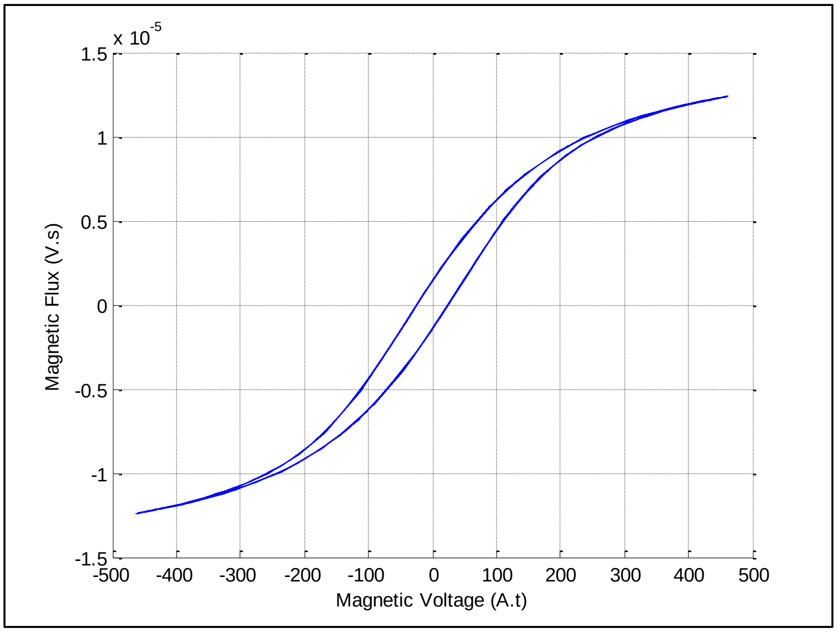

Figure 21: Variation of Permeance Flux versus Permeance Magnetic Voltage

The designed Transformer was excited by a sinusoidal voltage source of amplitude 100 V as shown in Figure 22. The transformer was loaded with a resistive load of 1 Ω. The output voltage and current are plotted below. As seen, the output voltage and current shows large spikes when the Permeance experiences large voltages.

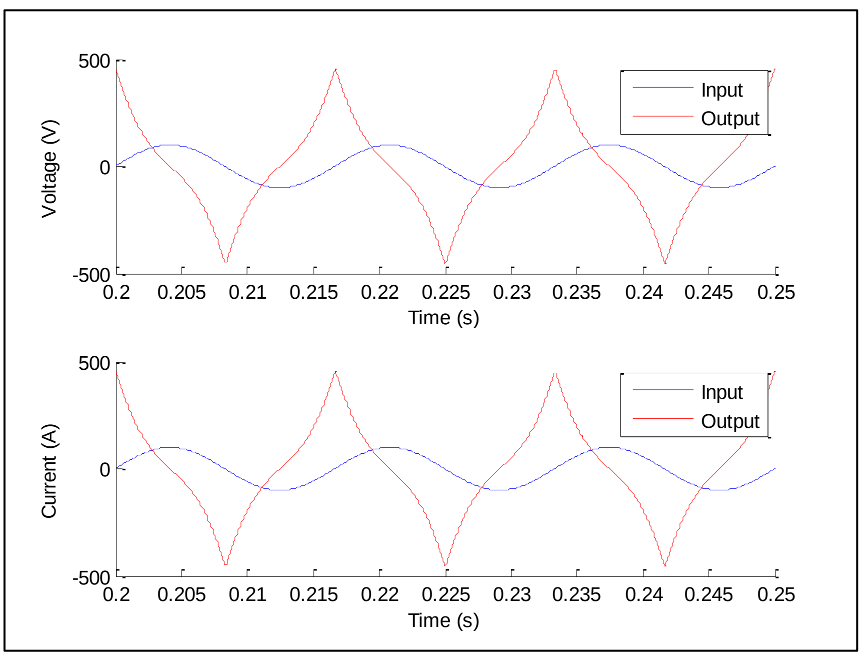

Figure 22: Transformer voltage and current response for sinusoidal excitation and resistive load

The Simulink Model for Isolated Buck Converter is shown in Figure 23. The Full Bridge is fed by a block that generates gate signals for electronic switches. The output of the Full Bridge is fed to the primary winding gyrator which converts electrical current to Magnetomotive force. The magnetic core is represented by a nonlinear permeance block. The current of the permeance is fed to the secondary winding gyrator which converts it into electromotive force. The secondary side consists of a full bridge rectifier and a low pass filter. This ensures constant voltage and current supply to the load.

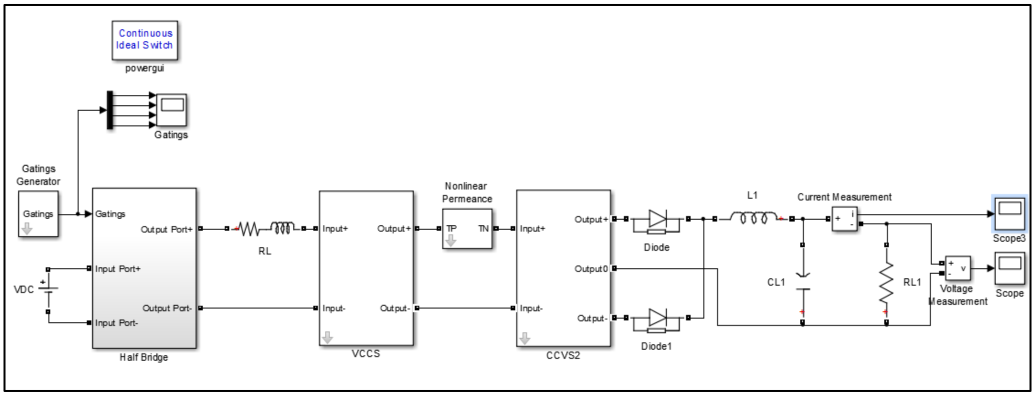

Figure 23: Simulink Model for Full Bridge Isolated Buck Converter

The Simulink Models for primary and secondary winding gyrators are shown in Figure 24 and 26. They convert Electric current to Magnetomotive force and Magnetic displacement current to electromotive force respectively.

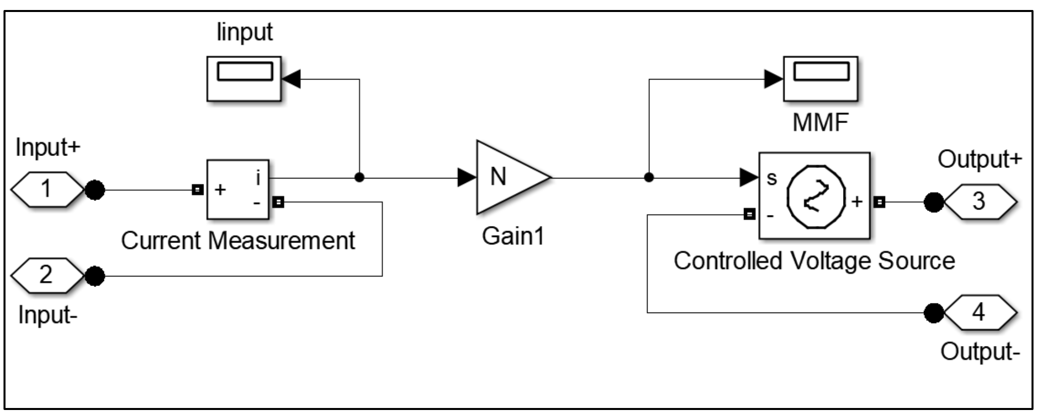

Figure 24: Simulink Model for Primary winding gyrator

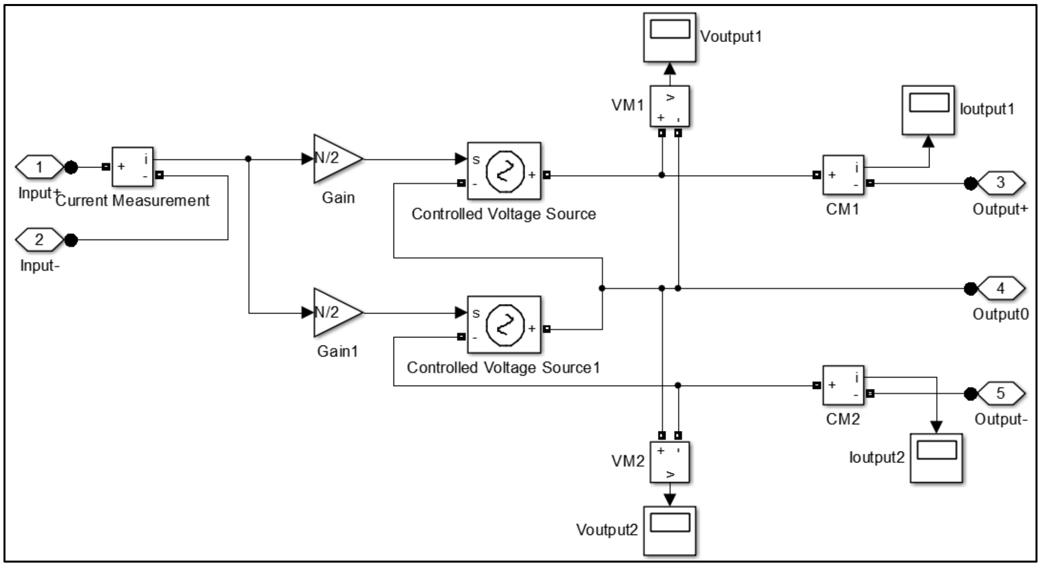

Figure 25: Simulink Model for secondary winding gyrator

The primary winding Electric voltage and Electric current are plotted in Figure 26. As desired, the voltage and current waveforms are sinusoidal waveforms.

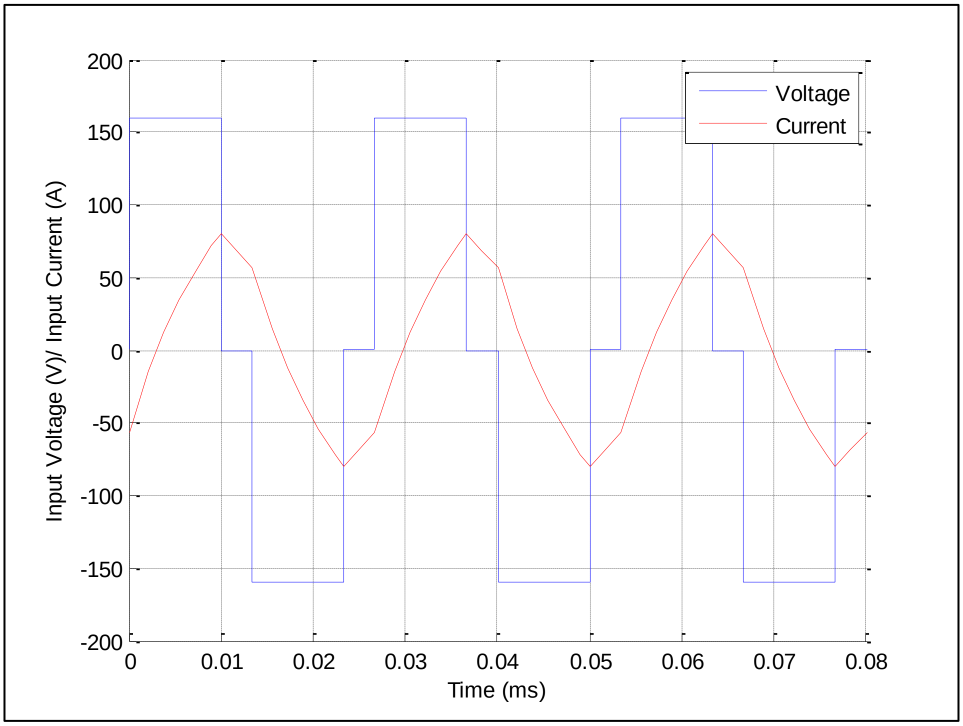

Figure 26: Primary winding voltage and current

The load Electric voltage and Electric current are plotted in Figure 27. As desired, the voltage and current ripple is about 5 percent.

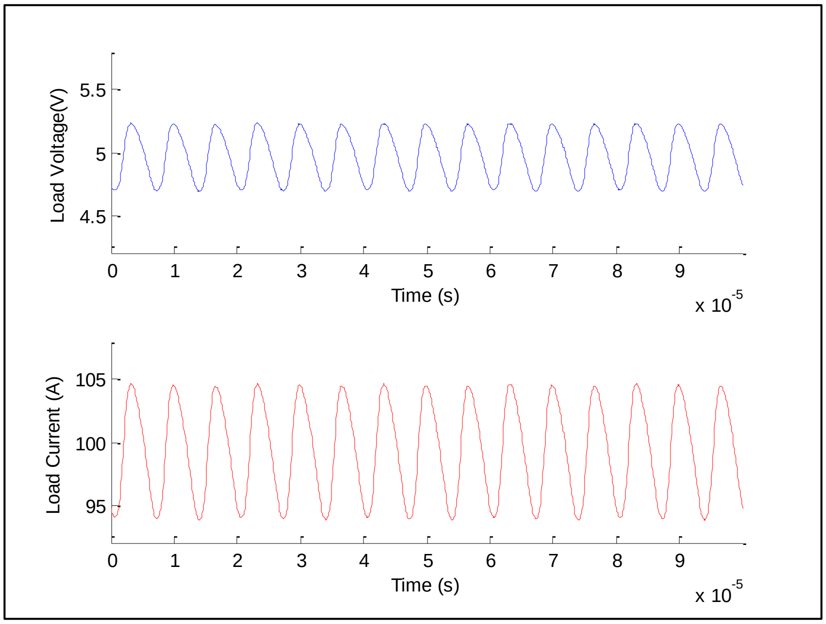

Figure 27: Load voltage and current

The Permeance Magnetic voltage and Magnetic displacement current are plotted in Figure 28. The Permeance saturates when the magnetic voltage becomes high hence magnetic current spikes are seen.

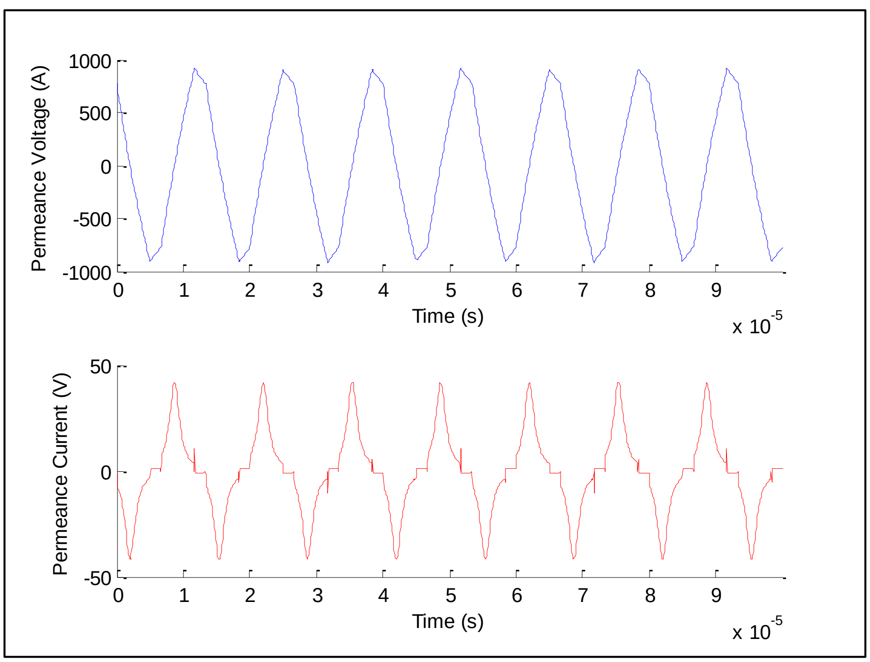

Figure 28: Permeance voltage and Current

The Permeance-Capacitance model is valuable for simulation of hysteresis in nonlinear cores.

3.3. Magnetic Transmission Line Model

This section presents the third model for magnetic elements called the Magnetic Transmission Line Model [22] - [26]. This model is based on the age old Electric transmission line model [22] - [26]. Like the Permeance-Capacitance Model, it also considers flux rate as the effective magnetic displacement current whereby magnetic permeability plays a similar role to electric conductivity by enhancing the magnetic displacement current inside the magnetic material.

In 2012, J. Faria and M. Pires presented Magnetic Transmission Line Model [22] - [26] based on Electric Transmission Line Model. The propagation of electromagnetic waves is governed by the Maxwell's Equations [55]:

$$\oint \boldsymbol{H}.dl = \oint \boldsymbol{J_e}\, dS + \frac{d}{dt}\int \boldsymbol{D}\, dS = \oint \boldsymbol{J_e}\, dS - \varepsilon_0 \frac{d}{dt}\int \boldsymbol{E}.dS - \varepsilon_0 \frac{d}{dt}\int \boldsymbol{E}.dS \quad (3.25)$$

$$\oint \boldsymbol{E}.dl = -\frac{d}{dt}\int \boldsymbol{B}.dS = -\mu_0 \frac{d}{dt}\int \boldsymbol{H}.dS - \mu_0 \frac{d}{dt}\int \boldsymbol{M}.dS \quad (3.26)$$

$$\oint \boldsymbol{B}.dS = 0 \quad (3.27)$$

$$\oint \boldsymbol{D}.dS = \iiint \rho_e\, dV \quad (3.28)$$

Analogous to the scalar Electric Potential, scalar magnetic potential V_m can be defined as

$$V_m = \int_a^b \boldsymbol{H}.dl \quad (3.29)$$

$$\boldsymbol{H} = \nabla V_m \quad (3.30)$$

The Magnetic Displacement Current I_m is defined as the rate of change of magnetic flux Φ_m:

$$\oint \boldsymbol{E}.dl = -\int \frac{d\boldsymbol{B}}{dt}.dS = -\oint \boldsymbol{J_m}\, dS = -\frac{d\Phi_m}{dt} = I_m \quad (3.31)$$

$$\nabla \times \boldsymbol{E} = -\boldsymbol{J_m} \quad (3.32)$$

The per unit length transverse magnetic inductance L_T represents a magnetic Energy storage element. It is defined in terms of per unit length Magnetic charge $\Phi_m$and scalar magnetic voltage V_m as

$$\Phi_m = L_T V_m \quad (3.33)$$

The per unit length longitudinal capacitance C_L represents an Electric Energy storage element [73]. It is defined in terms of electric displacement flux Ψ_e and magnetic displacement current I_m as

$$\Phi_e = C_L I_m \quad (3.34)$$

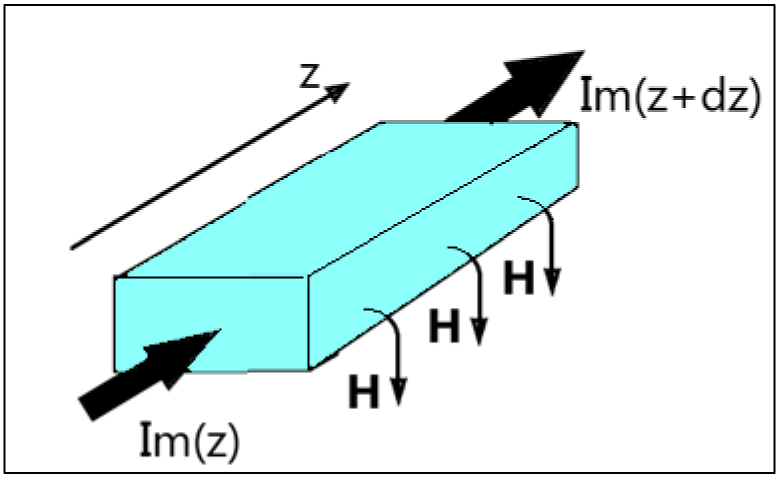

Figure 29: A section of Magnetic Transmission Line transmitting flux in z-direction

Assuming TEM-guided propagation in z-direction ($E_y = E_z = H_x = H_z = 0, \rho_e = J_e = 0$), the relation between the magnetic voltage and magnetic displacement current for a homogeneous magnetic transmission line [22] - [26] is derived by substituting the previous expressions in the Maxwell's Equations [55].

$$\frac{d}{dz}\int \boldsymbol{E_x} dx = -\mu \frac{d}{dt}\int \boldsymbol{H_y} dx \tag{3.35}$$

$$\frac{d}{dz}\int \boldsymbol{H_y} dy = -\varepsilon \frac{d}{dt}\int \boldsymbol{E_x} dy \tag{3.36}$$

The resulting Transmission Line Equations are

$$\frac{dI_m}{dz} = -L_T \frac{dV_m}{dt} \tag{3.37}$$

$$\frac{dV_m}{dz} = -C_L \frac{dI_m}{dt} \tag{3.38}$$

A forward travelling and a backward travelling wave can simultaneously exist on the transmission line. The solution for the Magnetic voltage and Magnetic displacement current is

$$V_m(z) = V_m^+ e^{-j\beta z + j\theta^+} + V_m^- e^{j\beta z + j\theta^-} \tag{3.39}$$

$$I_m(z) = \frac{V_m^+}{Z_o} e^{-j\beta z + j\theta^+ - j\theta_z} - \frac{V_m^-}{Z_o} e^{j\beta z + j\theta^- - j\theta_z} \tag{3.40}$$

The propagation constant is defined as

$$\beta = \sqrt{L_T C_L} \tag{3.41}$$

The characteristic impedance is the ratio of Magnetic displacement current to the Magnetic Voltage. It is calculated as

$$Z_m = \frac{I_m(z)}{V_m(z)} = \sqrt{\frac{L_T}{C_L}} \tag{3.42}$$

The average power flow in the Magnetic Transmission Line [22] - [26] can be represented in terms of three distinct components: the average power in the forward travelling wave, the average power in the backward travelling wave and the dissipated power.

$$P_{av}(z) = \frac{1}{2} Re\big(V(z) I^*(z)\big) \tag{3.43}$$

$$P_{av}(z) = \frac{1}{2} Re\Big(\big(V_m^+ e^{-\alpha z - j\beta z + j\theta^+} + V_m^- e^{\alpha z + j\beta z + j\theta^-}\big)\Big(\frac{V_m^+}{Z_o} e^{-\alpha z + j\beta z - j\theta^+ + j\theta_z} - \frac{V_m^-}{Z_o} e^{\alpha z - j\beta z - j\theta^- + j\theta_z}\Big)\Big) \tag{3.44}$$

$$P_{av}(z) = P_{av}^+(z) + P_{av}^-(z) + P_{loss}(z) \tag{3.45}$$

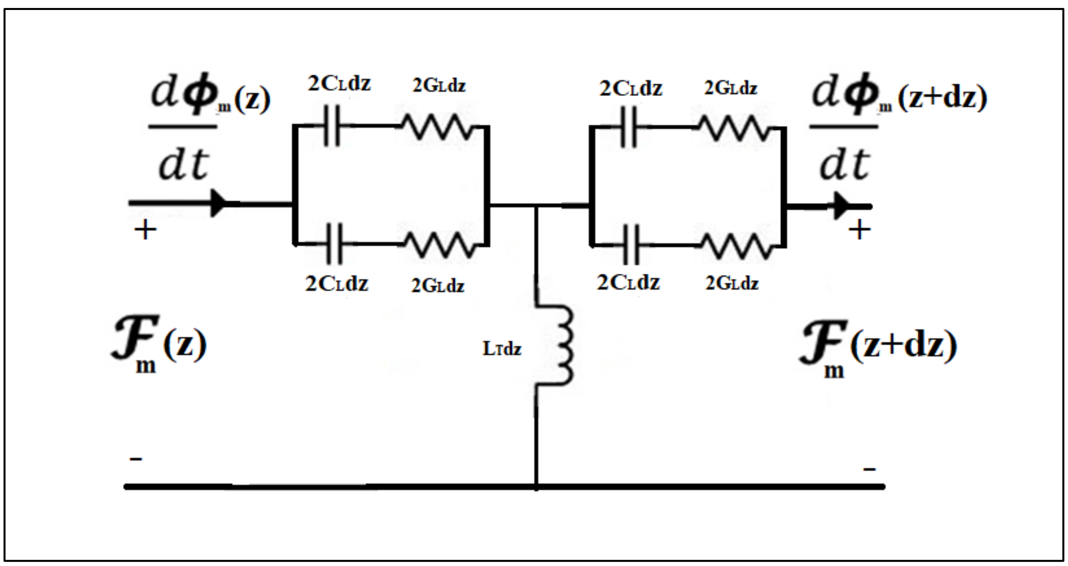

Figure 30: Equivalent circuit model for magnetic transmission line

In a non-ideal magnetic transmission line [22] - [26], magnetic voltage drop can be accounted by including magnetic reluctance/ conductance. It represents all the magnetization, polarization and conduction losses [20] due to electric conductivity, complex permittivity and complex permeability [72], [70], [35-36]. Magnetic Inductance and Magnetic Capacitance are energy storage elements in this model [74], [73].

$$G_L = \frac{\mathcal{R}_m}{j\omega} = \frac{V_m}{I_m} = \frac{\int \boldsymbol{H}.dl}{\oint \boldsymbol{E}.dl} \qquad [Ohm] \tag{3.46}$$

$$L_T = \frac{\phi_m}{V_m} = \frac{\int \boldsymbol{B}.dS}{\int \boldsymbol{H}.dl} \quad [Henry] \tag{3.47}$$

$$C_L = \frac{\phi_e}{I_m} = \frac{\int \boldsymbol{D}.dS}{\oint \boldsymbol{E}.dl} \quad [Farad] \tag{3.48}$$

Energy is dissipated in Magnetic Conductance:

$$P_{loss} = I_m^2 G_L \quad [Watt] \tag{3.49}$$

Electrical Energy is stored in Magnetic Capacitance [74], [73]; and Magnetic Energy is stored in Magnetic Inductance [22] - [26].

$$W_e = \frac{1}{2} C_L V_m^2 = \frac{1}{2} \int \boldsymbol{B}.\boldsymbol{H}\, dV \tag{3.50}$$

$$W_m = \frac{1}{2} L_T I_m^2 = \frac{1}{2} \int \boldsymbol{D}.\boldsymbol{E}\, dV \tag{3.51}$$

The resulting Magnetic Transmission Line Equations [22] - [26] are:

$$\frac{dI_m}{dz} = -L_T \frac{dV_m}{dt} \tag{3.52}$$

$$\frac{dV_m}{dz} = -G_L I_m - C_L \frac{dI_m}{dt} \tag{3.53}$$

$$\frac{d^2V_m}{dz^2} = L_T C_L \frac{d^2V_m}{dt^2} + L_T G_L \frac{dV_m}{dt} \tag{3.54}$$

$$\frac{d^2I_m}{dz^2} = L_T G_L \frac{d^2I_m}{dt^2} + L_T C_L \frac{dI_m}{dt} \tag{3.55}$$

Assuming sinusoidal steady state, the equations can be expressed in terms of phasor quantities as follows:

$$\frac{d^2V_m}{dz^2} = -\omega^2 L_T C_L V_m + j\omega L_T G_L V_m = (-\omega^2 L_T C_L + j\omega L_T G_L) V_m \tag{3.56}$$

$$\frac{d^2I_m}{dz^2} = -\omega^2 L_T G_L I_m + j\omega L_T C_L I_m = (-\omega^2 L_T G_L + j\omega L_T C_L) I_m \tag{3.57}$$

The Magnetic Transmission Line Equations [22] - [26] can be solved just like Electric Transmission Line Equations. The solutions are compared in the table below.

Electric Transmission Line	Magnetic Transmission Line
$\frac{dI_e}{dz} = -G_T V_e - C_T \frac{dV_e}{dt}$ $\frac{dV_e}{dz} = -R_L I_e - L_L \frac{dI_e}{dt}$	$\frac{dI_m}{dz} = -L_T \frac{dV_m}{dt}$ $\frac{dV_m}{dz} = -G_L I_m - C_L \frac{dI_m}{dt}$
$\frac{d^2 I_e}{dz^2} = L_L C_T \frac{d^2 I_e}{dt^2} + (L_L G_T + R_L C_T)\frac{dI_e}{dt} + R_L G_T I_e$ $\frac{d^2 V_e}{dz^2} = L_L C_T \frac{d^2 V_e}{dt^2} + (L_L G_T + R_L C_T)\frac{dV_e}{dt} + R_L G_T V_e$	$\frac{d^2 I_m}{dz^2} = L_T G_L \frac{d^2 I_m}{dt^2} + L_T C_L \frac{dI_m}{dt}$ $\frac{d^2 V_m}{dz^2} = L_T C_L \frac{d^2 V_m}{dt^2} + L_T G_L \frac{dV_m}{dt}$
$V_e(z) = V_{e_i}(0)e^{-\gamma z} + V_{e_r}(0)e^{+\gamma z}$ $I_e(z) = I_{e_i}(0)e^{-\gamma z} - I_{e_r}(0)e^{+\gamma z}$	$V_m(z) = V_{m_i}(0)e^{-\gamma z} + V_{m_r}(0)e^{+\gamma z}$ $I_m(z) = I_{m_i}(0)e^{-\gamma z} - I_{m_r}(0)e^{+\gamma z}$
$\gamma = \sqrt{(R_e + j\omega L_L)(G_e + j\omega C_T)}$ $\gamma = \sqrt{(\rho + j\omega\mu)(\sigma + j\omega\varepsilon)}$ $\gamma = \alpha + j\beta$	$\gamma = \sqrt{(j\omega L_T)(G_L + j\omega C_L)}$ $\gamma = \sqrt{(j\omega\mu)(\sigma + j\omega\varepsilon)}$ $\gamma = \alpha + j\beta$
$Z_w = \frac{V_e(z)}{I_e(z)} = \sqrt{\frac{R_L + j\omega L_L}{G_T + j\omega C_T}}$	$Z_w = \frac{I_m(z)}{V_m(z)} = \sqrt{\frac{j\omega L_T}{G_L + j\omega C_L}}$

For Electric Transmission Lines of same geometry described by $L_L$and C_T matrices, the magnetic Transmission Line parameter matrices are closely related:

$$L_T L_L = \mu_0^2 \tag{3.58}$$

$$L_T C_L = \mu_0 \varepsilon \tag{3.59}$$

$$\varepsilon_0 L_T = \mu_0 C_T \tag{3.60}$$

$$C_T C_L = \varepsilon_0 \varepsilon \tag{3.61}$$

Magnetic cores are often manufactured using layers of laminated magnetic sheets to prevent the flow of Eddy Currents. In such materials, magnetic flux from one transmission line can link with a neighboring magnetic transmission line [22] - [26] and disturb the information [21]. The Magnetic Transmission Line Model [22] - [26] can be extended to the generator-receptor Magnetic Transmission Line model [22] - [26]. This is well suited for studying Electromagnetic Coupling of Magnetic Transmission Lines [22] - [26] which are in close proximity.

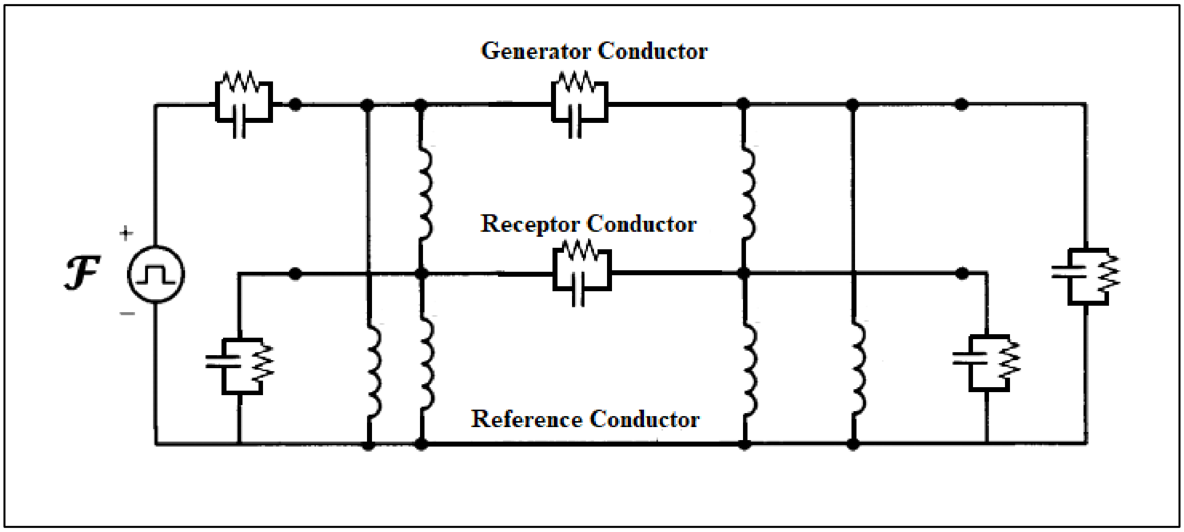

Figure 31: Equivalent circuit model for cross-talk between neighbouring Magnetic Transmission Lines

3.4. Summary

This chapter presented three different models for modeling magnetic elements. The age old reluctance model based on the Ohm's law analogy was found to violate power invariance property. It is only suitable for steady state simulations of magnetic cores with known reluctance profile. The Permeance-Capacitance model uses a nonlinear permeance to model nonlinearity and hysteresis losses of magnetic materials. It is valuable for simulating transient behavior of Ferromagnetic elements like RF inductors, transformers and filters. The third model was the magnetic transmission line model which is the most accurate model for modeling dispersive, inhomogeneous and lossy magnetic cores. It uses Transmission Line theory to predict magnetic parameters of ferromagnetic core. The three models are summarized in the table below.

	Reluctance Model	**Permeance-Capacitance Model**	**Transmission Line Model**
Conserved Quantity	?	Magnetic Flux [Volt-Second]	Magnetic Flux [Volt-Second]
Flow Variable	Magnetic Flux [Volt-Second]	Rate of change of Magnetic Flux [Volt]	Rate of change of Magnetic Flux [Volt]
Effort Variable	Magnetomotive Force [Ampere]	Magnetomotive Force [Ampere]	Magnetomotive Force [Ampere]
Energy Dissipation Element	Magnetic Reluctance $[\text{Henry}^{-1}]$	?	Magnetic Conductance [Ohm]
Electrical Energy Storage Element	?	?	Magnetic Capacitance [Farad]
Magnetic Energy Storage Element	?	Magnetic Permeance [Henry]	Magnetic Inductance [Henry]

4. Computational Electromagnetics

This chapter discusses the different time domain and frequency domain methods for solving Maxwell's Equations [55], [21], [39], [1]. Section 4.1 introduces different popular methods for computational electrodynamics. Section 4.2 discusses Finite Difference Time Domain method which will be used for simulating Magnetic Transmission Lines in MEEP Simulator [52] introduced in Section 4.3.

4.1. Methods for solving Maxwell's Equations

The Maxwell's Equations can be solved in time domain and frequency domain by solving Partial Differential Equations or Integral Equations [55], [39]. Some of the methods are listed in the table below.

Method	**Remark**
Adaptive Integral Method (AIM)	Provides efficient iterative procedure for matrix algebra for linearized version of Maxwell's equations.
Analytical closed form techniques	Approximate methods are used in cases with high degree of symmetry. Closed form solutions are not always possible.
Bi-conjugate gradient method with Fast Fourier Transform (BCG-FFT)	Useful in solving complex matrix equations resulting from the interactions of electromagnetic waves with surfaces.
Boundary Element Method (BEM)	Discretizes boundary elements to solve low frequency or steady state AC problems.
Conjugate Gradient Method (CGM)	Uses iterative method of conjugate gradients to solve systems involving large and sparse matrices.
Fast Multipole Method (FMM)	Uses approximations to solve for far field scalar potential.
Finite Difference Frequency Domain (FDFD)	Uses optimal discretization to solve time harmonic versions of linearized Maxwell's equations.
Finite Difference Time Domain (FDTD)	Maxwell's Equations are linearized using finite differences. Entire volume is uniformly discretized and fields are evolved by time stepping. Transient analysis of sharp edges increases resolution and computational time.
Finite Element Method (FEM)	Entire volume is non-uniformly discretized into homogeneous sub-regions. Field are computed by minimizing energy functions.
Finite Integration Technique (FIT)	Integral version of Maxwell's Equations are solved in a non-uniformly meshed volume with very high resolution.

Finite Volume Time Domain (FVTD)	Entire volume is non-uniformly discretized and fields are evolved by time stepping.
Generalized Multipole Technique (GMT)	Surface charges and currents are used to determine frequency domain analytical field solutions using method of weighted residuals.
Geometrical Optics (GO)	Used for exact ray tracing for light wave propagation in optical media.
Geometrical/ Uniform Theory of Diffraction (GTD/ UTD)	Used for high frequency ray tracing and asymptotic solutions are used for solving diffraction problems.
Hybrid Lumped Circuit and Quasi Transmission Line Method	A hybrid method to accurately model lumped elements in microwave applications.
Method of Moments (MoM)	Wire mesh currents and patch surface currents are used to analyze complex inhomogeneous structures through the method of weighted residuals.
Multiple Multipole (MMP)	Generalized point matching is used to find a series of homogeneous domain analytic solutions that compose the field.
Partial Element Equivalent Circuit (PEEC)	A circuit of small electrical elements is used to approximate PCB radiation patterns.
Shooting Bouncing Rays (SBR), Physical Optics (PO), Physical Theory of Diffraction (PTD)	Planar surfaces are irradiated with electromagnetic field by transmitters. Receivers use detected radiation to compute local field.
Singularity Expansion Method (SEM)	Laplace Transform with complex frequencies is used to detect characteristic resonance of complex scatterers.
Spectral Domain Approach (SDA)	Spatial Fourier Transform is used to solve fields in spectral domain.
Transmission Line Method (TLM)	Complex nonlinear materials can be modeled using virtual transmission lines. The Voltage and current inform about the fields.
Vector Parabolic Equation Technique (VPE)	Useful in radio communication systems.

After this brief review of Computational Electromagnetics, the next section discusses Finite Difference Time Domain Method which will be used to simulate nonlinear, anisotropic, inhomogeneous Magnetic Transmission Lines.

4.2. Introduction to Finite Difference Time Domain Method

Finite Difference Time Domain Method (FDTD) or K. S. Yee's Method (1966) is a differential numerical modeling technique for computational electrodynamics [68] - [69], [39], [21], [43], [64]. Finite Difference Time Domain Method [9] discretizes space into a grid of small elements called Yee Lattice (1966) [68] - [69], [64], [43]. Each element can have a different conductivity, permittivity and permeability [43], [39].

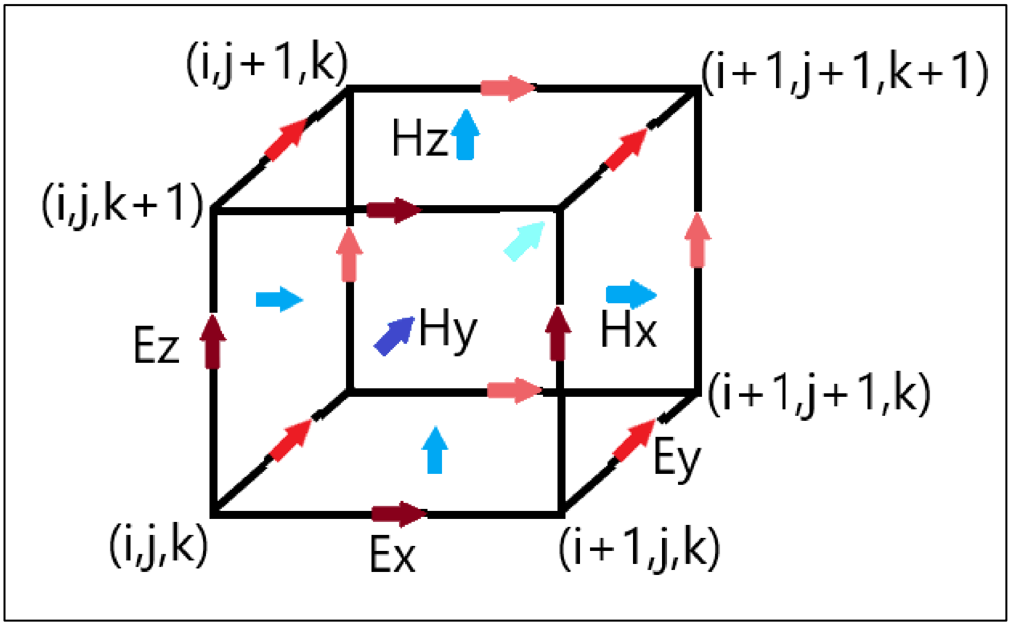

Figure 32: Location of different Field components in a Yee Cell

J. C. Maxwell's Equations (1861) [55] are discretized using central difference approximations to the space and time partial derivatives. For example, Faraday's Law can be expanded as follows:

$$\nabla \times \boldsymbol{E} = -\frac{d\boldsymbol{B}}{dt} \tag{4.1}$$

$$\nabla \times E = \left(\frac{\Delta E_z}{\Delta y} - \frac{\Delta E_y}{\Delta z}\right) a_x + \left(\frac{\Delta E_x}{\Delta z} - \frac{\Delta E_z}{\Delta x}\right) a_y + \left(\frac{\Delta E_y}{\Delta x} - \frac{\Delta E_x}{\Delta y}\right) a_z \tag{4.2}$$

$$\frac{\Delta E_y}{\Delta z} - \frac{\Delta E_z}{\Delta y} = \mu \frac{\Delta H_x}{\Delta t} \tag{4.3}$$

$$\frac{\Delta E_z}{\Delta x} - \frac{\Delta E_x}{\Delta z} = \mu \frac{\Delta H_y}{\Delta t} \tag{4.4}$$

$$\frac{\Delta E_x}{\Delta y} - \frac{\Delta E_y}{\Delta x} = \mu \frac{\Delta H_z}{\Delta t} \tag{4.5}$$

Similarly, Ampere's Law can be approximated as follows:

$$\nabla \times \boldsymbol{H} = \sigma \boldsymbol{E} + \frac{d\boldsymbol{D}}{dt} \tag{4.6}$$

$$\nabla \times H = \left(\frac{\Delta H_z}{\Delta y} - \frac{\Delta H_y}{\Delta z}\right) a_x + \left(\frac{\Delta H_x}{\Delta z} - \frac{\Delta H_z}{\Delta x}\right) a_y + \left(\frac{\Delta H_y}{\Delta x} - \frac{\Delta H_x}{\Delta y}\right) a_z \tag{4.7}$$

$$\frac{\Delta H_z}{\Delta y} - \frac{\Delta H_y}{\Delta z} = \sigma E_x + \varepsilon \frac{\Delta E_x}{\Delta t} \tag{4.8}$$

$$\frac{\Delta H_x}{\Delta z} - \frac{\Delta H_z}{\Delta x} = \sigma E_y + \varepsilon \frac{\Delta E_y}{\Delta t} \tag{4.9}$$

$$\frac{\Delta H_y}{\Delta x} - \frac{\Delta H_x}{\Delta y} = \sigma E_z + \varepsilon \frac{\Delta E_z}{\Delta t} \tag{4.10}$$

The different field components at a grid location are stored in the edges and faces of a cubic element called Yee's Cell. They are evolved in discrete time steps $t_n = n\Delta t$ [68] - [69].

$$\left(\frac{E_y\Big|_{i,j,k+\frac{1}{2}}^{n} - E_y\Big|_{i,j,k-\frac{1}{2}}^{n}}{\Delta z}\right) - \left(\frac{E_z\Big|_{i,j+\frac{1}{2},k}^{n} - E_z\Big|_{i,j-\frac{1}{2},k}^{n}}{\Delta y}\right) = \mu_{i,j,k}\left(\frac{H_x\Big|_{i,j,k}^{n+\frac{1}{2}} - H_x\Big|_{i,j,k}^{n-\frac{1}{2}}}{\Delta t}\right) \tag{4.11}$$

$$\left(\frac{E_z\Big|_{i+\frac{1}{2},j,k}^{n} - E_z\Big|_{i-\frac{1}{2},j,k}^{n}}{\Delta x}\right) - \left(\frac{E_x\Big|_{i,j,k+\frac{1}{2}}^{n} - E_x\Big|_{i,j,k-\frac{1}{2}}^{n}}{\Delta z}\right) = \mu_{i,j,k}\left(\frac{H_y\Big|_{i,j,k}^{n+\frac{1}{2}} - H_y\Big|_{i,j,k}^{n-\frac{1}{2}}}{\Delta t}\right) \tag{4.12}$$

$$\left(\frac{E_x\Big|_{i,j+\frac{1}{2},k}^{n} - E_x\Big|_{i,j-\frac{1}{2},k}^{n}}{\Delta y}\right) - \left(\frac{E_y\Big|_{i+\frac{1}{2},j,k}^{n} - E_y\Big|_{i-\frac{1}{2},j,k}^{n}}{\Delta x}\right) = \mu_{i,j,k}\left(\frac{H_z\Big|_{i,j,k}^{n+\frac{1}{2}} - H_z\Big|_{i,j,k}^{n-\frac{1}{2}}}{\Delta t}\right) \tag{4.13}$$

$$\left(\frac{H_z\Big|_{i,j+\frac{1}{2},k}^{n} - H_z\Big|_{i,j-\frac{1}{2},k}^{n}}{\Delta y}\right) - \left(\frac{H_y\Big|_{i,j,k+\frac{1}{2}}^{n} - H_y\Big|_{i,j,k-\frac{1}{2}}^{n}}{\Delta z}\right) = \sigma\Big|_{i,j,k}^{n}\left(E_x\Big|_{i,j,k}^{n}\right) + \varepsilon_{i,j,k}\left(\frac{E_x\Big|_{i,j,k}^{n+\frac{1}{2}} - E_x\Big|_{i,j,k}^{n-\frac{1}{2}}}{\Delta t}\right) \tag{4.14}$$

$$\left(\frac{H_x\Big|_{i,j,k+\frac{1}{2}}^{n} - H_x\Big|_{i,j,k-\frac{1}{2}}^{n}}{\Delta z}\right) - \left(\frac{H_z\Big|_{i+\frac{1}{2},j,k}^{n} - H_z\Big|_{i-\frac{1}{2},j,k}^{n}}{\Delta x}\right) = \sigma\Big|_{i,j,k}^{n}\left(E_y\Big|_{i,j,k}^{n}\right) + \varepsilon_{i,j,k}\left(\frac{E_y\Big|_{i,j,k}^{n+\frac{1}{2}} - E_y\Big|_{i,j,k}^{n-\frac{1}{2}}}{\Delta t}\right) \tag{4.15}$$

$$\left(\frac{H_y\Big|_{i+\frac{1}{2},j,k}^{n} - H_y\Big|_{i-\frac{1}{2},j,k}^{n}}{\Delta x}\right) - \left(\frac{H_x\Big|_{i,j+\frac{1}{2},k}^{n} - H_x\Big|_{i,j-\frac{1}{2},k}^{n}}{\Delta y}\right) = \sigma\Big|_{i,j,k}^{n}\left(E_z\Big|_{i,j,k}^{n}\right) + \varepsilon_{i,j,k}\left(\frac{E_z\Big|_{i,j,k}^{n+\frac{1}{2}} - E_z\Big|_{i,j,k}^{n-\frac{1}{2}}}{\Delta t}\right) \tag{4.16}$$

The location of field components and the central difference operations implicitly enforce the two Gauss's Laws [55].

The finite region of space must always be terminated with some boundary conditions. Some examples include:

1. Bloch-periodic Boundaries are used for simulation of periodic structures $f(x) = f(x+L)e^{-jkL}$. Periodic Bloch Boundaries copy the field component at one cell's edge and reinject them at a neighboring cell's edge.
2. At Metallic Walls, all fields are forced to be zero hence it is a perfect reflector with zero absorption and zero skin depth.
3. Perfectly Matched Layers allow all the fields to pass through with minial reflection. These absorbing boundary conditions (ABCs) absorb almost all of the incident field.

4.3. Introduction to MEEP Simulator

This section gives a brief introduction to MEEP [52] simulator designed for solving the Maxwell's Equations [55] using discrete time stepping. MEEP [52] is a script based Simulator for modeling the time domain [39] and frequency domain behavior of a variety of arbitrary materials.

1. A fully scriptable open source C++ interface is provided for generating optimized algorithms.
2. The use of normalized units for solving Maxwell's Equations provides exceptional resolution in frequency and time domain. The simulator can be run on multicore supercomputers to speed up execution and transient analysis.
3. A Material Library with sample data for several materials is provided in libraries for building accurate test structures.
4. A wide variety of electric or magnetic soft current sources can be simulated. G. Green's Functions (1835) give the Field Patterns from a localized point source at a particular frequency ω.
5. A frequency domain solver is also provided for multidimensional Fourier transformation (1822) and the decomposition of fields into travelling modes [59]. The 3 Dimensional Discrete Fourier transform (1822) of the response to a short impulse can give useful information about the transmitted power and losses [35-36], [59], [50], [21].
6. Averaging, symmetry and integration are allowed in cylindrical and rectangular three dimensional coordinates. Hence different homogeneous/inhomogeneous structures can be built inside the space. Electric/ Magnetic/ Thermal Energy Density, Poynting Flux etc. can be evaluated. The Transmitted Power can be computed using the integral of Poynting Vector (1884); over a surface on the far end of the transmission line. Transmitted power and incident power can be used to find power losses in transmission line.

$$P(\omega) = Re\left\{\hat{n}.\int E_{\omega}(x)^{*} \times H_{\omega}(x)\, d^{2}x\right\} \tag{4.17}$$

7. The fields can be printed as image or video files through Data Visualization features.

MEEP [52] can simulate anisotropic, dispersive [72], [16], non-linear [40] and gyrotropic media [54].

1. Anisotropic Media: For anisotropic media, non-diagonal susceptibility tensor is used to relate Polarization/ Magnetization and Field intensity.

$$\boldsymbol{P} = \begin{bmatrix} \chi_{\perp} & -j\eta & 0 \\ j\eta & \chi_{\perp} & 0 \\ 0 & 0 & \chi_{||} \end{bmatrix} \boldsymbol{E} \tag{4.18}$$

$$\boldsymbol{M} = \begin{bmatrix} \chi_{\perp} & -j\eta & 0 \\ j\eta & \chi_{\perp} & 0 \\ 0 & 0 & \chi_{||} \end{bmatrix} \boldsymbol{H} \tag{4.19}$$

2. Dispersive Media: Drude-Lorentzian Model (1900) models frequency dependent permittivity and permeability [72], [16]. It explains the electrodynamic properties of metals by regarding conduction band electrons as non-interacting electron gas. When the material is excited by an external source of resonant frequency, the material absorption loss increases greatly. Electromagnetic Energy is converted into other forms of energy. Flux Densities contain terms for infinite frequency response and frequency dependent Polarization vector [72].

$$\boldsymbol{D} = \varepsilon_{\infty}\boldsymbol{E} + \boldsymbol{P} \tag{4.20}$$

$$\boldsymbol{B} = \mu_{\infty}\boldsymbol{H} + \boldsymbol{M} \tag{4.21}$$

   ε and μ are represented as a sum of harmonic resonances [72], [12] and a term for frequency independent electric conductivity.

$$\varepsilon(\omega, x) = (1 + \frac{j\sigma_D}{\omega})(\varepsilon_{\infty}(\boldsymbol{x}) + \sum_N \frac{\sigma_n(\boldsymbol{x})\omega_n^2}{\omega_n^2 - \omega^2 + j\omega\gamma_n}) \tag{4.22}$$

$$\mu(\omega, x) = (1 + \frac{j\sigma_B}{\omega})(\mu_{\infty}(\boldsymbol{x}) + \sum_N \frac{\sigma_n(\boldsymbol{x})\omega_n^2}{\omega_n^2 - \omega^2 + j\omega\gamma_n}) \tag{4.23}$$

   σ_D/σ_B is the electrical/magnetic conductivity. σ_n is the oscillator strength, ω_n is the angular resonance frequency, γ_n is a damping factor.

3. Nonlinear Media: The Pockels and Kerr Non-linearity model (1875) explains how ε and μ can change as a function of the field intensity [40], [48]. Ferromagnetic materials are non-linear [48], [8], [39] as their permeability varies with the strength of applied field intensity. At high magnetic field intensity, the material saturates, limiting further increase of Magnetic Flux [48]. Hence, the susceptibility decreases rapidly.

$$\boldsymbol{D} = (\varepsilon_{\infty}(\boldsymbol{x}) + \chi^{(2)}(\boldsymbol{x}).diag(\boldsymbol{E}) + \chi^{(3)}(\boldsymbol{x}).|\boldsymbol{E}|^2)\boldsymbol{E} + \boldsymbol{P} \tag{4.24}$$

$$\boldsymbol{B} = (\mu_{\infty}(\boldsymbol{x}) + \chi^{(2)}(\boldsymbol{x}).diag(\boldsymbol{H}) + \chi^{(3)}(\boldsymbol{x}).|\boldsymbol{H}|^2)\boldsymbol{H} + \boldsymbol{M} \tag{4.25}$$

$\chi^{(2)}$sum is the Pockels effect constant; whereas $\chi^{(3)}$ sum is the Kerr effect constant.

4. Gyrotropic Media: Landau-Lifshitz-Gilbert model (1955) describes the precessional motion of saturated magnetic dipoles in a magnetic field [62], [54].

$$\frac{d\boldsymbol{M}_n}{dt} = \boldsymbol{b}_n \times \left(-\sigma_n \boldsymbol{H} + \omega_n \boldsymbol{M}_n + \alpha_n \frac{d\boldsymbol{M}_n}{dt}\right) - \gamma_n \boldsymbol{M}_n \tag{4.26}$$

$\boldsymbol{M}_n$describes the linear deviation of magnetization from its static equilibrium value. Precession occurs around this unit bias vector $\boldsymbol{b}_n$. σ_n represents oscillator strength, ω_n is the angular resonance frequency, γ_n is the oscillator damping factor.

MEEP uses normalized units for solving Maxwell's Equations. A conversion scheme from SI units to MEEP units is shown in the table below.

Property	Symbol	Reference Scale in SI Units	SI to MEEP Conversion Factor	Normalized MEEP Units
Length	a_0	1.00000×10^{-4} m	$\frac{1}{a_0} = 1.00000\times 10^{4}$	1
Speed of Light	c_0	$2.99792\times 10^{8}\ \frac{m}{s}$	$\frac{1}{c_0} = 3.33564\times 10^{-9}$	1
Current	I_0	1.00000 A	$\frac{1}{I_0} = 1.00000$	1
Time	t_0	$\frac{a_0}{c_0} = 3.33564\times 10^{-13}$ s	$\frac{1}{t_0} = 2.99792\times 10^{12}$	1
Frequency	f_0	$\frac{c_0}{a_0} = 2.99792\times 10^{12}$ Hz	$\frac{1}{f_0} = 3.33564\times 10^{-13}$	1
Permittivity	ε_0	$8.85418\times 10^{-12}\ \frac{F}{m}$	$\frac{1}{\varepsilon_0} = 1.12940\times 10^{11}$	1
Permeability	μ_0	$1.25663\times 10^{-6}\ \frac{H}{m}$	$\frac{1}{\mu_0} = 7.95774\times 10^{5}$	1
Electric Field Intensity	E_0	$\frac{I_0}{a_0\varepsilon_0 c_0} = 3.76730\times 10^{6}\ \frac{V}{m}$	$\frac{1}{E_0} = 2.65441\times 10^{-7}$	1
Electric Flux Density	D_0	$\frac{I_0}{a_0 c_0} = 3.33564\times 10^{-5}\ \frac{C}{m^2}$	$\frac{1}{D_0} = 2.99792\times 10^{4}$	1
Magnetic Field Intensity	H_0	$\frac{I_0}{a_0} = 1.00000\times 10^{4}\ \frac{A}{m}$	$\frac{1}{H_0} = 1.00000\times 10^{-4}$	1
Magnetic Flux Density	B_0	$\frac{I_0}{a_0\varepsilon_0 c_0 c_0} = 1.25663\times 10^{-2}\ \frac{Wb}{m^2}$	$\frac{1}{B_0} = 7.95774\times 10^{1}$	1
Electric Conductivity	σ_0	$\frac{\varepsilon_r\varepsilon_0 c_0}{a_0} = 2.65441\times 10^{1}\ \frac{A}{\mathrm{V}m}$	$\frac{1}{\sigma_0} = 3.7673\times 10^{-2}$	1
Electric Current Density	J_0	$\frac{I_0}{a_0 a_0} = 1.00000\times 10^{8}\ \frac{A}{m^2}$	$\frac{1}{J_0} = 1.00000\times 10^{-8}$	1
Energy Density	U_0	$\frac{I_0 I_0}{a_0 a_0\varepsilon_0 c_0 c_0} = 1.25663\times 10^{2}\ \frac{J}{m^3}$	$\frac{1}{U_0} = 7.95774\times 10^{-3}$	1
Poynting Vector	S_0	$\frac{I_0 I_0}{a_0 a_0\varepsilon_0 c_0} = 3.76730\times 10^{10}\ \frac{W}{m^2}$	$\frac{1}{S_0} = 2.65441\times 10^{-11}$	1
Courant Factor	S_{c0}	$\frac{1}{c_0} = 3.33564\times 10^{-9}\ \frac{s}{m}$	$\frac{1}{S_{c0}} = 2.99792\times 10^{8}$	1

5. Magnetic Transmission Line Simulation

This section presents an application of Magnetic Transmission Line Model for predicting the transient response of ferromagnetic materials. The results of the Transmission Line model will be verified by simulating the structure in MEEP simulator [52].

The Electromagnetic simulations will be carried out in MEEP [52] Simulator which is a script based Finite Difference Time Domain [68] - [69], [64], [43], [9] Electromagnetic Fields Simulator for solving Maxwell's Equations [55].

Lumped circuits [18] were used for studying linear, time invariant, distributed systems like Magnetic Transmission Lines [22] - [26]. The distributed parameters can be calculated using mathematical formulas. MATLAB will be used for modeling the time and frequency domain behavior of Magnetic Transmission Lines [22] - [26] in terms of simplified Lumped Circuits.

Finite Difference Time Domain [68] - [69], [64], [43], [9] Electromagnetic Field MEEP [52] Simulations will be carried out for dispersive [72], [16] Magnetic Transmission Lines [22] - [26] in anisotropic, inhomogeneous, non-linear media [40], [65], [39]. The Magnetic Transmission Lines [22] - [26] will be constructed using Drude-Lorentz susceptibility models for ferromagnetic conductors like Nickel, Iron and Cobalt alloys. The Transmission Lines will be excited using continuous point sources. The terminations can be modeled by Perfectly matched layers for Surge Impedance Loading; or as perfect reflectors for no load. Different Transmission Line structures can be simulated like the Wideband Transformer [67], [65], [31], [29], [14], [17], [35-36] and Transmission Line Transformer.

5.1. Simulation of Magnetic Transmission Line in MEEP

In order to study their frequency response to continuous sources, Finite Difference Frequency Domain [1] Electromagnetic Field MEEP [52] Simulations will be carried out. The multi-dimensional Fourier transform and mode decomposition will be used for this study. In order to simplify analysis, the Distributed System will be linearized to obtain a lumped model. The frequency Domain Behavior will also be studied using Transfer Function of Equivalent T-model Transmission Line circuit.

Multi-conductor Transmission Lines introduce many complexities like capacitive/ inductive coupling. MEEP [52] Simulations and MATLAB Lumped Circuit Simulations [18] will be carried out for studying cross talk between Conductors of multi-wire Magnetic Transmission Lines.

As in the case of Electric Transmission Lines, Power Flow Equations can be developed for Magnetic Transmission Lines [22] - [26] in terms of Lumped parameters; like per unit length transverse impedance and the per unit length longitudinal admittance. The results can be verified using electromagnetic simulations.

The Electromagnetic MEEP [52] Simulations will help to probe the stored Electric/ Magnetic Energy Density, geometric parameters, per unit length losses and Transmission Efficiency of Magnetic Transmission Lines. Among the different magnetic materials, the best alloy will be chosen based on desired performance metrics. A suitable candidate must exhibit minimal radiation and line losses. The transverse impedance and longitudinal admittance dictate the propagation of wave modes in magnetic transmission lines [22] - [26]. Simulations will be used to estimate per unit length transverse inductance and longitudinal capacitance [73], which contribute to the transverse impedance and longitudinal admittance respectively. These parameters are pivotal in determining the lumped model of the distributed Transmission Line system.

The Magnetic Transmission Lines [22] - [26] will be excited by continuous sources to examine their Frequency Response. The Fourier Transform will decompose the Fields into the various travelling wave modes. This will aid the study of the effects of magnetic hysteresis [48], [44-46] and saturation on power quality [9]. The T-model Equivalent Magnetic circuits [18] and coupled equations will be used to simplify analysis of the transient [9] and steady state behavior. According to theory, Magnetic Transmission Lines [22] - [26] must exhibit the behavior of a high pass filter, blocking all DC signals. DC signals produce the most severe transients in Electric Transmission Lines [9]; which behave like a low pass filter. However, this also implies that Magnetic Transmission Lines [22] - [26] must be operated at higher frequencies than Electric Transmission Lines. Poorly designed Magnetic Transmission Lines [22] - [26] may amplify high frequency noise which can be damaging for the power system. The imaginary part of Transmission Line Magnetic Reluctance, which is a strong function of frequency, contributes to line losses. Hysteresis losses [48], [44-46] also increase significantly at higher frequencies

[20], [9], [35-36]. Hence, an appropriate frequency must be chosen, considering the complex nature of the magnetic material.

The study of capacitive/ inductive coupling in Multi-Conductor Transmission Lines will provide useful knowledge about the Radiated/ Conducted Emissions and Susceptibility. The generator-receptor model is well suited for studying Electromagnetic Interference and Electromagnetic Compatibility of Magnetic Transmission Lines [22] - [26]. The results can be compared with mathematical formulas to build linear circuit models [18] for cross talk between Magnetic Transmission Lines [22] - [26]. The aim will be to minimize Electromagnetic Radiation; that can be picked up by intentional receivers like Radio and Television; or unintentional receivers like digital Computers. This will prevent malfunction of the sensitive electronic equipment.

Power Flow Equations for Magnetic Transmission Lines [22] - [26] will help to compare the Electromagnetic and Magnetic circuit models. The Power Flow will be represented in the form of Magnetic displacement current and Magnetic Voltage for circuit Model. For the Electromagnetic Model, the Power Flow will be represented in the form of Magnetic Field and Electric Field. Accurate Estimation of Lumped parameters; like per unit length transverse impedance and the per unit length longitudinal admittance is necessary for producing a valid lumped magnetic circuit [18] for Magnetic Transmission Lines [22] - [26].

The overview of the simulation algorithm is shown in Figure 33.

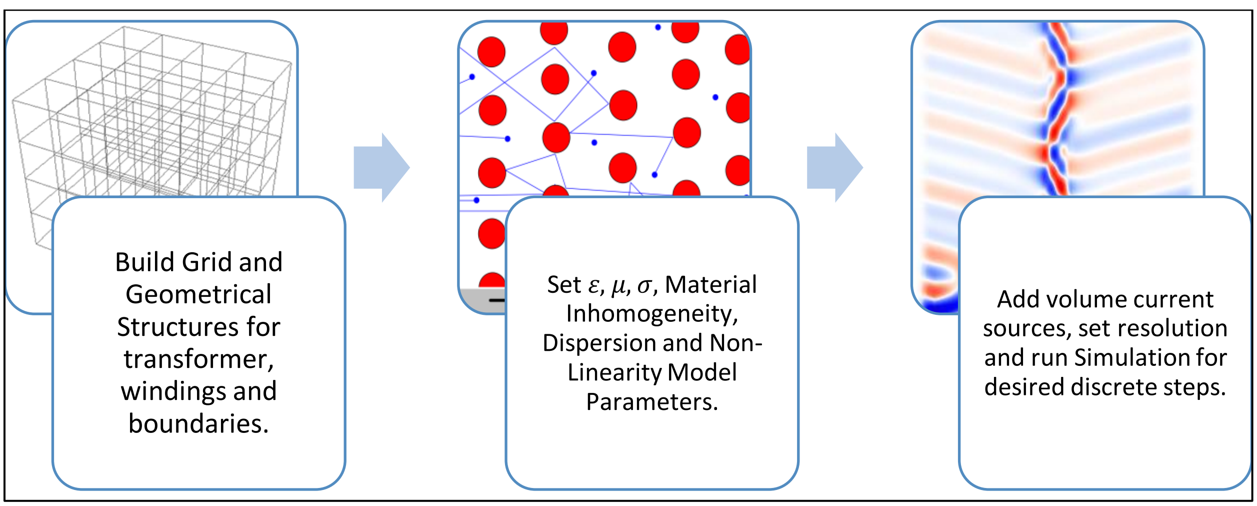

Figure 33: Overview of MEEP algorithm for simulation of Magnetic Transmission Line

The Magnetic Transmission Line [22] - [26] will be constructed for studying inhomogeneous, dispersive [72], [16], non-linear [40] ferromagnetic substances [8] like manganese, zinc, nickel and cobalt alloys. The Transmission Lines will be excited using continuous current sources. The terminations can be modeled by Perfectly matched layers for complete absorption; or as perfect reflectors for no load.

The relative permittivity of the Magnetic Transmission Line is 10 and the electric conductivity is $5 \times 10^{-3} S/m$. The magnetic permeability is a function of frequency as in Equation 4.23.

$$\mu(\omega, x) = \mu_\infty(\boldsymbol{x}) + \frac{\sigma_0(\boldsymbol{x})\omega_0^2}{\omega_0^2 - \omega^2 + j\omega\gamma_0} \tag{5.1}$$

where $\mu_\infty(\boldsymbol{x}) = 1$, $\sigma_0(\boldsymbol{x}) = -500$, $\omega_0 = 1\ GHz$, $\gamma_0 = 1$

The geometry of the simulated Magnetic Transmission Line is shown below. The electric current source is represented by a current loop at z = 0 mm. The magnet flux and magnetic displacement current flows in the z-direction.

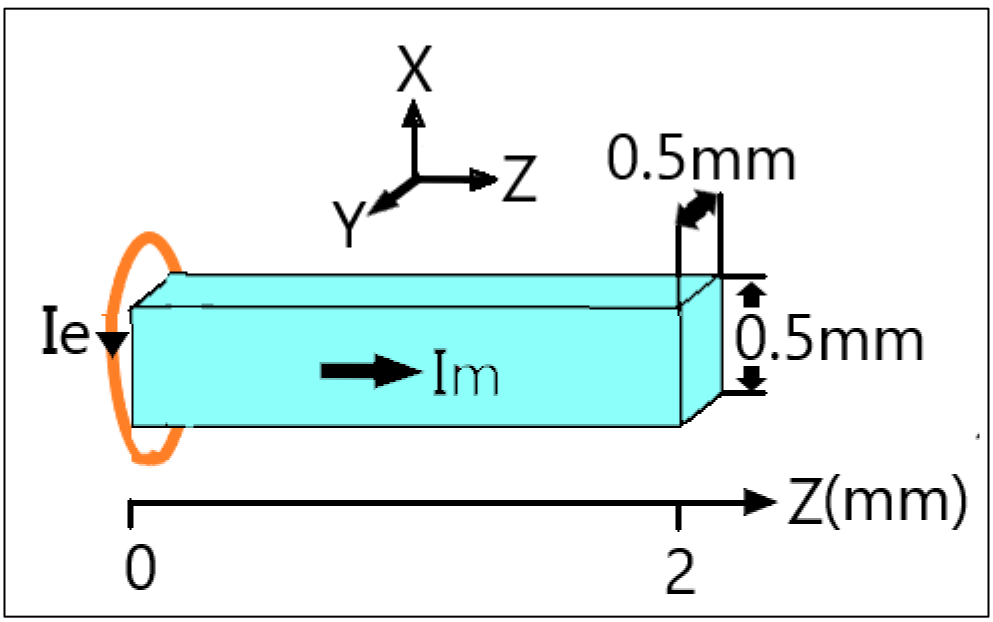

Figure 34: Geometry of Simulated Magnetic Transmission Line and Current Source

5.1.1.Visualization of Electromagnetic Fields

The Longitudinal Fields of the simulated transmission line are shown in the table below.

	Component		
Field	X	Y	Z
H	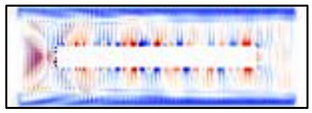	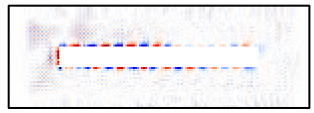	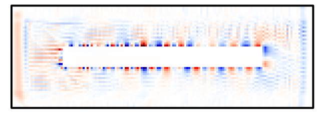
B	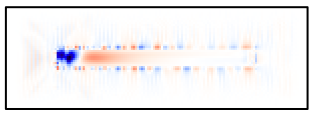	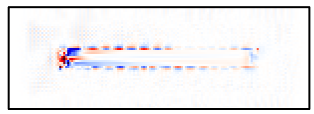	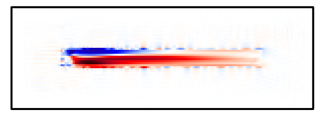
E		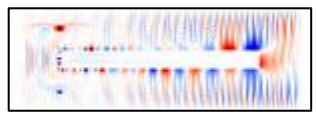	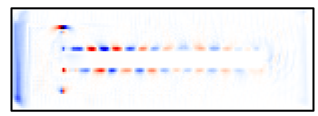
D		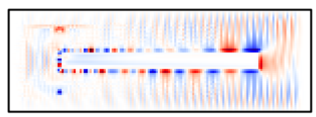	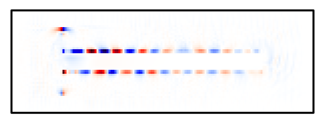

The magnetization fields Hx, Hy and Hz are almost zero inside the magnetic transmission line due to high magnetic permeability of the ferromagnetic material. The longitudinal magnetic field Bz is very intense inside the transmission line as a large amount of flux flows through it. The intense longitudinal Hx field around the transmission line results due to magnetic flux leakage. The transverse Ex, Ey, Dx and Dy show that electric fields encircle the transmission line.

The Transverse Fields of the simulated transmission line are shown in the table below.

	Component		
Field	X	Y	Z
H	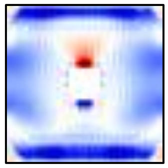		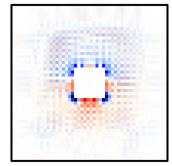
B	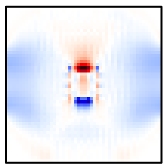	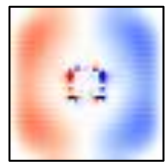	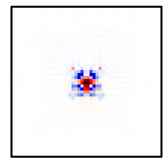
E	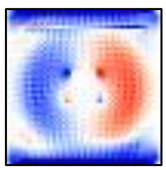	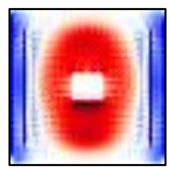	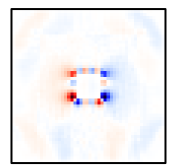
D	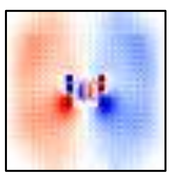		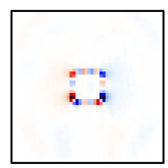

The magnetization fields Hx, Hy and Hz are almost zero inside the magnetic transmission line due to high magnetic permeability of the ferromagnetic material. Intense Transverse Hx and Hy fields show that H field radiates out from the magnetic transmission line in straight paths. The Magnetic Flux Density Bz is mainly confined inside the transmission Line. Bx and By components result from the magnetic leakage flux. The transverse Ex, Ey, Dx and Dy show that electric fields encircle the transmission line.

5.1.2. Variation of Permeability with Frequency

The variation of Permeability with frequency is shown in the figure 35. The relative permittivity of the Magnetic Transmission Line is 10 and the electric conductivity is $5 \times 10^{-3} S/m$.

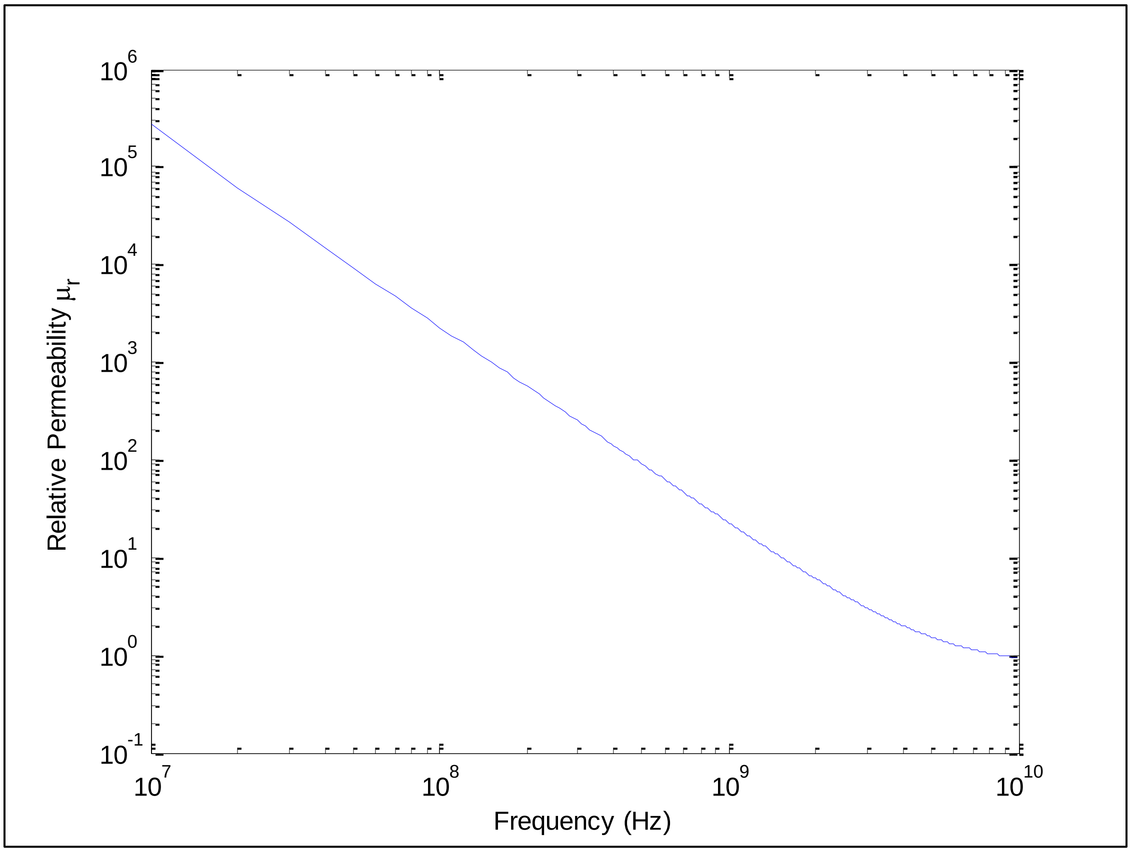

Figure 35: Variation of relative Permeability with applied Magnetic Field

5.1.3. Attenuation of Magnetic Field along the direction of propagation

The diagram below shows the decay of Magnetic Field along the length of the Magnetic path. The wave front of the axial Magnetic Field evolves over time, spreading across the length of the line. The field is plotted in logarithmic scale to show the decay of the wave front as it propagates. When the wave front hits the opposite end, it is reflected so the final profile approaches a standing wave of constant magnitude as shown in Figure 36.

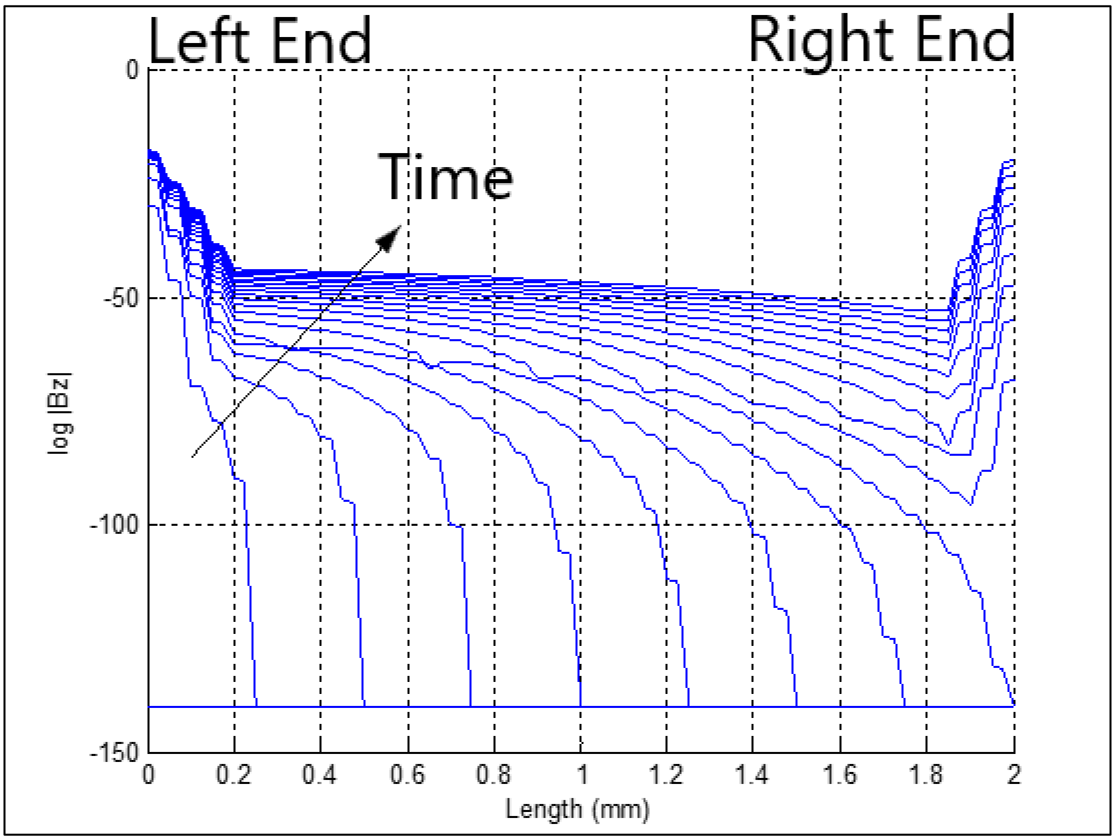

Figure 36: Evolution of pulse wave front across the length of the transmission line

5.1.4. Skin Effect in Magnetic Transmission Line

The Electromagnetic fields decay very strongly inside the lossy transmission line due to skin effect.

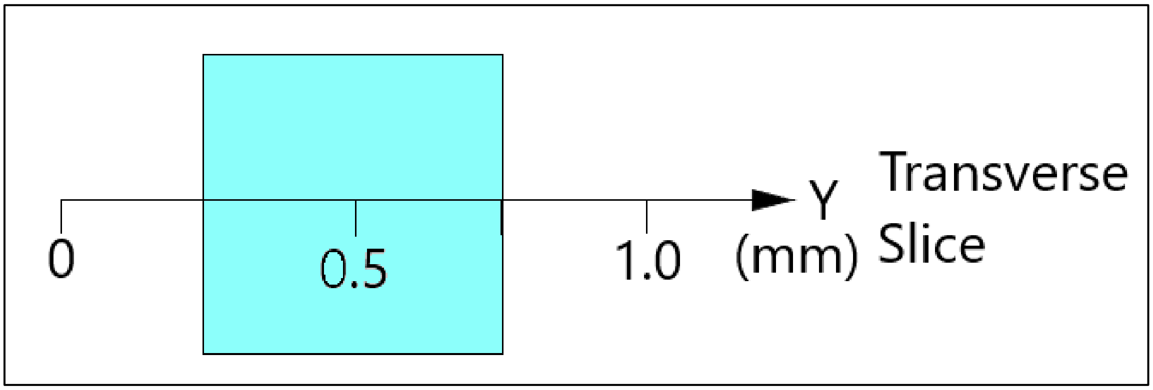

Figure 37: A Transverse slice of the Magnetic Transmission Line

The amplitudes of fields are plotted for a transverse slice of the ferromagnetic material in the Figure 38. The fields attenuate exponentially inside the ferromagnetic material. The attenuation increases at high frequencies.

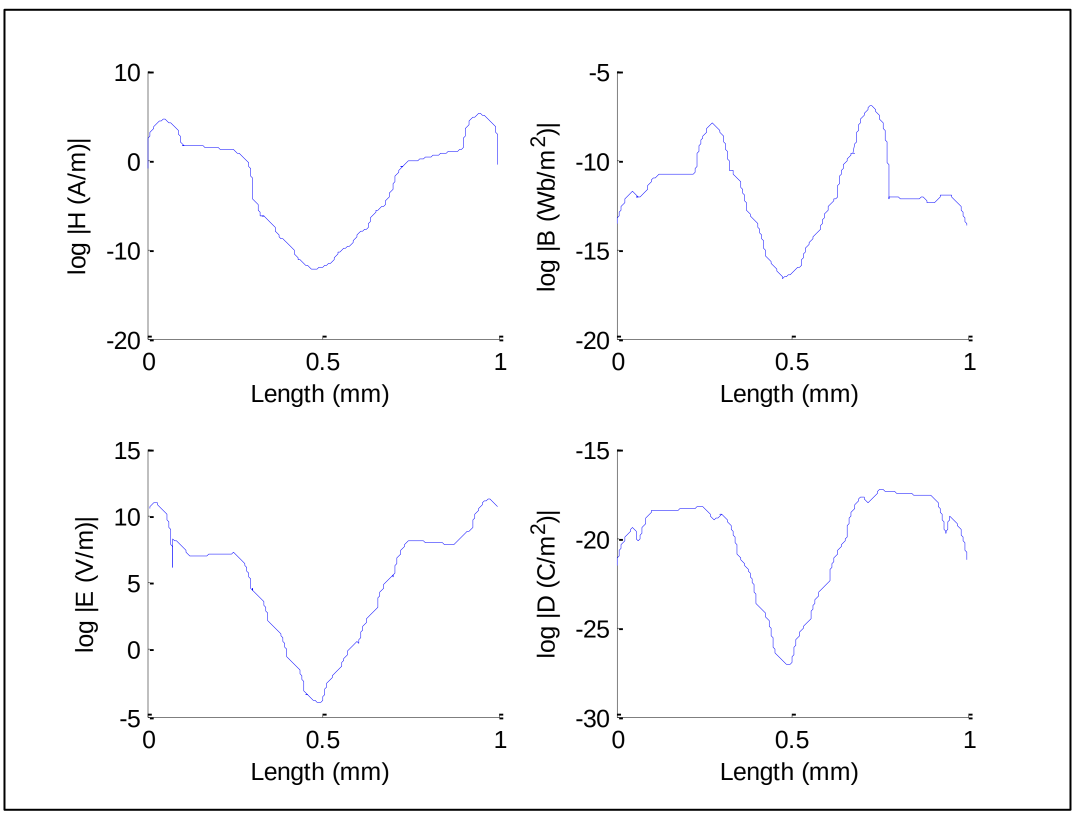

Figure 38: Decay of Electromagnetic Fields inside the lossy Magnetic Material

5.1.5. Evolution of Magnetic displacement current and Voltage

The evolution of magnetic voltage and current is shown in Figure 39.

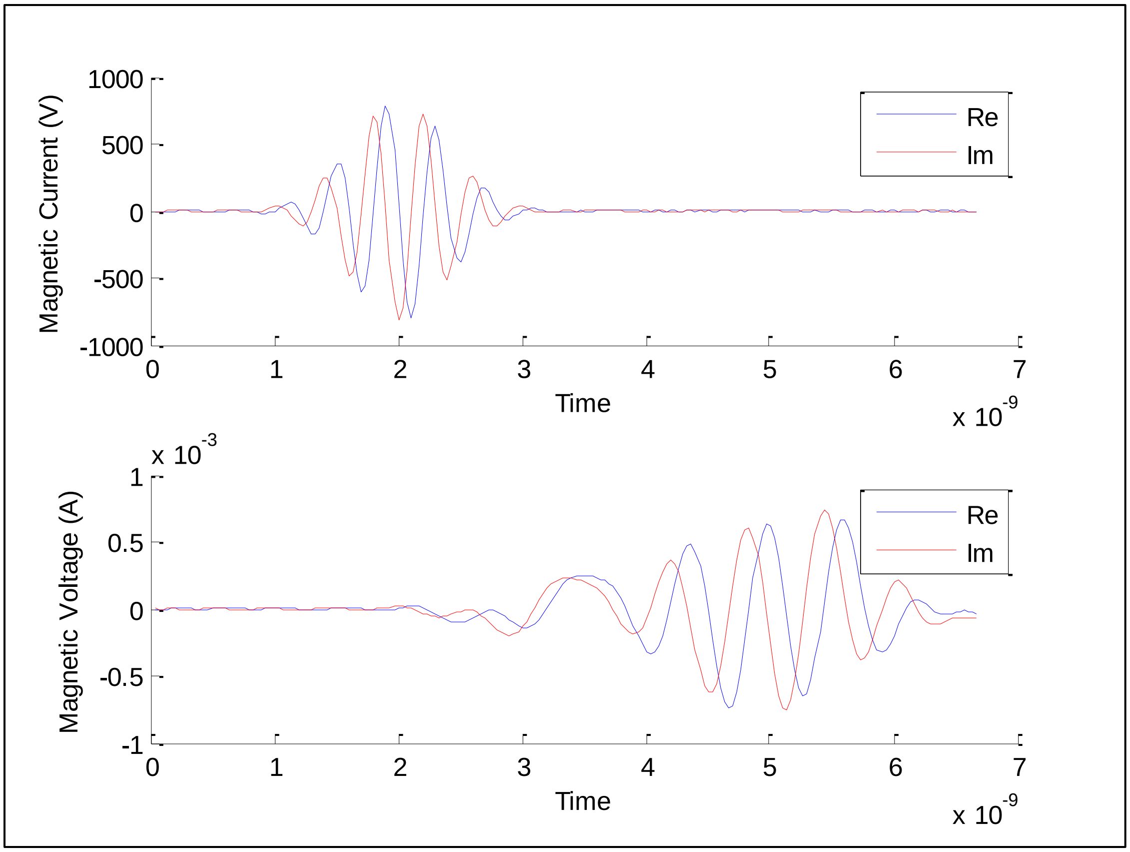

Figure 39: Evolution of Magnetic displacement current and Magnetic Voltage upon application of Gaussian Pulse

The magnetic voltage lags the magnetic current because the transmission line acts as an inductor which resists changes in magnetic voltage.

5.1.6. Intrinsic Wave Impedance of Magnetic Transmission Line

The intrinsic wave impedance was calculated using the following relationship:

$$Z_w(j\omega) = \frac{E_x(d)}{H_x(d)} = \sqrt{\frac{j\omega L_T}{G_L + j\omega C_L}} \tag{5.2}$$

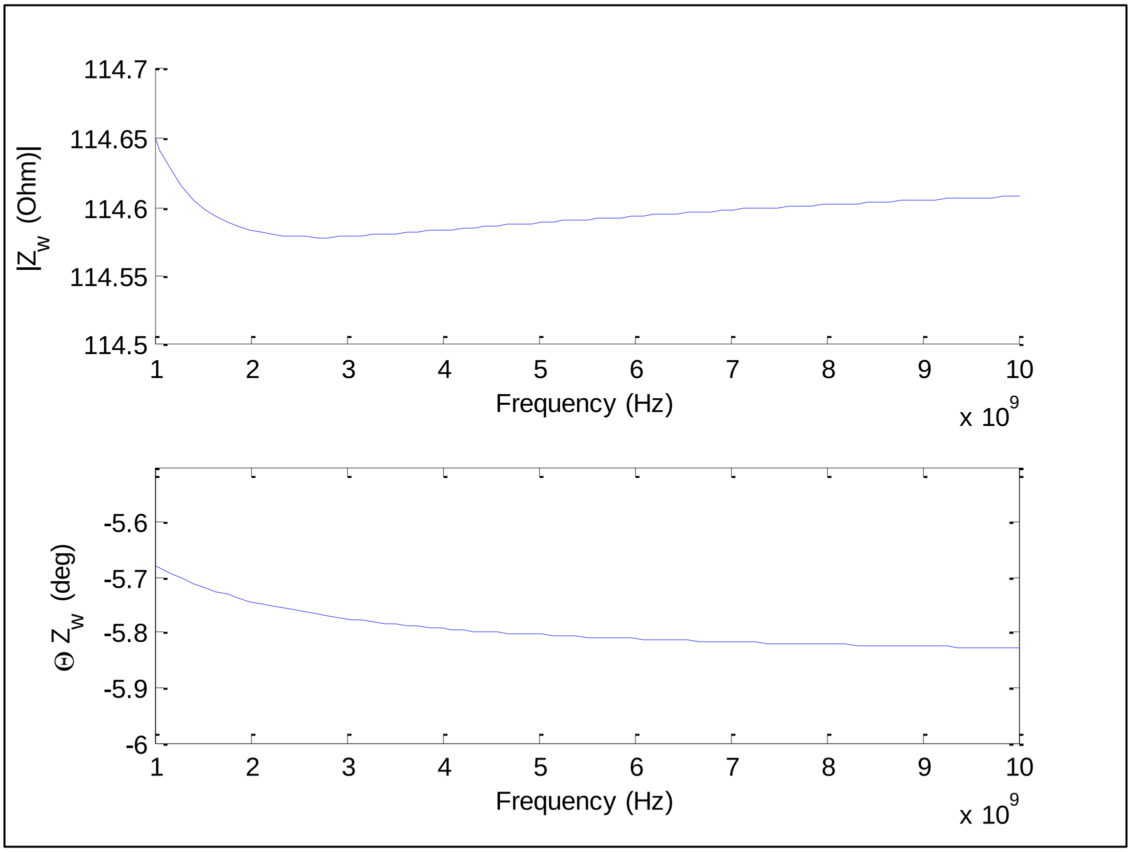

Figure 40: Variation of wave impedance magnitude and angle with frequency

The intrinsic wave impedance is high at low frequencies because of high agnetic permeability. At 10GHz, the core saturates and the intrinsic impedance approaches the estimated value of $\frac{377}{\sqrt{\varepsilon_r}} = \frac{377}{\sqrt{10}} = 119\Omega$.

5.1.7. Attenuation Constant and Phase Constant of Magnetic Transmission Line

The Attenuation constant was calculated using the following relation:

$$\gamma(j\omega) = \frac{-1}{L}\log\left(\frac{H_x(d=L)}{H_x(d=0)}\right) = \sqrt{(j\omega L_T)(G_L + j\omega C_L)} = \alpha + j\beta \tag{5.3}$$

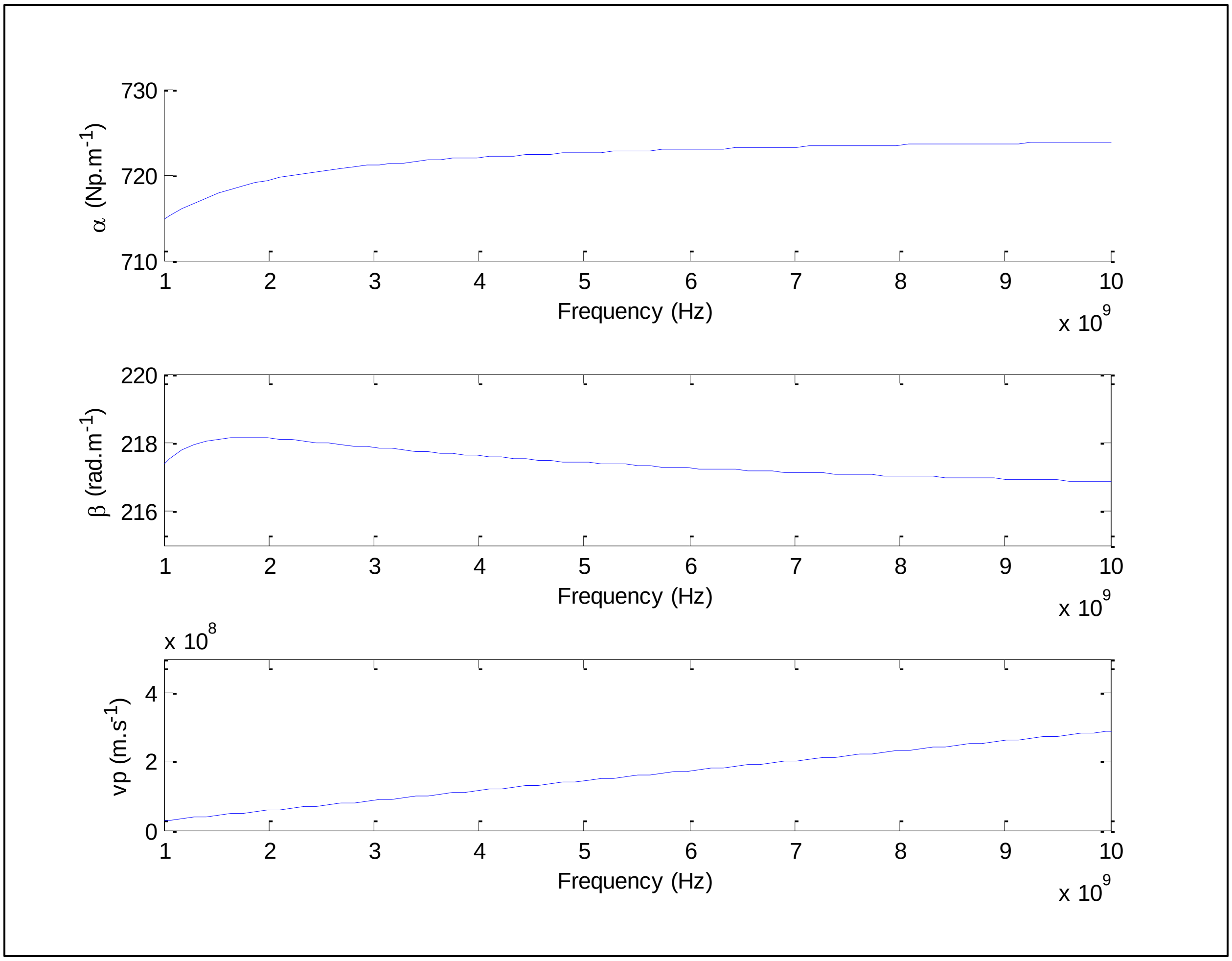

Figure 41: Variation of Attenuation Constant, Phase Constant and Phase Velocity with frequency

In Figure 41, the attenuation constant increases with frequency since the magnetic conductivity increases. As frequency increases, the phase constant drops because the magnetic permeability decreases sharply. The phase velocity approaches the free space velocity $3 \times 10^8\ m/s$ as the core saturates.

5.1.8. Magnetic Admittance of Magnetic Transmission Line

The Magnetic Admittance was calculated using the following relationship:

$$\frac{\gamma(j\omega)}{Z_w(j\omega)} = \sqrt{(j\omega L_T)(G_L + j\omega C_L)}\sqrt{\frac{G_L + j\omega C_L}{j\omega L_T}} = G_L + j\omega C_L = \frac{\mathcal{R}_{mskin}}{j\omega} + j\omega C_L \quad (5.4)$$

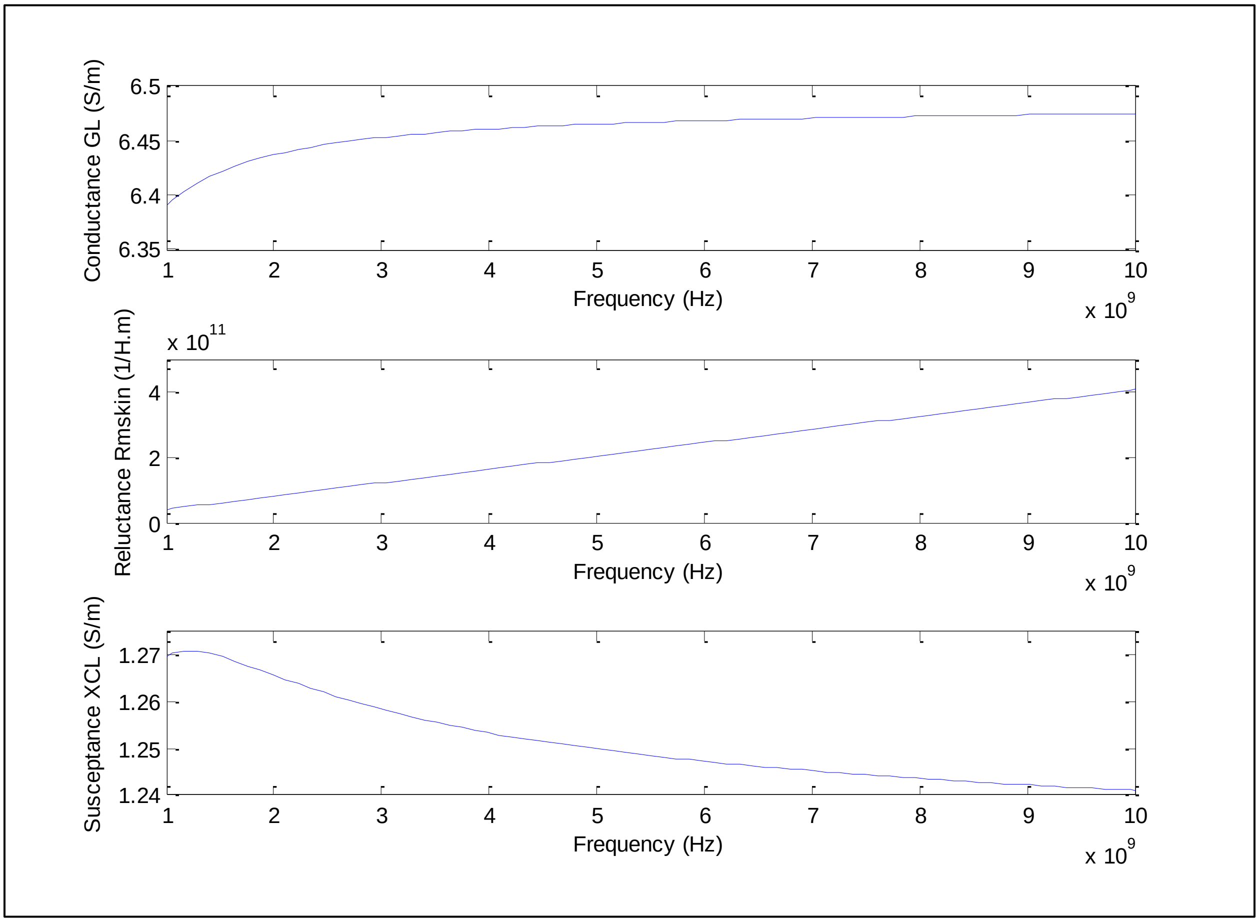

Figure 42: Variation of Magnetic Conductance, Magnetic Reluctance and Magnetic Capacitance with frequency

The Magnetic Conductance and magnetic susceptance are complex functions of material permittivity, permeability and geometry. As seen in Figure 42, the Magnetic reluctance increases with frequency hence magnetic losses increase as well.

5.1.9. Magnetic Impedance of Magnetic Transmission Line

The Magnetic Impedance was calculated using the following formula:

$$Z_w(j\omega)\gamma(j\omega) = \sqrt{(j\omega L_T)(G_L + j\omega C_L)}\sqrt{\frac{j\omega L_T}{G_L + j\omega C_L}} = j\omega L_T \quad (5.5)$$

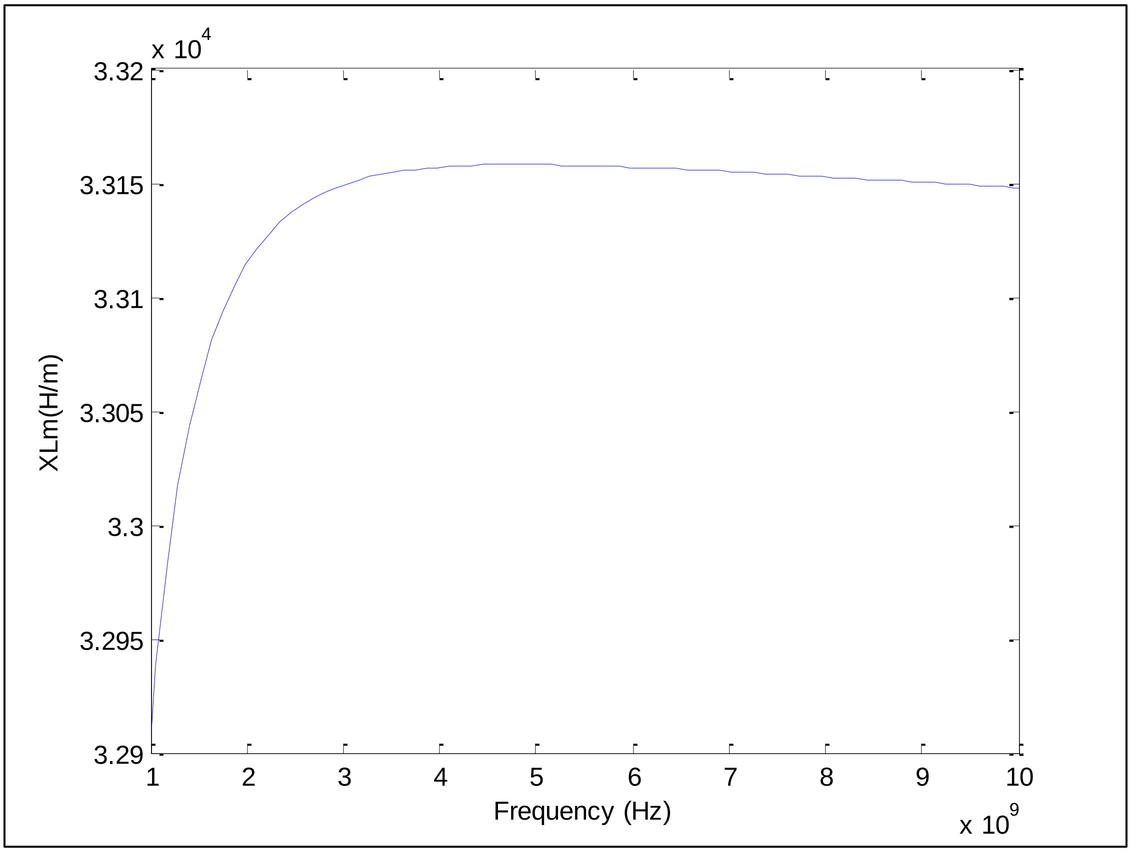

Figure 43: Variation of Magnetic Inductance with frequency

As seen in Figure 43, the Magnetic reactance is small at low frequencies. As the frequency is increased, it starts increasing at first, but soon the permeability decreases and the reactance drops. This is responsible for high frequency droop in wideband transformers.

The next section will discuss the application of these results for predicting the frequency response of a 300 MHz – 3 GHz wideband transformer.

5.2. Introduction to Wideband Transformers

Wideband Transformers are widely used in RF Electronics for voltage, current and impedance matching of unbalanced loads [35-36], [31], [29]. They provide DC isolation and common mode rejection for efficient AC transmission [67], [17], [14].

Wideband Transformers [29] provide impedance matching for interfacing different systems through accurate current and voltage transformation [35-36], [14]. The impedance transformation ratio is dictated by the square of the effective turns ratio between the primary and secondary side [31], [67].

Unlike an unbalanced network, a balanced network has none of its terminals connected to ground. It is difficult to interface balanced systems with unbalanced systems due to common mode currents [67], [31]. Balun transformer is used for providing DC isolation and maximum power transfer between a balanced and an unbalanced system. A Unun transformer is used for interfacing two unbalanced impedances, whereas a Balbal transformer connects two balanced systems [14].

Usually wideband transformers [29] are required in high frequency communication applications that require processing of small amounts of RF power in a wide frequency range [35-36], [17], [14], [31], [67]. For high power applications in Base Station Amplifiers, Repeaters, Satellites, Radar and VFDs, the power limitations of the core and winding must be controlled along with the parasitic losses [35-36], [65], [31], [20].

1. Telecommunication Applications: 4G, CDMA, EDGE, GSM, LMDS, LTE, MMDS, Handsets (Cellular, PHS, DECT, TV), Node B, Pagers, TD-SCDMA, TMA, UMTS, W-CDMA, Wi-Fi, WiMAX, Wireline (DSL, ADSL, DSLAM etc.), W-LAN, WLL.
2. Automotive Applications: IVHS, GPS, Tracking
3. Wireless Communication: Audio Systems, AMR, EPIRB, Marine Radar, Marine GPS, RFID Reader/ TAGS, Security Monitoring Systems, Radio Astronomy, Jammers.
4. STATCOM: DBS, LNBs, MODEMs, TMBs, V-SAT.
5. Medical Applications: CT, MR, Ultrasound, Telemetry.
6. Cable/ CATV and Broadband Fiber Communication: BPON, Cable (Set Top Box), Fiber Optic, FTTH, GPON, Hybrid Fiber Coax Network, MOCA.
7. Broadcast Applications: Radio, TV, LMDS.
8. Avionics: Radar, Surveillance Radar, MLS, TACAN, TCAS.

The performance of a wideband transformer [35-36], [29], [14], [17] can be analyzed by the following performance parameters:

Bandwidth is the range of frequencies between the two maximum allowable attenuation (1 dB/ 2 dB/ 3 dB) points f_{min} and f_{max} [31]. A high fractional bandwidth $\frac{f_{max}}{f_{min}}$ of 1000 or more can only be achieved if the primary and secondary windings are strongly coupled [29], [35-36], [67]. Besides attenuation, wideband transformer may also introduce undesirable phase noise in the system causing distortion of RF signal. The transformer must be designed to have a flat phase response in the desired frequency range [65], [31].

Insertion Loss is the ratio of power transfer between the source and an ideal load upon direct connection; and when the transformer is used for the connection. It is indicative of the power loss through the transformer under matched conditions [67], [35-36], [31]. For a typical wideband transformer, the insertion loss increases at low frequencies due to the low magnetizing reactance [29]. At high frequencies, the insertion loss increases due to the inter-winding capacitance and the leakage inductance [65], [29], [20]. Often, mid-band insertion loss (e.g. 0.5 dB) is taken as reference value [31], [67].

$$Insertion\ Loss = 10\ log_{10} \frac{P_{Load}(Direct\ connection\ between\ source\ and\ ideal\ load)}{P_{Load}\ (Transformer\ inserted\ between\ source\ and\ ideal\ load)} \quad (5.6)$$

Return Loss is the ratio of applied power and reflected power due to impedance mismatch between the source and load [31]. Optimal impedance matching must maximize the return loss (e.g. 14 - 25 dB) over the entire operational bandwidth i.e. minimum input power must be reflected back to the source [35-36], [67], [65], [29].

$$Return\ Loss = 10\ log_{10} \frac{P_{source}}{P_{reflected}} \quad (5.7)$$

Amplitude balance is the absolute difference in signal amplitude between the outputs of a center-tapped transformer [35-36], [67], [65], [29], [31].

Phase balance is the absolute difference in signal phase between the outputs of a center-tapped transformer [35-36], [67], [65], [29], [31].

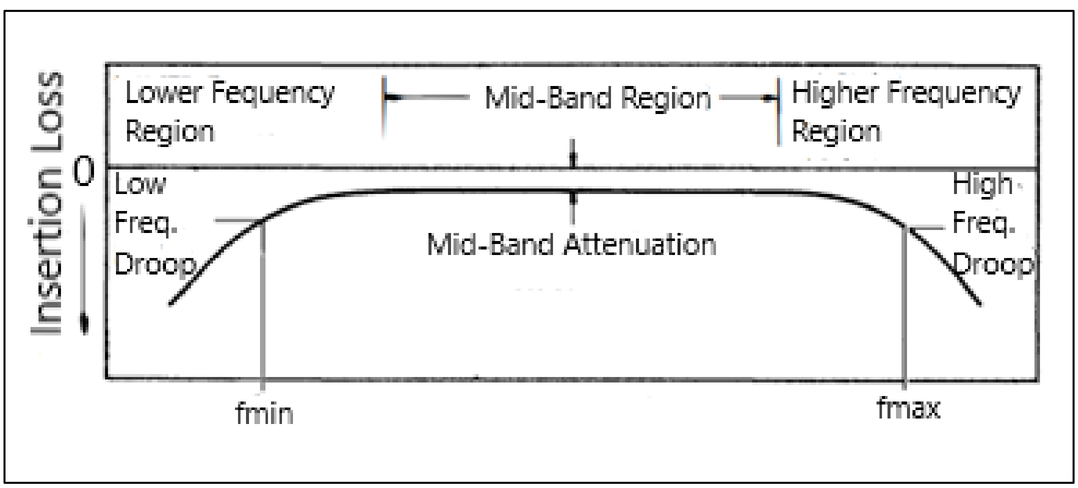

Figure 44: Variation of Wideband Transformer Insertion Loss with frequency

5.2.1.Electrical Circuit for Wideband Transformer

The equivalent electrical circuit diagram of a wideband transformer [35-36], [67], [31], [17], [14] is given below.

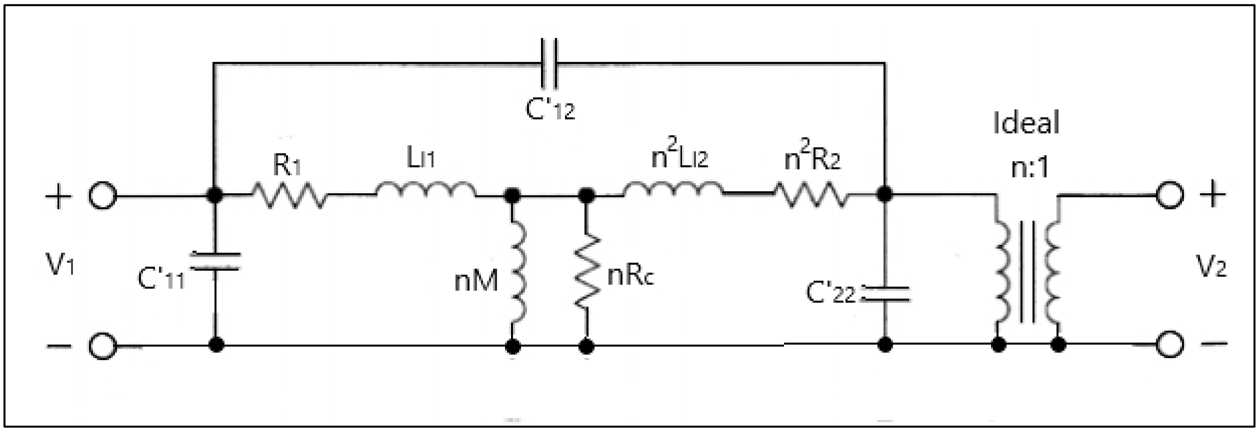

Figure 45: Electrical circuit for wideband transformer

In Figure 45,

L_{l1}represents the primary leakage inductance.

n^2L_{l2} represents the secondary leakage inductance referred to the primary side.

R_1represents the primary winding resistance.

n^2R_2 represents the secondary winding resistance referred to the primary side.

$nR_c$is the shunt resistance representing core loss.

nM is the magnetizing inductance of the core.

$C'_{11}$is the shunt capacitance associated with the primary windings.

C'_{22} is the shunt capacitance associated with the secondary windings.

C'_{12} is the capacitance between the primary and secondary windings.

The operation of wideband transformer [29], [17], [14] can be divided into three distinct segments:

1. Low Frequency Region: The low frequency droop in the transfer characteristics is attributed to the diminishing shunt magnetizing reactance [67], [31], [29]. The loss can be reduced by inserting capacitance in series with the primary or secondary winding [65], [31], [35-36].

2. Mid-band Region: The parasitic inductances and capacitances can be ignored in the mid-band region [31]. The response is mainly effected by the series resistance of the windings and the shunt resistance of the core [67], [65], [35-36], [29].

3. High Frequency Region: The high frequency droop results from the losses in leakage inductances and shunt capacitances of the windings [31]. The reactance of leakage inductances increases greatly whereas the reactance of shunt capacitance decreases at high frequencies [67], [65], [29], [35-36].

5.2.2. Magnetic Circuit for Wideband Transformer

The Magnetic circuit for the Wideband Transformer is shown below. It consists of a primary gyrator with gyration constant Np. The secondary side gyrator has a gyration constant of Ns.

The magnetic core is represented by a short transmission line section consisting of longitudinal Magnetic Capacitance C_L which stores electric energy, longitudinal Magnetic Conductance G_L which dissipated energy and Transverse Magnetic Inductance L_T which stores magnetic energy.

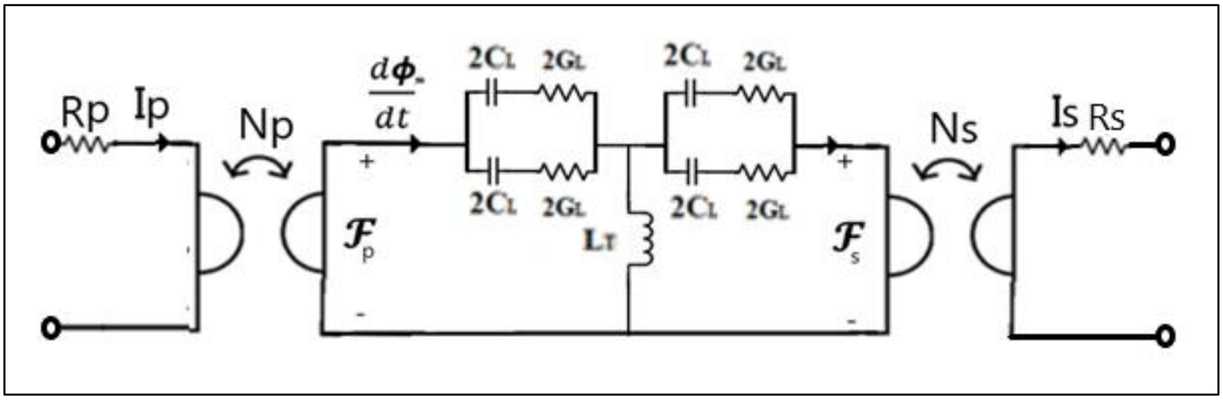

Figure 46:Magnetic circuit for wideband transformer based on small magnetic transmission line

The operation of wideband transformer can be divided into three distinct segments:

1. Low Frequency Region: The low frequency droop in the transfer characteristics is attributed to the diminishing shunt magnetizing reactance and high series capacitive reactance.

2. Mid-band Region: The parasitic inductances and capacitances can be ignored in the mid-band region. The response is mainly effected by the series resistance of the windings.

3. High Frequency Region: The high frequency droop results from increased losses in series conductance of the windings. The reactance of shunt inductance decreases greatly whereas the permeability drops at high frequencies.

5.2.3. Simulation of Wideband Transformer in MEEP

In this section, a 300 MHz – 3 GHz wideband transformer will be simulated to study the effects of Magnetic Transmission Lines parameters on its frequency response.

Wideband transformers [29], [14], [17] pass a frequency band of several decades and are usually designed to handle complex waveforms like rectangular pulses [67], [59]. They are used for impedance matching, voltage/ current transformation, DC isolation, mixing, power splitting, coupling and signal inversion [65], [31].

The 300 MHz – 3 GHz wideband transformer [14], [17] will be excited by a small Gaussian pulse to examine the Frequency Response [67], [59]. The 3 dimensional discrete Fourier Transform will be used to determine Transmittance and Broadband Response [67], [65], [59], [50], [17], [29], [31]. The MEEP algorithm is explained in the Figure 47.

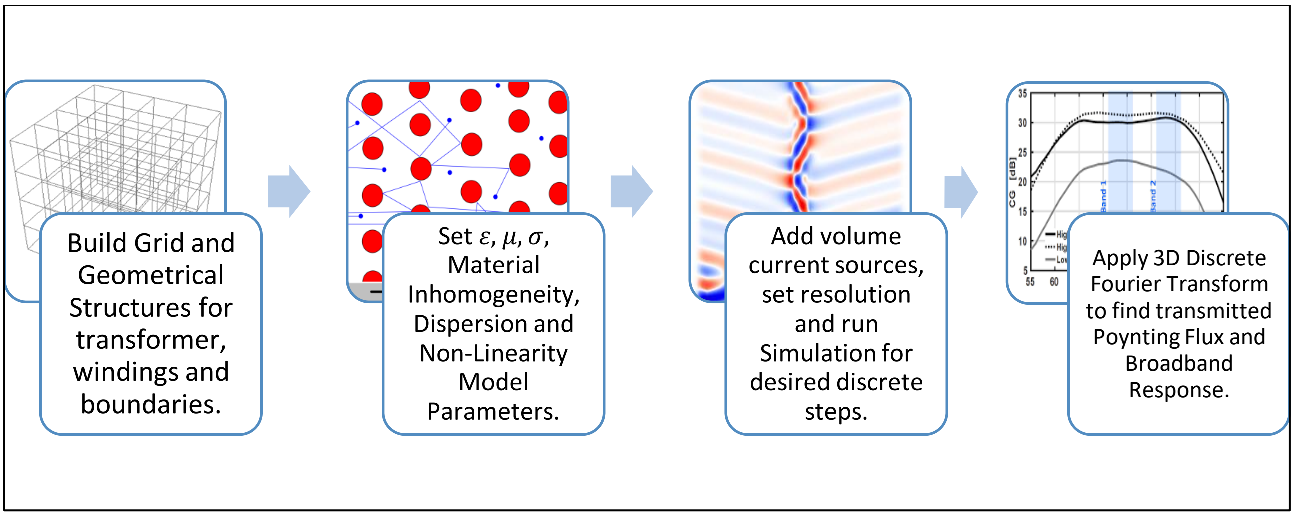

Figure 47: Outline of MEEP Algorithm for simulation of wideband transformer

The Geometry of the simulated wideband transformer is shown in Figure 48.

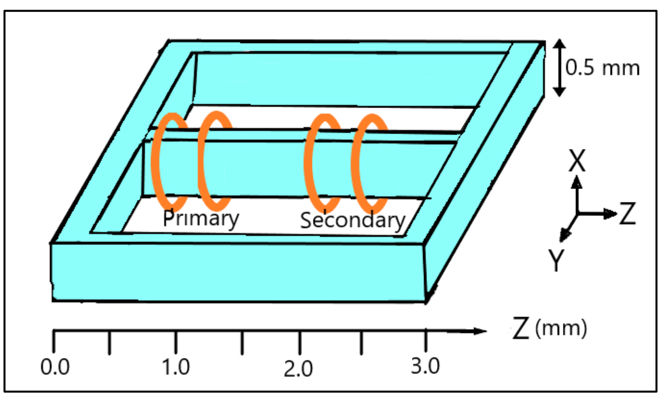

Figure 48: Geometry of wideband transformer simulated in MEEP

5.2.4. Visualization of Electromagnetic Fields

The Transverse Fields of the wideband transformer are shown in the table below.

	Component		
Field	X	Y	Z
H	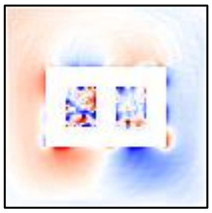	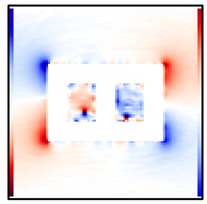	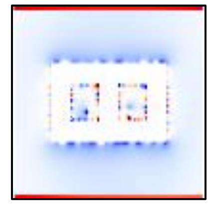
B	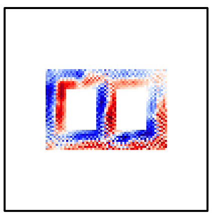	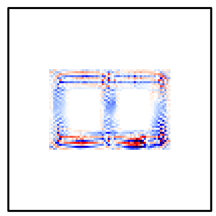	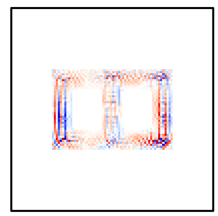
E	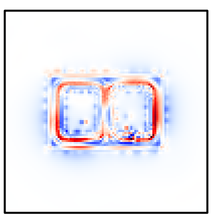	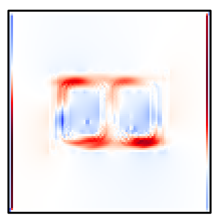	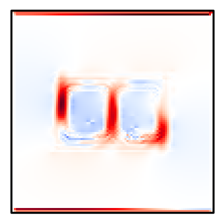
D	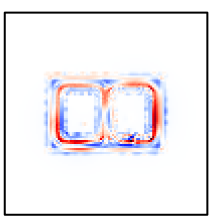	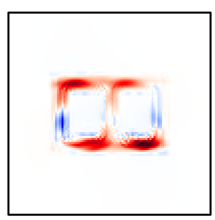	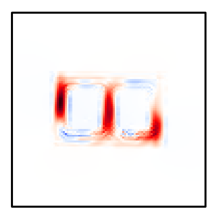

The Hx, Hy and Hz fields are zero inside the core due to high magnetic permeability. The magnetic flux density is intense inside the core as magnetic flux takes the least resistive path. The longitudinal magnetic capacitance is responsible for storing electric energy in E field while the transverse magnetic inductance stores the magnetic energy in H field.

5.2.5. Calculating Bandwidth of Wideband Transformer

The discrete Fourier Transform of the flux linkage of primary winding and secondary winding was used to determine the Insertion loss of the Wideband Transformer shown in Figure 49.

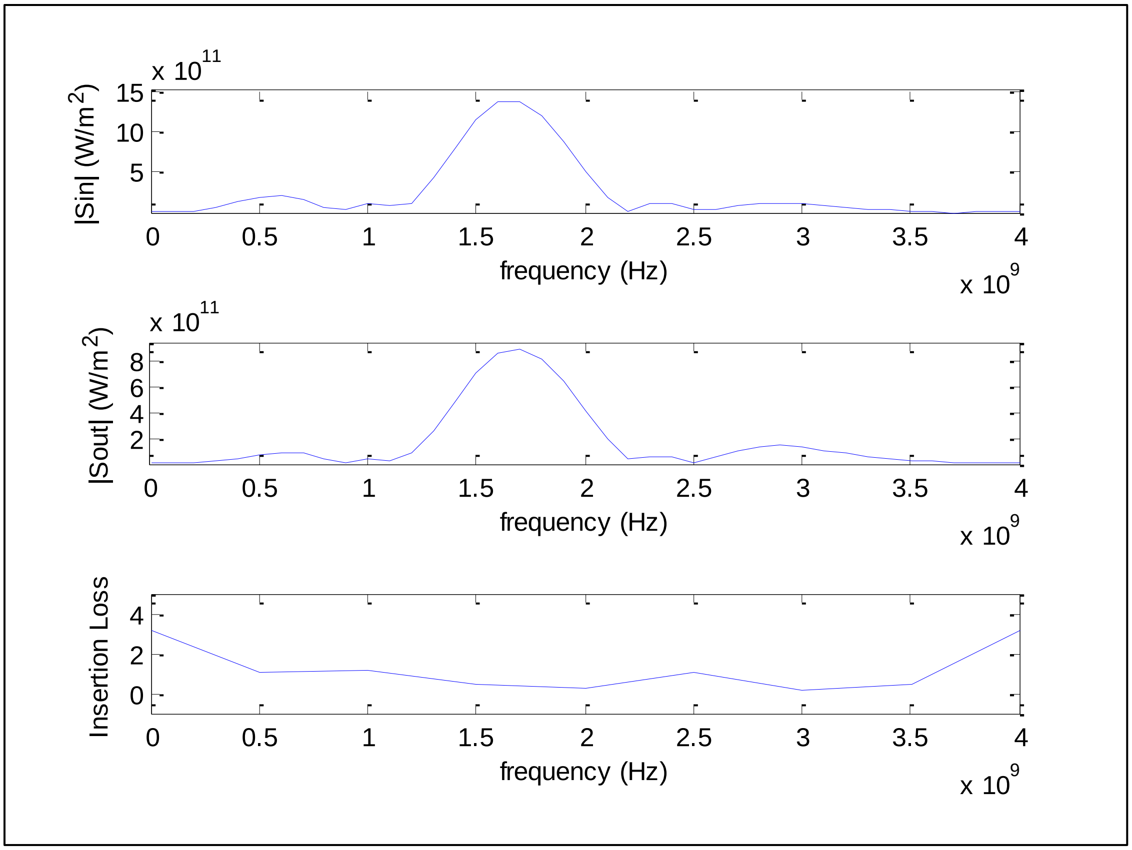

Figure 49: Input Poynting Flux, Output Poynting Flux and insertion loss of wideband transformer

The low frequency droop below 300 MHz in the transfer characteristics is attributed to the diminishing shunt magnetizing reactance and high series capacitive reactance.

The mid-band insertion loss is attributed to loss across the magnetic conductance.

The attenuation constant increases with frequency since the magnetic conductivity increases. As the frequency is increased, the permeability decreases and the shunt magnetic reactance drops. The Magnetic reluctance increases with frequency hence magnetic losses increase as well. This is responsible for high frequency droop above 3.5 GHz in the wideband transformer.

6. Conclusion

This chapter presented three different models for modeling magnetic elements. The age old reluctance model based on the Ohm’s law analogy was found to violate power invariance property. An application of modeling a DC compounded generator was presented as well and the was only suitable for steady state simulations of magnetic cores with known reluctance profile.

The Permeance-Capacitance model uses a nonlinear permeance to model nonlinearity and hysteresis losses of magnetic materials. It is valuable for simulating transient behavior of Ferromagnetic elements like RF inductors, transformers and filters. A full bridge isolated Buck converter was designed to study its response. The model can be improved as it does not feature an electric energy storage element or an energy dissipation element.

The third model was the magnetic transmission line model which is the most accurate model for modeling dispersive, inhomogeneous and lossy magnetic cores. It uses Transmission Line theory to predict magnetic parameters of ferromagnetic core. The MEEP simulation results for a 300MHz – 3 GHz wideband transformer were presented to verify Magnetic Transmission Line theory. The model was very useful in predicting the frequency response of the wideband transformer. The simulator could not model Magnetostriction, Accoustic effects, Relativistic Effects, Piezomagnetism and Gravitomagnetism

Troughout this research, non-linear [40] components were used for simulating complex effects such as DC Resistance Losses, Skin Effect Losses, Proximity Effect Losses, Self-Capacitance Dielectric Losses, Self-Capacitance Circulating Currents Losses, Core Residual Losses, Core Eddy Current Losses and Core Hysteresis Losses. Network Equivalent Magnetic circuits [18] and coupled equations were used to simplify analysis of the transient [9] and steady state behavior.

The conclusion of the research is that magnetic coupling between magnetic transmission lines [22] - [26] results in sharing of electromagnetic energy. This division of power is very useful in design of DC and AC machines, DC converters and high frequency wideband transformers. The study of capacitive and inductive coupling in Multi-Conductor Transmission Lines provides useful knowledge about the Radiated/ Conducted Emissions and Radiated/ Conducted Susceptibility.

The power invariant Magnetic Transmission Line model [22] - [26] can also be used for accurate modeling of AC and DC Machines [20], Micro-strip Antennas, Gyromagnetic NLTLs [71], [62], [61], [54], Magnetic Transistors, Spintronic devices etc. Due to the versatility of the Magnetic Transmission Line model, different Transmission Line structures can be simulated like shielded transmission line and multi-wire transmission lines.

7. References

[1] H. Al-Barqawi, N. Dib and M. Khodier, “A Full-Wave Two-Dimensional Finite-Difference Frequency-Domain Analysis of Ferrite-Loaded Structures”. Mosharaka International Conference on Communications, Propagation and Electronics, 2008.

[2] J. Allmeling, W. Hammer, and J. Schonberger, “Transient simulation of magnetic circuits using the permeance-capacitance analogy,” *2012 IEEE 13th Workshop on Control and Modeling for Power Electronics (COMPEL)*, 2012.

[3] B. Anderson and R. Newcomb, “A capacitor-transformer gyrator realization,” *Proceedings of the IEEE*, vol. 53, no. 10, 1965.

[4] G. Antonini, “A general framework for the analysis of metamaterial transmission lines.” Prog. Electromagn. Res. B., pp. 353–373, 2010.

[5] J. Atulasimha and S. Bandyopadhyay, *Nanomagnetic and Spintronic Devices for energy-efficient memory and computing*. Chichester, West Sussex: Wiley, 2016.

[6] S. Blundell, *Magnetism in condensed matter*. Oxford: Oxford University Press, 2014.

[7] I. Boldea and S. Nasar, *Linear electric actuators and generators*. Cambridge: Cambridge University Press, 1997.

[8] J. Bragg, J. Dickens, and A. Neuber, “Material selection considerations for coaxial, ferrimagnetic-based nonlinear transmission lines,” *Journal of Applied Physics*, vol. 113, no. 6, 2013.

[9] M. Brignone, D. Mestriner, R. Procopio, A. Piantini, and F. Rachidi, “On the Stability of FDTD-Based Numerical Codes to Evaluate Lightning-Induced Overvoltages in Overhead Transmission Lines,” *IEEE Transactions on Electromagnetic Compatibility*, vol. 62, no. 1, pp. 108–115, 2020.

[10] C. Caloz and T. Itoh, *Electromagnetic Metamaterials: Transmission Line Theory and Microwave Applications*, Wiley-IEEE Press, pp. 27-58, 2006.

[11] S. Chapman, *Electric machinery fundamentals*. New York: McGraw-Hill, 2012.

[12] S. Chua, Y. Chong, A. D. Stone, M. Soljacic and J. Bravo-Abad, “Low-threshold lasing action in photonic crystal slabs enabled by Fano resonances” Optics Express, vol. 19, no. 2, 2011.

[13] G. Cividjian, “Corner 2D Capacitance,” *2018 20th International Symposium on Electrical Apparatus and Technologies (SIELA)*, 2018.

[14] R. Darraji, M. Honari, R. Mirzavand, F. Ghannouchi, and P. Mousavi, “Wideband Two-Section Impedance Transformer With Flat Real-to-Real Impedance Matching,” *IEEE Microwave and Wireless Components Letters*, vol. 26, no. 5, pp. 313–315, 2016.

[15] S. Demokritov, *Magnonics: From Fundamentals to Applications.* Berlin: Springer, 2013.

[16] T. Deng and Z. Chen, "Design of frequency-dispersive magnetic material for application of microwave attenuation," *2016 46th European Microwave Conference (EuMC)*, 2016.

[17] D. Dinulovic, M. Shousha, M. Haug, and K. Shafey, "Miniaturized Planar Transformer Embedded in Ferrite Substrate for Isolated High- Frequency Low-Power Applications," *2019 20th International Symposium on Power Electronics*, 2019.

[18] T. Edwards and M. Steer, *Foundations for Microstrip Circuit Design*, 4th ed. Wiley-IEEE Press, pp. 576-607, 2016.

[19] I. Eichwald, S. Breitkreutz, G. Ziemys, G. Csaba, W. Porod, and M. Becherer, "Majority logic gate for 3D magnetic computing," *Nanotechnology*, vol. 25, no. 33, 2014.

[20] R. Erickson, D. Maksimovic, *Fundamentals of Power Electronics*, 2nd ed. Kluwer, 2004.

[21] L. Er-Ping, "Computational Electromagnetics for Electromagnetic Compatibility/ Signal Integrity Analysis", IEEE EMC DL Talk, University of Missouri, 2008.

[22] J. Faria, "Multimodal propagation in multiconductor transmission lines." J. Electromag. Waves Appl. 2014.

[23] J. Faria, "Formulation of Multiwire Magnetic Transmission-Line Theory", Progress in Electromagnetics Research B, Vol. 49, 2013.

[24] J. Faria, "Matrix theory of wave propagation in hybrid electric/magnetic multiwire transmission line systems", Journal of Electromagnetic Waves and Applications, Vol. 29, No. 7, 2015.

[25] J. Faria, "A physical model of the ideal transformer based on magnetic transmission line theory", Journal of Electromagnetic Waves and Applications, Vol. 27, No. 3, 2013.

[26] J. Faria, *Electromagnetic Foundations of Electrical Engineering*, Chichester: John Wiley and Sons, 2008.

[27] A. Goldman, *Modern Ferrite Technology*, New York, NY: Springer, 2010.

[28] G. González and M. Ehsani, "Power-Invariant Magnetic System Modeling," *International Journal of Magnetics and Electromagnetism*, vol. 4, no. 1, pp. 1–9, Dec. 2018.

[29] F. Grecki and B. Wunsch, "Validation of Power Transformer Wideband Modeling Using standard sFRA method with VNA Equipment," *2019 IEEE PES Asia-Pacific Power and Energy Engineering Conference (APPEEC)*, 2019.

[30] A. Guimaraes, *Principles of Nanomagnetism*. Cham: Springer, 2018.

[31] B. Gustavsen, "A hybrid measurement approach for wide-band characterization and modeling of power transformers," *2011 IEEE Power and Energy Society General Meeting*, 2011.

[32] D. Hamill, “Gyrator-capacitor modeling: a better way of understanding magnetic components,” *Proceedings of 1994 IEEE Applied Power Electronics Conference and Exposition - ASPEC94*, 1994.

[33] V. Harris, “Modern Microwave Ferrites,” *IEEE Transactions on Magnetics*, vol. 48, no. 3, pp. 1075–1104, 2012.

[34] M. Holynska, *Single-Molecule Magnets: Molecular Architectures and Building Blocks for Spintronics*. Newark: John Wiley and Sons, 2019.

[35] “IEEE Guide for Loss Evaluation of Distribution and Power Transformers and Reactors," in IEEE Std C57.120-2017 (Revision of IEEE Std C57.120-1991), vol., no., pp.1-53, 18 Oct. 2017.

[36] “IEEE Standard for Pulse Transformers," in ANSI/IEEE Std 390-1987, vol., no., pp.1-32, 14 Oct. 1987.

[37] “IEEE Recommended Practice for Validation of Computational Electromagnetics Computer Modeling and Simulations," in IEEE Std 1597.2-2010, vol., no., pp.1-124, 25 Feb. 2011.

[38] M. Imtaar, P. Li, E. Varga, G. Csaba, G. Bernstein, G. Scarpa, W. Porod, and P. Lugli, “Nanomagnetic logic devices fabrication using nanoimprint lithography,” *2013 13th IEEE International Conference on Nanotechnology (IEEE-NANO 2013)*, 2013.

[39] W. Sui, *Time Domain Computer Analysis of Nonlinear Hybrid Systems*, pp. 251-283, 2018.

[40] S. Karelin, “FDTD analysis of nonlinear magnetized ferrites: application to modeling of oscillation forming in coaxial line with ferrite,” *Radiofizika I Elektronika*, vol. 22, no. 1, pp. 51–56, 2017.

[41] A. Khitun and A. Kozhanov, “Magnonic Logic Devices,” *Nanomagnetic and Spintronic Devices for Energy-Efficient Memory and Computing*, pp. 189–219, May 2016.

[42] M. Leuenberger and D. Loss, “Quantum computing in molecular magnets,” *Nature*, vol. 410, no. 6830, pp. 789–793, 2001.

[43] Y. Li, X. Li, and J. Mao, “Time domain analysis of transmission line based on WLP-FDTD,” *2013 IEEE International Wireless Symposium (IWS)*, 2013.

[44] M. Luo, D. Dujic, and J. Allmeling, “Modelling hysteresis of soft core materials using permeance-capacitance analogy for transient circuit simulations,” *2017 19th European Conference on Power Electronics and Applications (EPE17 ECCE Europe)*, 2017.

[45] M. Luo, D. Dujic, and J. Allmeling, “Modeling Frequency Independent Hysteresis Effects of Ferrite Core Materials Using Permeance–Capacitance Analogy for System-Level Circuit Simulations,” *IEEE Transactions on Power Electronics*, vol. 33, no. 12, 2018.

[46] M. Luo, D. Dujic, and J. Allmeling, “Permeance based modeling of magnetic hysteresis with inclusion of eddy current effect,” *2018 IEEE Applied Power Electronics Conference and Exposition (APEC)*, 2018.

[47] R. Mack and J. Sevick, *Sevick's Transmission Line Transformers: Theory and practice*, 5th ed. Edison, NJ: Scitech Publishing, 2014.

[48] J. Macías-Díaz, "Persistence of nonlinear hysteresis in fractional models of Josephson transmission lines," *Communications in Nonlinear Science and Numerical Simulation*, vol. 53, pp. 31–43, 2017.

[49] A. Moryc and W. Gwarek, "An equivalent lumped circuit describing magnetized plasma and its application in FD-TD modeling," *15th International Conference on Microwaves, Radar and Wireless Communications*, 2004.

[50] M. Nitu, M. Nicola, M. Duta, and M. Benea, "Methods for Determining Dielectric Stresses in the Windings of a Transformer Subjected to Lightning Impulse," *2019 International Conference on Electromechanical and Energy Systems (SIELMEN)*, 2019.

[51] G. Nnachi, A. Akumu, C. Richards, and D. Nicolae, "Estimation of no-Load Losses in Distribution Transformer Design Finite Element Analysis Techniques in Transformer Design," *2018 IEEE PES/IAS PowerAfrica*, 2018.

[52] A. Oskooi, D. Roundy, M. Ibanescu, P. Bermel, J. Joannopoulos, and S. Johnson, "MEEP: A flexible free-software package for electromagnetic simulations by the FDTD method", Computer Physics Communications, Vol. 181, pp. 687-702, 2010.

[53] U. Ozgur, Y. Alivov, and H. Morkoc, "ChemInform Abstract: Microwave Ferrites. Part 2. Passive Components and Electrical Tuning," *ChemInform*, vol. 41, no. 36, Dec. 2010.

[54] J. Parson, A. Neuber, J. Dickens and J. Mankowski, "Investigation of a stripline transmission line structure for gyromagnetic nonlinear transmission line [61] high power microwave sources", Review of Scientific Instruments, Vol. 87, pp. 1-7, 2016.

[55] C. Paul, K. Whites and S. Nasar, *Introduction to electromagnetic fields*, 4th ed. Boston: WCB/McGraw-Hill, pp.586-589, 1998.

[56] C. Paul, *Introduction to Electromagnetic Compatibility*, 2nd ed. Kentucky: John Wiley and Sons, pp. 559-710, 2006.

[57] C. Paul, *Analysis of Multiconductor Transmission Lines*, 2nd ed. Hoboken: Wiley-Interscience, pp. 240-342, 2008.

[58] D. Pozar, *Microwave Engineering*, 4nd ed. Kentucky: John Wiley and Sons, pp. 1-271, 2012.

[59] J. Lehr, P. Ron, *Foundations of Pulsed Power Technology*: John Wiley and Sons, pp. 63–96, Jul. 2017.

[60] P. Ripka and M. Janosek, "Advances in magnetic sensors," *2008 IEEE Sensors*, 2008.

[61] I. Romanchenko, P. Priputnev, and V. Rostov, "RF pulse formation dynamics in gyromagnetic nonlinear transmission lines," *Journal of Physics: Conference Series*, vol. 830, Apr. 2017.

[62] J. Rossi, F. Yamasaki, E. Schamiloglu, and J. Barroso, "Analysis of nonlinear gyromagnetic line operation using LLG equation," *2017 IEEE 21st International Conference on Pulsed Power (PPC)*, 2017.

[63] K. Sato, E. Saitoh A. Willoughby and P. Capper, *Spintronics for next generation Innovative Devices*. John Wiley and Sons, 2015.

[64] J. Schneider, *Understanding the Finite-Difference Time-Domain Method*, p. 33-74, 2017.

[65] N. Shirdel, A. Akbari, H. Mirzaei, and M. Abrishamian, "Three-dimensional simulation of UHF signal propagation in transformer using FDTD method," *2011 International Conference on Power Engineering, Energy and Electrical Drives*, 2011.

[66] R. Slatter, "High accuracy, high bandwidth magnetoresistive current sensors for spacecraft power electronics," *2015 17th European Conference on Power Electronics and Applications (EPE15 ECCE-Europe)*, 2015.

[67] E. Snelling, *Soft Ferrites: Properties and Applications*. Mendham, NJ: PSMA, 2005.

[68] A. Taflove and S. Hagness, *Computational Electrodynamics: The Finite-Difference Time-Domain Method*, 3rd ed. Boston: Artech House, 2005.

[69] A. Taflove, A. Oskooi and S. Hagness, *Advances in FDTD computational electrodynamics: photonics and nanotechnology*, 3rd ed. Boston: Artech House, 2013, p. 567-592.

[70] N. Tiwari, A. Jha, S. Singh, and M. Akhtar, "Estimation of Broadband Complex Permeability using SIW Cavity based Multimodal Approach," *IEEE Transactions on Instrumentation and Measurement*, 2020.

[71] M. Ulmasculov, K. Sharypov, S. Shunailov, V. Shpak, M. Yalandin, M. Pedos, and S. Rukin, "Gyromagnetic nonlinear transmission line generator of high voltage pulses modulated at 4 GHz frequency with 1000 Hz pulse repetition rate," *Journal of Physics: Conference Series*, vol. 830, Apr. 2017.

[72] J. Xu, M. Koledintseva, Y. Zhang, Y. He, B. Matlin, R. Dubroff, J. Drewniak, and J. Zhang, "Complex Permittivity and Permeability Measurements and Finite-Difference Time-Domain Simulation of Ferrite Materials," *IEEE Transactions on Electromagnetic Compatibility*, vol. 52, no. 4, 2010.

[73] H. Zhao, Y. Li, Q. Lin, and S. Wang, "The Parasitic Capacitance of Magnetic Components with Ferrite Cores Due to Time-Varying Electromagnetic (EM) Field," *2018 IEEE Energy Conversion Congress and Exposition (ECCE)*, 2018.

[74] D. Zyatkov, V. Balashov, V. Yurchenko, V. Cherepanov, and Z. Kochnev, "Capacitive Sensing Element with a Magnetic Fluid for Detecting of Change of Magnetic Field," *2019 Photonics & Electromagnetics Research Symposium - Spring (PIERS-Spring)*, 2019.

8. Appendix

8.1. MEEP Code

```
#include <iostream>
#include <fstream>
#include <stdio.h>
#include <stdlib.h>
#include <string.h>
#include <complex>
#include "meep.hpp"
#include "ctl-math.h"
#include <mpb.h>
#include "ctlgeom.h"
#include "meepgeom.hpp"
#include <math.h>
#ifndef DATADIR
#define DATADIR "./"
#endif

using namespace meep;
using namespace std;

typedef std::complex<double> cdouble;

//SI Conversion Factors
double epsr=10;
double a0=1e-4;//0.1mm
double c0=2.99792458e8;//Speed of Light (m/s)
double f0=c0/a0;//3000GHz
double t0=1/f0;//0.33e-12 (s)
double mu0=4*pi*(1e-7);// (H/m)
double eps0=8.854187817e-12;// (F/m)
double I0=1; //(A)
double E0=I0/(a0*eps0*c0);//Electric Field
double D0=I0/(a0*c0);//Electric Displacement Field
double B0=I0/(a0*eps0*c0*c0);//Magnetic Field
double H0=I0/(a0);//Magnetizing Field
double sigmaD0=(epsr*eps0*c0)/a0;//Electric Conductivity
double J0=I0/(a0*a0);//Electric Current Density
double u0=(I0*I0)/(eps0*c0*c0*a0*a0);//Energy Density
double S0=(I0*I0)/(eps0*c0*a0*a0);//Poynting Vector
double Sc0=1/(c0);//Courant Factor

double xcen=0.0, ycen=0.0, zcen=0.0;
double dxmin=0.0, dxmax=02.5, dymin=0.0, dymax=02.5, dzmin=0.0, dzmax=10.0;
double wcore=2.0*dymax;
double winding_thickness_p=01.0,insulation_thickness_p=02.5,
pml_thickness=1.0;
double mu_core=1;
int Np=1;//must be odd
int Ns=1;//must be odd
double margin=02.0;
```

```
double amplitude=1.0;
double divisions=2;

int numcoord=0;
int corecoord=0;
double k=2*pi*Np/(2*dzmin);
double theta=0.0;
double rp=(wcore/2.0)+(winding_thickness_p/2.0)+insulation_thickness_p;
double * xpcoord=new double [1000000];
double * ypcoord=new double [1000000];
double * zpcoord=new double [1000000];
double * xscoord=new double [1000000];
double * yscoord=new double [1000000];
double * zscoord=new double [1000000];
double * xccoord=new double [1000000];
double * yccoord=new double [1000000];
double * zccoord=new double [1000000];

double annulus(const vec & v, double xcen, double ycen, double zcen, double
dxmin, double dxmax, double dymin, double dymax, double dzmin, double dzmax,
double control, double special, double std = 0.0)
{
  double mu=control;

  double dx=v.x() - xcen;
  double dy=v.y() - ycen;
  double dz=v.z() - zcen;

  if ( (abs(dx)<=dxmax) && (abs(dy)<=dymax) && (abs(dz)<=dzmax) )
  {
    {mu= gaussian_random(special,std);}
  }

  if ( (abs(dx)<=dxmin) && (abs(dy)<=dymin) && (abs(dz)<=dzmin) )
  {
    mu= control;
  }

    return mu;
}

bool inside_box(const vec & v, double xcen, double ycen, double zcen, double
dxmax, double dymax, double dzmax)
{
  bool ans=false;

  double dx=v.x() - xcen;
  double dy=v.y() - ycen;
  double dz=v.z() - zcen;


  if ( (abs(dx)<=dxmax) && (abs(dy)<=dymax) && (abs(dz)<=dzmax) )
  {
    {ans=true;}
  }
```

```
  return ans;
}


cdouble line_integral_x(fields & f, component C, double dx, double xmin,
double xmax, double y, double z)
{
  cdouble sum(0.0,0.0);
  cdouble deltax(dx,0.0);
  for (double x=xmin; x<=xmax; x=x+dx)
  {
    monitor_point p;
    f.get_point(&p, vec(x,y,z));
    cdouble dF = p.get_component(C);
    sum += dF*deltax;
  }
  return sum;
}

cdouble line_integral_y(fields & f, component C, double dy, double ymin,
double ymax, double x, double z)
{
  cdouble sum(0.0,0.0);
  cdouble deltay(dy,0.0);
  for (double y=ymin; y<=ymax; y=y+dy)
  {
    monitor_point p;
    f.get_point(&p, vec(x,y,z));
    cdouble dF = p.get_component(C);
    sum += dF*deltay;
  }
  return sum;
}

cdouble line_integral_z(fields & f, component C, double dz, double zmin,
double zmax, double x, double y)
{
  cdouble sum(0.0,0.0);
  cdouble deltaz(dz,0.0);
  for (double z=zmin; z<=zmax; z=z+dz)
  {
    monitor_point p;
    f.get_point(&p, vec(x,y,z));
    cdouble dF = p.get_component(C);
    //cout<<dF.real()<<" , "<<dF.imag()<<endl;
    sum += dF*deltaz;
    //cout<<dF.real()<<" , "<<dF.imag()<<endl;
  }
  return sum;
}

cdouble compute_Im(fields & f, double z)
{
  cdouble Iyf=line_integral_y(f,Ey,0.001,ycen-dymax,ycen+dymax,xcen+dxmax,z);
```

```
    cdouble Iyb=line_integral_y(f,Ey,0.001,ycen-dymax,ycen+dymax,xcen-
dxmax,z);
    cdouble Ixt=line_integral_x(f,Ex,0.001,xcen-dxmax,xcen+dxmax,ycen-
dymax,z);
    cdouble Ixb=line_integral_x(f,Ex,0.001,xcen-
dxmax,xcen+dxmax,ycen+dymax,z);
    cdouble Im=Ixt+Iyf-Ixb-Iyb;
    return Im;
}

cdouble compute_Ie(fields & f, double z)
{
  cdouble Iyf=line_integral_y(f,Hy,0.001,ycen-dymax,ycen+dymax,xcen+dxmax,z);
    cdouble Iyb=line_integral_y(f,Hy,0.001,ycen-dymax,ycen+dymax,xcen-
dxmax,z);
    cdouble Ixt=line_integral_x(f,Hx,0.001,xcen-dxmax,xcen+dxmax,ycen-
dymax,z);
    cdouble Ixb=line_integral_x(f,Hx,0.001,xcen-
dxmax,xcen+dxmax,ycen+dymax,z);
    cdouble Ie=Ixt+Iyf-Ixb-Iyb;
  return Ie;
}

cdouble compute_Vm(fields & f, double z)
{
  //cdouble Vy=line_integral_y(f,Hy,0.001,ycen-dymin,y,xcen,zcen-dzmin);
  cdouble Vz=line_integral_z(f,Hz,0.001,zcen-dzmax,z,xcen,ycen);
  //cdouble Vm=Vy+Vz;
  return Vz;
}

cdouble compute_Ve(fields & f, double z)
{
  //cdouble Vy=line_integral_y(f,Ey,0.001,ycen-dymin,y,xcen,zcen-dzmin);
  cdouble Vz=line_integral_z(f,Ez,0.001,zcen-dzmax,z,xcen,ycen);
  //cdouble Ve=Vy+Vz;
  return Vz;
}

double mu(const vec &v)
{
  return 1.0;
}

double eps(const vec &v)
{
  return 1.0;
}

double conductivity(const vec &v)
{
}

class core_material : public material_function {
  public:
```

```
};

class winding_material : public material_function {
  public:
};


typedef struct my_material_func_data {
  double rxInner, ryInner, rOuter;
  bool with_susceptibility;
} my_material_func_data;

void my_material_func(vector3 p, void *user_data, meep_geom::medium_struct
*m) {
  my_material_func_data *data = (my_material_func_data *)user_data;

    bool in_middle=false;

    double dx=p.x - xcen;
    double dy=p.y - ycen;
    double dz=p.z - zcen;

    for (int i=0; i<corecoord; i++) {
    double dxp=p.x - xccoord[i];
    double dyp=p.y - yccoord[i];
    double dzp=p.z - zccoord[i];
    double drp=sqrt(dxp*dxp+dyp*dyp+dzp*dzp);
    if((dxp<=(wcore/2.0))&&(dyp<=(wcore/2.0))&&(dzp<=(wcore/2.0))){
        in_middle=true;
    }
    }

  // set permittivity and permeability
  double nn = in_middle ? sqrt(mu_core) : 1.0;
  double mm = in_middle ? sqrt(10.0) : 1.0;
  m->epsilon_diag.x = m->epsilon_diag.y = m->epsilon_diag.z = mm * mm;
  //m->epsilon_offdiag.x.re = m->epsilon_offdiag.x.im = epsilon_offdiag.y.re
= m->epsilon_offdiag.y.im = epsilon_offdiag.z.re = m->epsilon_offdiag.z.im =
nn * nn;
  m->mu_diag.x = m->mu_diag.y = m->mu_diag.z = nn*nn;

  //m->mu_offdiag.x.re = m->mu_offdiag.x.im = mu_offdiag.y.re = m-
>mu_offdiag.y.im = mu_offdiag.z.re = m->mu_offdiag.z.im = nn * nn;
  m->E_chi2_diag.x = m->E_chi2_diag.y = m->E_chi2_diag.z = 1.0;
  m->E_chi3_diag.x = m->E_chi3_diag.y = m->E_chi3_diag.z = 1.0;
  m->H_chi2_diag.x = m->H_chi2_diag.y = m->H_chi2_diag.z = 1.0;
  m->H_chi3_diag.x = m->H_chi3_diag.y = m->H_chi3_diag.z = 1.0;
  //m->D_conductivity_diag.x = m->D_conductivity_diag.y = m-
>D_conductivity_diag.z = nn * nn;
  //m->B_conductivity_diag.x = m->B_conductivity_diag.y = m-
>B_conductivity_diag.z = 0.0;

  if (in_middle)
  {
    m->H_susceptibilities.num_items = 1;
```

```
    m->H_susceptibilities.items = new meep_geom::susceptibility[1];

    m->H_susceptibilities.items[0].sigma_offdiag.x = 0.0;
    m->H_susceptibilities.items[0].sigma_offdiag.y = 0.0;
    m->H_susceptibilities.items[0].sigma_offdiag.z = 0.0;
    m->H_susceptibilities.items[0].sigma_diag.x =
gaussian_random(1.0,1.0);//NiFe_sig;
    m->H_susceptibilities.items[0].sigma_diag.y =
gaussian_random(1.0,1.0);//NiFe_sig;
    m->H_susceptibilities.items[0].sigma_diag.z =
gaussian_random(1.0,1.0);//NiFe_sig;
    m->H_susceptibilities.items[0].bias.x = gaussian_random(1.0,1.0);
    m->H_susceptibilities.items[0].bias.y = gaussian_random(1.0,1.0);
    m->H_susceptibilities.items[0].bias.z = gaussian_random(1.0,1.0);
    m->H_susceptibilities.items[0].frequency = (0.2e6)/f0;//NiFe_frq;
    m->H_susceptibilities.items[0].gamma = 100.0*((0.2e6)/f0);//NiFe_gam;
    m->H_susceptibilities.items[0].alpha =
gaussian_random(1.0,1.0);//NiFe_alpha;
    m->H_susceptibilities.items[0].noise_amp = 0.01;
    m->H_susceptibilities.items[0].drude = false;
    m->H_susceptibilities.items[0].saturated_gyrotropy = true;
    m->H_susceptibilities.items[0].is_file = false;
    m->D_conductivity_diag.x = m->D_conductivity_diag.y = m-
>D_conductivity_diag.z = (5e-3)/sigmaD0;
  }

  for (int i=0; i<numcoord; i++) {
    double dxp=p.x - xpcoord[i];
    double dyp=p.y - ypcoord[i];
    double dzp=p.z - zpcoord[i];
    double drp=sqrt(dxp*dxp+dyp*dyp+dzp*dzp);
    if(drp<=(winding_thickness_p/2.0)){
        m->D_conductivity_diag.x = m->D_conductivity_diag.y = m-
>D_conductivity_diag.z = 5.8e7/sigmaD0;
    }
    double dxs=p.x - xscoord[i];
    double dys=p.y - yscoord[i];
    double dzs=p.z - zscoord[i];
    double drs=sqrt(dxs*dxs+dys*dys+dzs*dzs);
    if(drs<=(winding_thickness_p/2.0)){
        m->D_conductivity_diag.x = m->D_conductivity_diag.y = m-
>D_conductivity_diag.z = 5.8e7/sigmaD0;
    }
  }

  if ( (p.z<(zcen-dzmax))||(p.z>(zcen+dzmax)) ) {
  }

}



int main(int argc, char *argv[]) {

  initialize mpi(argc,argv);
```

```
const char *mydirname = "MMTL-out";
  std::ofstream Time;
  std::ofstream Space;
  std::ofstream FieldsIn;
  std::ofstream FieldsOut;
  std::ofstream Fluxes;
  std::ofstream Skin;
  Time.open ("TimeEvolution.txt");
  Space.open ("SpaceEvolution.txt");
  FieldsIn.open ("FieldEvolutionIn.txt");
  FieldsOut.open ("FieldEvolutionOut.txt");
  Fluxes.open ("Flux.txt");
  Skin.open ("Skin.txt");
  //trash_output_directory(mydirname);
  double xsize=10;
  double ysize=10;
  double zsize=50;

  for (double z = -04.0; z <= -1.0; z=z+0.1)
  {
      theta=k*(z+04.0);
      xpcoord[numcoord]=-rp*sin(theta);
      ypcoord[numcoord]=rp*cos(theta);
      zpcoord[numcoord]=z;
      xscoord[numcoord]=-rp*sin(theta);
      yscoord[numcoord]=rp*cos(theta);;
      zscoord[numcoord]=z+05.0;
      numcoord++;
  }

  for(double y=-12.5;y<=12.5;y=y+12.5)
  {for (double z=-07.5;z<=07.5;z=z+00.1){
      xccoord[corecoord]=xcen;
      yccoord[corecoord]=y;
      zccoord[corecoord]=z;
      corecoord++;
  }}

  for(double z=-07.5;z<=07.5;z=z+15.0)
  {for (double y=-12.5;y<=12.5;y=y+00.1){
      xccoord[corecoord]=xcen;
      yccoord[corecoord]=y;
      zccoord[corecoord]=z;
      corecoord++;
  }}


  grid_volume gv = vol3d(xsize, ysize, zsize, divisions);
  //grid_volume vol3d(double xsize, double ysize, double zsize, double a);
  gv.center_origin();
  //void center_origin(void) { shift_origin(-icenter()); }


  structure transformer(gv, eps, pml(pml_thickness));
```

```
    transformer.set_output_directory(mydirname);

    meep_geom::medium_struct my_medium_struct;
    my_medium_struct.epsilon_diag.x = 1.0;
    my_medium_struct.epsilon_diag.y = 1.0;
    my_medium_struct.epsilon_diag.z = 1.0;
    my_medium_struct.mu_diag.x=1.0;
    my_medium_struct.mu_diag.y=1.0;
    my_medium_struct.mu_diag.z=1.0;
    my_medium_struct.H_chi2_diag.x=1.0;
    my_medium_struct.H_chi2_diag.y=1.0;
    my_medium_struct.H_chi2_diag.z=1.0;
    my_medium_struct.H_chi3_diag.x=1.0;
    my_medium_struct.H_chi3_diag.y=1.0;
    my_medium_struct.H_chi3_diag.z=1.0;

    my_medium_struct.E_chi2_diag.x=1.0;
    my_medium_struct.E_chi2_diag.y=1.0;
    my_medium_struct.E_chi2_diag.z=1.0;
    my_medium_struct.E_chi3_diag.x=1.0;
    my_medium_struct.E_chi3_diag.y=1.0;
    my_medium_struct.E_chi3_diag.z=1.0;

    my_medium_struct.H_susceptibilities.num_items = 1;
    my_medium_struct.H_susceptibilities.items = new
meep_geom::susceptibility[1];

    my_medium_struct.H_susceptibilities.items[0].sigma_offdiag.x = 0.0;
    my_medium_struct.H_susceptibilities.items[0].sigma_offdiag.y = 0.0;
    my_medium_struct.H_susceptibilities.items[0].sigma_offdiag.z = 0.0;
    my_medium_struct.H_susceptibilities.items[0].sigma_diag.x =
gaussian_random(1.0,1.0);
    my_medium_struct.H_susceptibilities.items[0].sigma_diag.y =
gaussian_random(1.0,1.0);
    my_medium_struct.H_susceptibilities.items[0].sigma_diag.z =
gaussian_random(1.0,1.0);
    my_medium_struct.H_susceptibilities.items[0].bias.x =
gaussian_random(1.0,1.0);
    my_medium_struct.H_susceptibilities.items[0].bias.y =
gaussian_random(1.0,1.0);
    my_medium_struct.H_susceptibilities.items[0].bias.z =
gaussian_random(1.0,1.0);
    my_medium_struct.H_susceptibilities.items[0].frequency = (0.2e6/f0);
    my_medium_struct.H_susceptibilities.items[0].gamma = 100.0*(0.2e6/f0);
    my_medium_struct.H_susceptibilities.items[0].alpha =
gaussian_random(1.0,1.0);
    my_medium_struct.H_susceptibilities.items[0].noise_amp = 0.01;
    my_medium_struct.H_susceptibilities.items[0].drude = false;
    my_medium_struct.H_susceptibilities.items[0].saturated_gyrotropy = true;
    my_medium_struct.H_susceptibilities.items[0].is_file = false;

    my_material_func_data data;
    data.with_susceptibility = true;
```

```
  meep_geom::material_type default_material =meep_geom::make_dielectric(1.0);
  default_material->medium=my_medium_struct;
  default_material->user_func = my_material_func;
  default_material->user_data = (void *) &data;
  default_material->do_averaging = false;

  meep_geom::material_type my_user_material
=meep_geom::make_user_material(my_material_func, (void *)&data, false);

  geometric_object objects[5];
  vector3 center = {0.0, 0.0, 0.0};
  vector3 center1 = {0.0, -12.5, 0.0};
  vector3 center2 = {0.0, 0.0, 0.0};
  vector3 center3 = {0.0, 12.5, 0.0};
  vector3 center4 = {0.0, 0.0, 07.5};
  vector3 center5 = {0.0, 0.0, -07.5};
  double radius = 3.0;
  double height = 1.0e20;
  vector3 xhat1 = {1.0, 0.0, 0.0};
  vector3 yhat1 = {0.0, 1.0, 0.0};
  vector3 zhat1 = {0.0, 0.0, 1.0};
  vector3 size1 = {wcore, wcore, 20.0};
  vector3 size2 = {wcore, wcore, 20.0};
  vector3 size3 = {wcore, wcore, 20.0};
  vector3 size4 = {wcore, 30.0, wcore};
  vector3 size5 = {wcore, 30.0, wcore};

  objects[0] = make_block(my_user_material, center1, xhat1, yhat1, zhat1,
size1);
  objects[1] = make_block(my_user_material, center2, xhat1, yhat1, zhat1,
size2);
  objects[2] = make_block(my_user_material, center3, xhat1, yhat1, zhat1,
size3);
  objects[3] = make_block(my_user_material, center4, xhat1, yhat1, zhat1,
size4);
  objects[4] = make_block(my_user_material, center5, xhat1, yhat1, zhat1,
size5);
  geometric_object_list g = {5, objects};




    meep_geom::absorber_list al= new meep_geom::absorber_list_type;

    meep_geom::material_type_list mtl= meep_geom::material_type_list();
    mtl.num_items=1;
    mtl.items=new meep_geom::material_type;
    mtl.items[0]=my_user_material;
    cout<<"MAIN "<<mtl.num_items<<endl;
    bool use_anisotropic_averaging = false;
    bool ensure_periodicity = true;
    set_materials_from_geometry(&transformer, g, center,
use_anisotropic_averaging,DEFAULT_SUBPIXEL_TOL,
DEFAULT_SUBPIXEL_MAXEVAL,ensure_periodicity, default_material,al,mtl);
```

```
    fields f(& transformer);
    //fields(structure *, double m = 0, double beta = 0, bool
zero_fields_near_cylorigin = true);


 for (double fp=0.0;fp<=3.0*(1e9/f0);fp=fp+0.5*(1e9/f0))
    { cout<<fp<<endl;
      for (double yp = -20.0; yp <= 20.0; yp=yp+10.0)
      {
        cout<<f.get_mu(vec(0.0,yp,(dzmin+dzmax)/2.0),fp)-10000<<" ";
      }
      cout<<endl;
    }


    double xcenp=xcen;
    double ycenp=ycen-dymin-(0.5*wcore);
    double zcenp=zcen;
    double dxminp=dxmax+insulation_thickness_p;
    double dxmaxp=dxminp+winding_thickness_p;
    double dyminp=(0.5*wcore)+insulation_thickness_p;
    double dymaxp=dyminp+winding_thickness_p;
    double dzminp=0;
    double dzmaxp=0.5*winding_thickness_p;
    zcenp=zcen-(0.5*double(Np-1)*insulation_thickness_p)-(0.5*double(Np-
1)*winding_thickness_p);

    double fcen = (1e10)/f0; // ; pulse center frequency
    double df = 0.999999*((1e10)/f0);    // ; df

    for (int i=0;i<numcoord;i++)
    {
        theta=k*(zpcoord[i]+05.0);
      const volume vsrc1 =volume(vec(xpcoord[i],ypcoord[i],zpcoord[i]),
vec(xpcoord[i],ypcoord[i],zpcoord[i]));
      {
        //continuous_src_time src(cdouble(fr/f0,0.0));
        gaussian_src_time src(fcen,df);
        f.add_volume_source(Ex, src, vsrc1, cdouble(amplitude*cos(theta),0));
        f.add_volume_source(Ey, src, vsrc1, cdouble(-
amplitude*sin(theta),0));
      }

    }

    xcenp=xcen;
    ycenp=ycen-dymin-(05.0*wcore);
    zcenp=zcen;
    volume box1( vec(dxmax,-dymax,-05.0), vec(-dxmax,dymax,0.0) );
    ycenp=ycen+dymin+(0.5*wcore);
    volume box2( vec(dxmax,-dymax,0.0), vec(-dxmax,dymax,05.0) );

    fcen = (1e10)/f0; // ; pulse center frequency
    df = 0.001*(fcen/f0);    // ; df
```

```
    double fmin = 0, fmax = (1e11)/f0;
    int Nfreq = 1000;
    dft_flux flux1 = f.add_dft_flux_box(box1, fmin, fmax, Nfreq);
    dft_flux flux2 = f.add_dft_flux_box(box2, fmin, fmax, Nfreq);
    double init_energy = f.field_energy_in_box(box1);


  //integral of flux = change in energy of box
  f.step();
  f.step();
  f.step();
  f.step();
  f.step();

    volume vxy=volume(vec(-xsize+10,-ysize+10,0),vec(xsize-10,ysize-10,0));
    volume vxz=volume(vec(-xsize+10,0,-zsize+10),vec(xsize-10,0,zsize-10));
    volume vyz=volume(vec(0,-ysize+10,-zsize+10),vec(0,ysize-10,zsize-10));

int stop=0;

    for(int i=1;i<=1000000;i++)
    {
        if(!stop)
           {f.step();}
       if (stop)
       {
         i=1000001;
       }

    if ((i%100)==0)
    {
    f.output_hdf5(Hx,vyz);
    f.output_hdf5(Hy,vyz);
    f.output_hdf5(Hz,vyz);
    f.output_hdf5(Bx,vyz);
    f.output_hdf5(By,vyz);
    f.output_hdf5(Bz,vyz);
    f.output_hdf5(Ex,vyz);
    f.output_hdf5(Ey,vyz);
    f.output_hdf5(Ez,vyz);
    f.output_hdf5(Dx,vyz);
    f.output_hdf5(Dy,vyz);
    f.output_hdf5(Dz,vyz);
    f.output_hdf5(Sx,vyz);
    f.output_hdf5(Sy,vyz);
    f.output_hdf5(Sz,vyz);

    }

      {
        cdouble Vm=compute_Vm(f,ycen);
        cdouble Im=compute_Im(f,ycen);
        cdouble Ve=compute_Ve(f,ycen);
        cdouble Ie=compute_Ie(f,ycen);
```

```
        Time<<Im.real()<<" , "<<Im.imag()<<" , "<<Vm.real()<<" ,
"<<Vm.imag()<<" , "<<Ie.real()<<" , "<<Ie.imag()<<" , "<<Ve.real()<<" ,
"<<Ve.imag()<<endl;
        //Im , Vm , Ie , Ve

        monitor_point pin;
        f.get_point(&pin, vec(xcen,ycen,-02.5));
        cdouble E1i = pin.get_component(Ex);
        cdouble E2i = pin.get_component(Ey);
        cdouble E3i = pin.get_component(Ez);
        cdouble D1i = pin.get_component(Dx);
        cdouble D2i = pin.get_component(Dy);
        cdouble D3i = pin.get_component(Dz);
        cdouble H1i = pin.get_component(Hx);
        cdouble H2i = pin.get_component(Hy);
        cdouble H3i = pin.get_component(Hz);
        cdouble B1i = pin.get_component(Bx);
        cdouble B2i = pin.get_component(By);
        cdouble B3i = pin.get_component(Bz);

        monitor_point po;
        f.get_point(&po, vec(xcen,ycen,02.5));
        cdouble E1o = po.get_component(Ex);
        cdouble E2o = po.get_component(Ey);
        cdouble E3o = po.get_component(Ez);
        cdouble D1o = po.get_component(Dx);
        cdouble D2o = po.get_component(Dy);
        cdouble D3o = po.get_component(Dz);
        cdouble H1o = po.get_component(Hx);
        cdouble H2o = po.get_component(Hy);
        cdouble H3o = po.get_component(Hz);
        cdouble B1o = po.get_component(Bx);
        cdouble B2o = po.get_component(By);
        cdouble B3o = po.get_component(Bz);

        FieldsIn<<H1i.real() <<" , "<<H1i.imag()<<" , "<<H2i.real()<<" ,
"<<H2i.imag()<<" , "<<H3i.real()<<" , "<<H3i.imag()<<" , "<<B1i.real()<<" ,
"<<B1i.imag()<<" , "<<B2i.real()<<" , "<<B2i.imag()<<" , "<<B3i.real()<<" ,
"<<B3i.imag()<<" , "<<E1i.real()<<" , "<<E1i.imag()<<" , "<<E2i.real()<<" ,
"<<E2i.imag()<<" , "<<E3i.real()<<" , "<<E3i.imag()<<" , "<<D1i.real()<<" ,
"<<D1i.imag()<<" , "<<D2i.real()<<" , "<<D2i.imag()<<" , "<<D3i.real()<<" ,
"<<D3i.imag()<<endl;
        FieldsOut<<H1o.real()<<" , "<<H1o.imag()<<" , "<<H2o.real()<<" ,
"<<H2o.imag()<<" , "<<H3o.real()<<" , "<<H3o.imag()<<" , "<<B1o.real()<<" ,
"<<B1o.imag()<<" , "<<B2o.real()<<" , "<<B2o.imag()<<" , "<<B3o.real()<<" ,
"<<B3o.imag()<<" , "<<E1o.real()<<" , "<<E1o.imag()<<" , "<<E2o.real()<<" ,
"<<E2o.imag()<<" , "<<E3o.real()<<" , "<<E3o.imag()<<" , "<<D1o.real()<<" ,
"<<D1o.imag()<<" , "<<D2o.real()<<" , "<<D2o.imag()<<" , "<<D3o.real()<<" ,
"<<D3o.imag()<<endl;
        //Hx , Hy , Hz , Bx , By , Bz , Ex , Ey , Ez , Dx , Dy , Dz
      }

      if((i%1000)==0)
      {
        cout<<"End? (1/0):";
        cin>>stop;
```

```
      }

    }


    double *fl1 = flux1.flux();
    double *fl2 = flux2.flux();
    cout<<"Flux Harmonics"<<endl;
    for (int i = 0; i < Nfreq; ++i) {
      Fluxes<<(fmin + i * flux1.dfreq)<<" , "<<fl1[i]<<" , "<<fl2[i]<<endl;
      //freq , fluxin , fluxout
    }

    int num_bands=1;
    int * bands=new int [num_bands];
    double * vgrp=new double [num_bands*Nfreq];
    cdouble * coeffs=new cdouble [2*num_bands*Nfreq];
    bands[0]=1;
    for (int i = 1; i <= Nfreq; ++i) {
      vgrp[i]=0.0;
    }

    cout<<"Skin Effect"<<endl;
    for (double y=-05.0;y<=05.0;y=y+00.01)
    {
        monitor_point pin;
        f.get_point(&pin, vec(xcen,y,zcen));
        cdouble E1i = pin.get_component(Ex);
        cdouble E2i = pin.get_component(Ey);
        cdouble E3i = pin.get_component(Ez);
        cdouble D1i = pin.get_component(Dx);
        cdouble D2i = pin.get_component(Dy);
        cdouble D3i = pin.get_component(Dz);
        cdouble H1i = pin.get_component(Hx);
        cdouble H2i = pin.get_component(Hy);
        cdouble H3i = pin.get_component(Hz);
        cdouble B1i = pin.get_component(Bx);
        cdouble B2i = pin.get_component(By);
        cdouble B3i = pin.get_component(Bz);
        Skin<<H1i.real() <<" , "<<H1i.imag()<<" , "<<H2i.real()<<" ,
"<<H2i.imag()<<" , "<<H3i.real()<<" , "<<H3i.imag()<<" , "<<B1i.real()<<" ,
"<<B1i.imag()<<" , "<<B2i.real()<<" , "<<B2i.imag()<<" , "<<B3i.real()<<" ,
"<<B3i.imag()<<" , "<<E1i.real()<<" , "<<E1i.imag()<<" , "<<E2i.real()<<" ,
"<<E2i.imag()<<" , "<<E3i.real()<<" , "<<E3i.imag()<<" , "<<D1i.real()<<" ,
"<<D1i.imag()<<" , "<<D2i.real()<<" , "<<D2i.imag()<<" , "<<D3i.real()<<" ,
"<<D3i.imag()<<endl;
    }

    cout<<"SpaceEvolution"<<endl;
    //for (double y=(ycen-dymin);y<=(ycen+dymin);y=y+0.001)
    for (double z=-05.0;z<=05.0;z=z+00.1)
    {
      cdouble Im=compute_Im(f,z);
      cdouble Ie=compute_Ie(f,z);
      cdouble Vm=compute_Vm(f,z);
      cdouble Ve=compute_Ve(f,z);
```

```
      Space <<Im.real()<<" , "<<Im.imag()<<" , "<<Vm.real()<<" , 
"<<Vm.imag()<<" , "<<Ie.real()<<" , "<<Ie.imag()<<" , "<<Ve.real()<<" , 
"<<Ve.imag()<<endl;
      //Im , Vm , Ie , Ve
    }

    Time.close();
    Space.close();
    FieldsIn.close();
    FieldsOut.close();
    Fluxes.close();
    return 0;
}
```

8.2. MATLAB Codes

8.2.1. Plotting Magnetic Susceptibility and Hysteresis Loop for Ferromagnetic material

```
clc;clear all;
max=2000;
MMF(1:max+1)=(0:max)-(max/2);
ind=1;

for ind=1:max+1
        chip(ind)=10000*exp(-(abs(MMF(ind)-500))*(abs(MMF(ind)-500))/50000);
        chin(ind)=-10000*exp(-(abs(MMF(ind)+500))*(abs(MMF(ind)+500))/50000);
end

B(1)=2.5;
Hmax=1000;
Happ=[Hmax:-1:(-Hmax) (-Hmax):1:(Hmax)];
hold on;
for ind=2:length(Happ)
    if (Happ(ind)>Happ(ind-1))
        munet=(chip(Happ(ind)+(Hmax+1))+1);
        dB=(Happ(ind)-Happ(ind-1))*munet*(4*pi*1e-7);
    else
        munet=(chin(Happ(ind)+(Hmax+1))+1);
        dB=(-Happ(ind)+Happ(ind-1))*munet*(4*pi*1e-7);
    end
    B(ind)=B(ind-1)+dB;
end
```

8.2.2. Evolution of Magnetic displacement current and Voltage for Magnetic Transmission Line

```
clc;clear all;
f=fopen('TimeEvolution.txt');
l=fgetl(f);
i=1;
while ischar(l)
    %%disp(l);
    text{i}=l;
    data{i}=sscanf(text{i},'%f , %f , %f , %f , %f , %f , %f , %f');
    A1(i)=data{i}(1);
    A2(i)=data{i}(2);
    A3(i)=data{i}(3);
    A4(i)=data{i}(4);
    A5(i)=data{i}(5);
    A6(i)=data{i}(6);
    A7(i)=data{i}(7);
    A8(i)=data{i}(8);
    l=fgetl(f);
    i=i+1;
end

epsr=0.9999;
a0=1e-4;%0.1mm
c0=2.99792458e8;%Speed of Light (m/s)
f0=c0/a0;%3000GHz
t0=1/f0;%0.33e-12 (s)
mu0=4*pi*(1e-7);% (H/m)
eps0=8.854187817e-12;% (F/m)
I0=1; %(A)
E0=I0/(a0*eps0*c0);%Electric Field
D0=I0/(a0*c0);%Electric Displacement Field
B0=I0/(a0*eps0*c0*c0);%Magnetic Field
H0=I0/(a0);%Magnetizing Field
V0=I0/(eps0*c0);%Electric Field

hold on;
A1=A1*V0;A2=A2*V0;
A3=A3*I0;A4=A4*I0;
A5=A5*I0;A6=A6*I0;
A7=A7*V0;A8=A8*V0;

t=100*t0*(1:length(A1));
subplot(2,1,1)
hold on;plot(t,A1);plot(t,A2,'r');%Im
ylabel('Magnetic Current (V)');
xlabel('Time');
legend('Re','Im');
subplot(2,1,2)
hold on;plot(t,A3);plot(t,A4,'r');%Vm
ylabel('Magnetic Voltage (A)');
xlabel('Time');
legend('Re','Im');
```

8.2.3. Calculation of Intrinsic Impedance, Propagation Constant, per unit length Conductance, per unit length Reluctance and per unit length Susceptance for Magnetic Transmission Line

```
clc;clear all;
%hold on;
%%
f=fopen('F1.txt');
File=1;
l=fgetl(f);
in=1;
Prev=1600*(File-1);
while ischar(l)
%for kj=1:81
    %%disp(l);
    text{in}=l;
    data{in}=sscanf(text{in},'%f , %f , %f , %f , %f , %f , %f , %f , %f , %f
, %f , %f , %f , %f , %f , %f , %f , %f , %f , %f , %f , %f , %f , %f , %f ,
%f');
    Hx(data{in}(1)-Prev,(((data{in}(2)+10)*4)+1))=data{in}(3)+1i*data{in}(4);
    Hy(data{in}(1)-Prev,(((data{in}(2)+10)*4)+1))=data{in}(5)+1i*data{in}(6);
    Hz(data{in}(1)-Prev,(((data{in}(2)+10)*4)+1))=data{in}(7)+1i*data{in}(8);

    Bx(data{in}(1)-
Prev,(((data{in}(2)+10)*4)+1))=data{in}(9)+1i*data{in}(10);
    By(data{in}(1)-
Prev,(((data{in}(2)+10)*4)+1))=data{in}(11)+1i*data{in}(12);
    Bz(data{in}(1)-
Prev,(((data{in}(2)+10)*4)+1))=data{in}(13)+1i*data{in}(14);

    Ex(data{in}(1)-
Prev,(((data{in}(2)+10)*4)+1))=data{in}(15)+1i*data{in}(16);
    Ey(data{in}(1)-
Prev,(((data{in}(2)+10)*4)+1))=data{in}(17)+1i*data{in}(18);
    Ez(data{in}(1)-
Prev,(((data{in}(2)+10)*4)+1))=data{in}(19)+1i*data{in}(20);

    Dx(data{in}(1)-
Prev,(((data{in}(2)+10)*4)+1))=data{in}(21)+1i*data{in}(22);
    Dy(data{in}(1)-
Prev,(((data{in}(2)+10)*4)+1))=data{in}(23)+1i*data{in}(24);
    Dz(data{in}(1)-
Prev,(((data{in}(2)+10)*4)+1))=data{in}(25)+1i*data{in}(26);

    l=fgetl(f);
    in=in+1;
end

epsr=10;
a0=1e-4;%0.1mm
c0=2.99792458e8;%Speed of Light (m/s)
f0=c0/a0;%3000GHz
t0=1/f0;%0.33e-12 (s)
mu0=4*pi*(1e-7);% (H/m)
```

```
eps0=8.854187817e-12;% (F/m)
I0=1; %(A)
E0=I0/(a0*eps0*c0);%Electric Field
D0=I0/(a0*c0);%Electric Displacement Field
B0=I0/(a0*eps0*c0*c0);%Magnetic Field
H0=I0/(a0);%Magnetizing Field
sigmaD0=(epsr*eps0*c0)/a0;

hold on;

subplot(4,1,1)
hold on;
T=t0;
Fs=1/T;
L=45;
L=2^nextpow2(L);
% NFFT=2^nextpow2(L);
% FHxi=(fft(Hx(1:L,5)*H0,NFFT)/L)();
% FHxi(2:end-1)=
% f=Fs/2*linspace(0,1,NFFT/2+1);

FHxi=(fft(Hx(1:L,2)*H0,L));
FHxi=FHxi(1:L/2+1);
%FHxi(2:end-1)=2*FHxi(2:end-1)
f=Fs*(0:L/2+1);
f=f';

FHxo=(fft(Hx(1:L,12)*H0,L));
FHxo=FHxo(1:L/2+1);
%FHxo(2:end-1)=2*FHxo(2:end-1);

Gamma=log(FHxo./FHxi)/(-(10/80)*(2e-3));

subplot(3,1,1)
hold on;%plot(mag3(mag(A13,A14),mag(A15,A16),mag(A17,A18)));%E
plot(f(2:L/2+1),real(Gamma(2:L/2+1)));
xlabel('Frequency (Hz)')
ylabel('\alpha (Np.m^-^1)');
axis([0 5e11 1.32e5 1.38e5])

subplot(3,1,2)
plot(f(2:L/2+1),abs(imag(Gamma(2:L/2+1))));
ylabel('\beta (rad.m^-^1)');
xlabel('Frequency (Hz)')
axis([0 5e11 1e4 1.3e4])

subplot(3,1,3)
plot(f(2:L/2+1),f(2:L/2+1)./abs(imag(Gamma(2:L/2+1))));
ylabel('vp (m.s^-^1)');
xlabel('Frequency (Hz)')
axis([0 5e11 0 5e7])
% X = 1/(4*sqrt(2*pi*0.01))*(exp(-t.^2/(2*0.01)));

T=t0;
Fs=1/T;
```

```
L=45;
NFFT=2^nextpow2(L);
FEx=fft(Ex(1:L,2)*E0,NFFT)/L;
f=Fs/2*linspace(0,1,NFFT/2+1);
FHx=fft(Hx(1:L,2)*H0,NFFT)/L;
f=Fs/2*linspace(0,1,NFFT/2+1);
Z=FEx./FHx;


subplot(2,1,1)
hold on;%plot(mag3(mag(A13,A14),mag(A15,A16),mag(A17,A18)));%E
plot(f(2:NFFT/2+1),2*abs(Z(2:NFFT/2+1)));
xlabel('Frequency (Hz)')
ylabel('|Z_w (Ohm)|');
axis([0 5e11 3.3e4  3.45e4])

subplot(2,1,2)
plot(f(2:NFFT/2+1),angle(Z(2:NFFT/2+1))*(180/pi));
ylabel('\Theta Z_w (deg)');
xlabel('Frequency (Hz)');
axis([0 5e11 170 190])


XLm=(imag(Gamma(1:NFFT/2+1).*Z(1:NFFT/2+1)));
Gm=(real(Gamma(1:NFFT/2+1)./Z(1:NFFT/2+1)));
Rm=(Gm')*(-1).*(2*pi*f);%Reluctance
XCm=(imag(Gamma(1:NFFT/2+1)./Z(1:NFFT/2+1)));

subplot(4,1,1);
plot(f,(XLm(1:NFFT/2+1)));
ylabel('XLm(H/m)');
xlabel('Frequency (Hz)');
%axis([0 1e11 -5e9 5e9])

subplot(3,1,1);
plot(f(2:NFFT/2+1),(Gm(2:NFFT/2+1)));
ylabel('Conductance GL (S/m)');
xlabel('Frequency (Hz)');
axis([0 5e11 -8.5 -7.5])

subplot(3,1,2);
plot(f(2:NFFT/2+1),(Rm(2:NFFT/2+1)));
ylabel('Reluctance Rmskin (1/H.m)');
xlabel('Frequency (Hz)');
axis([0 5e11 0 3e13])

subplot(3,1,3);
plot(f(2:NFFT/2+1),(XCm(2:NFFT/2+1)));
ylabel('Susceptance XCL (S/m)');
xlabel('Frequency (Hz)');
axis([0 5e11 0 1])
```

8.2.4. Plotting Wideband Transformer Bandwidth calculated using Fourier Transform of Poynting Fluxes

```
clc;clear all;
f=fopen('Flux.txt');
l=fgetl(f);
i=1;
while ischar(l)
    %%disp(l);
    text{i}=l;
    data{i}=sscanf(text{i},'%f , %f , %f');
    A1(i)=data{i}(1);
    A2(i)=data{i}(2);
    A3(i)=data{i}(3);
    l=fgetl(f);
    i=i+1;
end

epsr=0.9999;
a0=1e-4;%0.1mm
c0=2.99792458e8;%Speed of Light (m/s)
f0=c0/a0;%3000GHz
t0=1/f0;%0.33e-12 (s)
mu0=4*pi*(1e-7);% (H/m)
eps0=8.854187817e-12;% (F/m)
I0=1; %(A)
E0=I0/(a0*eps0*c0);%Electric Field
D0=I0/(a0*c0);%Electric Displacement Field
B0=I0/(a0*eps0*c0*c0);%Magnetic Field
H0=I0/(a0);%Magnetizing Field
S0=(I0*I0)/(eps0*c0*a0*a0);%//Poynting Vector
sigmaD0=(epsr*eps0*c0)/a0;%Electric Conductivity

hold on;
subplot(3,1,1)
plot(A1*f0,abs(-A2*S0));
axis([0 4e9 S0*0.01 S0*40]);
ylabel('|Sin| (W/m^2)');
xlabel('frequency (Hz)');

subplot(3,1,2)
plot(A1*f0,abs(-A3*S0));
axis([0 4e9 S0*0.01 S0*25]);
ylabel('|Sout| (W/m^2)');
xlabel('frequency (Hz)');

subplot(3,1,3)
C=log(A2./A3);
C=C(1:5:1000);
A1=A1(1:5:1000);
plot((f0*A1),(abs(C)));
axis([0 4e9 -1 5]);
ylabel('Insertion Loss');
xlabel('frequency (Hz)');
```